

Advances in Preclinical Mantle Cell Lymphoma Research: A Novel Combination
Regimen and a Novel Mouse Model

Dissertation

Presented in Partial Fulfillment of the Requirements for the Degree Doctor of Philosophy
in the Graduate School of The Ohio State University

By

Fiona Dora Brown, B.S.

Graduate Program in Biomedical Sciences

The Ohio State University

2023

Dissertation Committee

Robert A Baiocchi MD PhD, Adviser

Rosa Lapalombella PhD, Co-Adviser

Monica Venere, PhD

Sameek Roychowdhury, MD PhD

Copyright by
Fiona Dora Brown
2023

Abstract

Mantle Cell Lymphoma (MCL) is a B cell lymphoma distinguished from other B cell lymphomas by an t(11;14)(q13;q32) translocation juxtaposing the *CCND1* gene downstream of the immunoglobulin heavy locus (*IgH*) promoter. *CCND1* and *SOX11*, a neural transcription factor, are the most commonly upregulated genes in MCL. The average patient with MCL is ~70 years of age and male with a 3:1 skew in sex. Current treatments include induction therapy with chemotherapeutics, first line therapy with targeted agents such as ibrutinib, and additional lines with more experimental agents. Stem cell transplant is possible after induction therapy in a small percentage of patients due to the physical strain. Relapse is basically universal with targeted therapies and frequently occurs after stem cell transplant. MCL is considered incurable today.

Many clinical trials are ongoing to develop novel treatment strategies. Many of the targeted therapy trials utilize the BCL-2 inhibitor venetoclax, an FDA approved agent for use in CLL, and second or third generation BTK inhibitors such as acalabrutinib. Immunotherapy is a rapidly expanding field for MCL, with many trials using CD19 CAR T cells, bi- or tri-specific antibodies, and drug-antibody conjugates. Despite these advances, more targets are needed to broaden the options available to patients.

We tested a potent and specific protein arginine methyltransferase 5 (PRMT5) inhibitor in combination with BH3 mimetics for synergistic cell death in *in vitro* and *in vivo*. PRMT5 inhibition causes the upregulation of many pro-apoptotic members of the BCL-2 family of proteins, which are responsible for triggering intrinsic apoptosis.

Mechanistic studies showed that response to PRMT5 inhibition and a combination treatment varied by cell line, but we saw significant survival advantages in our PDX models of MCL. PRMT5 inhibition with venetoclax provided the greatest advantage and disease was rendered undetectable via flow cytometry in two PDX models.

Beyond new treatment strategies, there is a need for an immune competent murine model of MCL to study and test novel immunotherapy strategies. Previous transgenic models were driven by genes representative of only a subset of MCL cases. To address this limitation, the E μ -SOX11CCND1 transgenic model was created by crossing two previously established mouse models. These mice show elevated levels of aberrant B cells in circulation and spontaneously develop lethal lymphomas. Cells from a spontaneous mouse were passaged in WT C57Bl/6 mice to develop the adoptive transfer model, increasing penetrance and shortening time to early removal criteria (ERC). This model showed an immune environment similar to published data on MCL and was found to be resistant to ibrutinib. This model is a novel immunocompetent murine model of aggressive, conventional MCL that can be used for preclinical immunotherapy research.

In total, this work supports the field of MCL research in two ways: 1) development of a novel treatment strategy, using compounds currently in clinical trials, and 2) characterization of novel transgenic murine model that supports all MCL researchers interested in the interaction between the immune system and cancer.

Dedication

I would like to dedicate this work to my parents, Melanie N. Brown and James D. Brown Jr., who inspired a love for all things science.

Acknowledgments

I want to begin by acknowledging the amazing mentorship of Drs Robert Baiocchi and Rosa Lapalombella. They have both provided outstanding guidance as well as real world examples of successful scientists and impeccable human beings. Their support made this work possible in every sense of the word. Many thanks to Drs. Monica Venere and Sameek Roychowdhury for serving on my doctoral committee and bringing insightful discussion to every meeting.

Thank you to my collaborators, especially the faculty of the Lymphoma Research group including Drs. Lapo Alinari, Polina Shindiapina, Walter Hanel, and Wing Chan. Thank you to our collaborators at Prelude Therapeutics, especially Drs. Peggy Scherle and Neha Bhagwat, who provided material and scientific support throughout these studies. Thank you to our collaborators at Weill Cornell Medicine, especially Drs. Jihye Paik and Selina Chen-Kiang. Thank you to Dr. Samir Parekh at Mount Sinai for help with the mouse model.

My lab mates in the Baiocchi became my family over the last six years and I want to acknowledge their scientific and social support that went into this work. Thank you to Drs. Shelby Sloan and Mackenzie Long for their support with ideas, animal related studies, and remembering who is presenting at lab meeting this week. Thank you to Eric Brooks for always knowing how to fix the strange sound and night owl conversations. I want to thank Claire Hinterschied for being the most amazing mentee and co-worker; I couldn't have asked for a better partner in cell culture. Thank you to Alex Prouty, JoBeth Helmig-Mason, Kaylee Harrison, Aneeq Yasin, Archisha Sharma, and Ian Hout for being an

amazing animal team. Thank you to Dr. Jihyun Chung for providing help at the bench from day one. Thanks to Dr. Christoph Weigel for being my sounding board and part-time German tutor. Thanks to Elshafa Ahmed for being my desk mate and always bringing joy to the day. Thanks to Dr. Lynda Villagomez for showing me how much I have learned and hosting the best happy hours. Thanks to Dr. Betsy Pray, Kinnari Sorathia, Shamama Nishat, Ethan Baiocchi, and the rest of the Alinari team for being a joy to share space with.

The other graduate students and members of the Experimental Hematology Laboratory on the fourth floor of Wiseman Hall provided the best support network anyone could ask for. Thank you to Dr. Janani Ravikrishnan for being my in-lab BFF. Thank you to Drs. Matthew Cannon, Libby Muhowski, Janek Walker, Eileen Hu, and Pu Zhang for your friendship and covering me whenever a reagent ran out. Thanks to Dr. Steven Sher for being a one-man hype team. Thank you to Charlene Mao and Matthew Purcell for all the flow cytometry guidance and support.

The Biomedical Sciences Graduate Program (SIB T32) and Pelotonia (Graduate Fellowship) made this work possible through their financial support of my work. Financial support also came from the OSU Graduate School through the Presidential Fellowship. Thank you for the investment and I hope to pay it forward.

This work would not have been possible without the support of my family. My mother Melanie Brown, and father, Jamie Brown, raised me to believe anything was possible and encouraged my interest in science from a very young age. Thanks to my brother, Keegan Brown, for reminding me to unwind and laugh whenever I can. Thank you to my in-laws, the Burkes, for being my cheer squad and for giving me a second home. My

amazing Verlobter Keith Burke needs to be acknowledged and given an award for how infrequently he complained about the late nights and long weekends, the missed dinners and long rants about flow protocols, the parties that turned into impromptu conferences. He supported my every dream and made sure that I got to this point, even when I wasn't sure I would make it.

Vita

1994	Born – Juneau, Alaska, USA
2012	Juneau-Douglas High School YADAA.AT KALÉ, Juneau, Alaska, USA
2016	Bachelor of Science in Bioengineering, Focus in nano and molecular engineering, University of Washington, Seattle, Washington, USA
2017 to present	Graduate Research Associate, Department of Hematology, The Ohio State University

Publications

Brown F, Hwang I, Sloan S, Hinterschied C, Helmig-Mason J, Long M, Chan W K, Prouty A, Chung J, Zhang Y, Youssef Y, Bhagwat N, Chen Z, Chen-Kiang S, Di Liberto M, Elemento O, Sehgal L, Alinari L, Vaddi K, Scherle P, Lapalombella R, Paik J, and Baiocchi R A. PRMT5 Inhibition Drives Therapeutic Vulnerability to Combination Treatment with BCL-2 Inhibition in Mantle Cell Lymphoma. (Under review) February 2023

Sloan S, **Brown F**, Long M, Koirala S, Chung J, Pray B, Villagomez L, Hinterschied C, Helmig-Mason J, Prouty A, Brooks E, Youssef Y, Hanel W, Parekh S, Chan W K, Chen Z, Lapalombella R, Vaddi K, Scherle P, Chen-Kiang S, Di Liberto M, Elemento O, Meydan C, Foox J, Butler D, Mason C E, Baiocchi R A and Alinari L. PRMT5 supports multiple oncogenic pathways in mantle cell lymphoma. (Under review) February 2023

Hing, Z. A., J. S. Walker, E. C. Whipp, L. Brinton, M. Cannon, P. Zhang, S. Sher, C. B. Cempre, **F. Brown**, P. L. Smith, C. Agostinelli, S. A. Pileri, J. N. Skinner, K. Williams, H. Phillips, J. Shaffer, L. P. Beaver, A. Pan, K. Shin, C. T. Gregory, G. H. Ozer, S. A. Yilmaz, B. K. Harrington, A. M. Lehman, L. Yu, V. Coppola, P. Yan, P. Scherle, M. Wang, P. Pitis, C. Xu, K. Vaddi, S. Chen-Kiang, J. Woyach, J. S. Blachly, L. Alinari, Y. Yang, J. C. Byrd, R. A. Baiocchi, B. W. Blaser, and R. Lapalombella. January 2023. "Dysregulation of PRMT5 in chronic lymphocytic leukemia promotes progression with high risk of Richter's transformation." *Nat Commun* 14 (1): 97. <https://doi.org/10.1038/s41467-022-35778-1>.

Sloan, S. L., K. A. Renaldo, M. Long, J. H. Chung, L. E. Courtney, K. Shilo, Y. Youssef, S. Schlotter, **F. Brown**, B. G. Klamer, X. Zhang, A. S. Yilmaz, H. G. Ozer, V. E. Valli, K. Vaddi, P. Scherle, L. Alinari, W. C. Kisseberth, and R. A. Baiocchi. 2021. "Validation of protein arginine methyltransferase 5 (PRMT5) as a candidate therapeutic target in the spontaneous canine model of non-Hodgkin lymphoma." *PLoS One* 16 (5): e0250839. <https://doi.org/10.1371/journal.pone.0250839>.

Field of Study

Biomedical Sciences Graduate Program

Table of Contents

Abstract	ii
Dedication	iv
Acknowledgments.....	v
Vita.....	viii
Table of Contents	x
List of Tables	xiii
List of Figures	xiv
Chapter 1 Introduction	1
1.1 Mantle Cell Lymphoma	1
1.1.a Pathology and Incidence	1
1.1.b Genetic Drivers and Risk Factors	3
1.1.c Staging and MIPI Score	9
1.1.d Current Treatments	13
1.1.e Prognosis and outcomes.....	21
1.2 PRMT5.....	23
1.2.a Protein Structure and Function.....	23
1.2.b PRMT5 in Cancer	28

1.2.c PRMT5 inhibitors.....	30
1.3 BCL-2 Family Proteins.....	35
1.3.a Class and Function.....	35
1.3.b BCL-2 Proteins in Lymphoma.....	39
1.3.c BH3 mimetics.....	40
1.4 Mouse Models.....	43
1.4.a Mouse Models of Lymphomas.....	43
1.4.b Mouse Models of MCL.....	44
Chapter 2: PRMT5 Inhibition Reactivates FOXO1 and Leads to Synthetic Lethality with BCL-2 Inhibitor Venetoclax	47
2.1 Background and Rationale.....	47
2.2 Methods.....	50
2.3 Results.....	53
2.4 Conclusions.....	86
Chapter 3: PRMT5 Inhibitors and BH3 Mimetics for the Treatment of MCL.....	89
3.1 Background and Rationale.....	89
3.2 Methods.....	92
3.3 Results.....	97
3.4 Conclusions.....	119

Chapter 4: E μ -SOX11CCND1 Murine Model of Mantle Cell Lymphoma.....	122
3.1 Background and Rationale.....	122
3.2 Methods.....	124
3.3 Results.....	130
3.4 Conclusion	153
Chapter 5: Discussion and Future Directions	156
PRMT5 inhibition and BH3 mimetics	156
E μ -SOX11CCND1 Model of MCL.....	159
Overview.....	162
Appendix A. Active Clinical Trials with Targeted Therapies	163
Appendix B. Active Clinical Trials with Immunotherapeutic Agents.....	183
Appendix C: Supplemental Table 1 for Chapter 2.....	188
Appendix D: Supplemental Table 2 for Chapter 2	189
Appendix E: Supplementary Materials and Methods for Chapter 2.....	190
Bibliography	163

List of Tables

Table 1-1: Ann Arbor staging of lymphomas.....	10
Table 1-2: Lugano Classification of Lymphoma Stages.....	11
Table 1-3: Current PRMT5 inhibitors in clinical trials or published as tool compounds.	30
Table 1-4: Table of primary BCL-2 Family proteins.....	36
Table 1-5: Table of published transgenic murine models of MCL.....	46
Table 3-1: Table of peptide sequences used for BH3 profiling.....	93
Table 4-1: Table of flow cytometry antibodies used to monitor disease progression in transgenic colony	125
Table 4-2: Table of flow cytometry antibodies used to monitor disease progression in the adoptive transfer model.....	126
Table 4-3: Spectral flow panel with marker, fluorochrome, volume per test and catalog number	127
Table A-1: List of clinical trials open with targeted therapies for NHLs including MCL.	180
Table B-1: Active Clinical Trials using immunotherapeutic agents.....	183
Table C-1: PRT382 and venetoclax doses used in Chapter 2.....	188
Table D-1: CHIP qPCR and qPCR primers used for Chapter 2	189

List of Figures

Figure 1-1: Pie chart of targeted agent clinical trials by target.....	18
Figure 1-2: Pie chart of immunotherapy based active clinical trials	20
Figure 1-3: A diagram of the roles of PRMT5	25
Figure 1-4: Diagram of major BCL-2 family proteins indicating their subclass and binding affinities	37
Figure 1-5: Table of half maximal effective concentration (EC50) of BH3 only peptides binding to anti-apoptotic truncated peptides.....	38
Figure 2-1: PRT382 is a selective and effective inhibitor of PRMT5	61
Figure 2-2: PRT382 dosing provides a survival advantage in <i>in vivo</i> model of MCL	62
Figure 2-3: PRMT5 inhibition disrupts the AKT:FOXO1 interaction and causes FOXO1 nuclearization.....	64
Figure 2-4: ChIP seq of FOXO1 and ChIP qPCR show <i>BAX</i> as a target of FOXO1 and significantly upregulated with PRMT5i.....	66
Figure 2-5: PRMT5 induces increased mRNA levels of multiple pro-apoptotic genes ...	68
Figure 2-6: PRMT5i induces expression of pro-apoptotic BCL-2 family proteins	69
Figure 2-7: Six of nine MCL cell lines show synergistic killing with treatment with PRT382 and BCL-2 inhibitor, venetoclax	71
Figure 2-8: BCL-2 expression coorelates to synergy score observed between PRMT5 and BCL-2 inhibition.....	73
Figure 2-9: Expression of key proteins and correlation of synergy score to p53 status ...	75

Figure 2-10: PRMT5i and BCL-2i combination therapy induces intrinsic apoptotsis within 48 hours of treatment	76
Figure 2-11: PRMT5i and BCL-2i synergy is dependent on BAX expression	78
Figure 2-12: PRT543 is synergistic with venetoclax in Granta-519 CDX model of MCL	80
Figure 2-13: PRT382 and venetoclax are synergistic in the PDX.AA model of MCL	82
Figure 2-14: PRT382 and venetoclax are synergistic in the PDX.IR.96069 model of MCL	84
Figure 3-1: BH3 profiling reveals varied response to mitochondrial insult across MCL cell lines	104
Figure 3-2: PRMT5 inhibition reduces mitochondria function and shifts response to mitochondrial insult	106
Figure 3-3: PRMT5 inhibition upregulates pro-apoptotic transcriptional profiles.....	107
Figure 3-4: PRMT5 inhibition upregulates the expression of pro-apoptotic activator and sensitizers in MCL cell lines.....	108
Figure 3-5: PRMT5 inhibition increases expression of anti-apoptotic BCL-2 family proteins.....	110
Figure 3-6: IC50s of navitoclax, A852, and PRT1419 for MCL cell lines	111
Figure 3-7: PRT382 and BH3 mimetics synergize in MCL cell lines.....	112
Figure 3-8: iBH3 profiling of PDX and primary MCL cells	114
Figure 3-9: PRT808 and navitoclax are synergistic <i>in vivo</i>	115

Figure 3-10: Platelet count for PRT808 and navitoclax combination treatment <i>in vivo</i> experiment.....	116
Figure 3-11: H&E of PRT808 and navitoclax combination <i>in vivo</i> experiment	117
Figure 4-1: Construct of E μ -SOX11CCND1 and survival of single and double transgenic colonies	138
Figure 4-2: Flow cytometry plots of WT, E μ -SOX11, E μ -CCND1 and E μ -SOX11CCND1 showing percentage of CD5+/CD19+ cells	139
Figure 4-3: Expansion of CD5+/CD19+ cells in the E μ -SOX11CCND1 model	140
Figure 4-4: Effects of sex and age on lymphomagenesis	141
Figure 4-5: Creation and immune profiling of the adoptive transfer E μ -SOX11CCND1 model.....	142
Figure 4-6: H&E of a WT C57Bl/6 mouse and an adoptive transfer E μ -SOX11CCND1 at ERC.....	144
Figure 4-7: Systemic and subcutaneous E μ -SOX11CCND1 adoptive transfer model survival and immune environment.....	145
Figure 4-8: Immune analysis of blood, spleen, and tumor for a subcutaneously engrafted E μ -SOX11CCND1 mouse	146
Figure 4-9: PD1 and PD-L1 expression in splenocytes of a subcutaneously engrafted E μ -SOX11CCND1 mouse	148
Figure 4-10: Survival curves of ibrutinib and venetoclax in systemically engrafted E μ -SOX11CCND1 mice.....	149
Figure 4-11: PRMT5 inhibition in the E μ -SOX11CCND1 adoptive transfer model	150

Figure 4-12: CAR T therapy in the E μ -SOX11CCND1 adoptive transfer model 151

Chapter 1 Introduction

1.1 Mantle Cell Lymphoma

1.1.a Pathology and Incidence

Mantle cell lymphoma (MCL) is a CD5+/CD19+ B cell non-Hodgkin Lymphoma (NHL), defined by the t(11;14)(q13;q32) translocation juxtaposing the *CCND1* gene downstream of the immunoglobulin heavy locus (*IgH*) promoter. This promoter is constitutively active in mature B cells, resulting in the overexpression of Cyclin D1. Fluorescence *in situ* hybridization (FISH) of this canonical translocation is used to distinguish this cancer from other mature B cell lymphomas [1] which is present in 97% of MCL cells [2]. The average age of MCL patients at diagnosis is 68-71 years old with the majority of cases being of males (3:1) [3, 4]. This disease is significantly enriched in non-Hispanic white populations compared to black (2.8:1), Hispanic (1.4:1), and Asian and Pacific Islander (2.9:1) patients [3]. MCL comprises up to 6% of NHL cases diagnosed annually [5] or about 3320 new cases in the United States each year as of 2016 [3]. The incidence of MCL has been increasing in the United States with the rate per 100,000 doubling from 0.34 to 0.79 from 1992 to 2009 [6]. Patients commonly present with palpable lymphadenopathy, with 30% also presenting “B symptoms” referring to fever, night sweats, and unexplained rapid weight loss [1, 7]. Other symptoms include physical discomfort due to splenomegaly or other organ involvement, and abnormal blood counts due to bone marrow involvement [1].

There are two major presentations of MCL; classical, which includes blastoid and pleomorphic histologies, and leukemic non-nodal [8]. Conventional MCL (cMCL) arises from mature B cells that have not entered the germinal center, carry few to none *IgH* variable region (*IgHV*) mutations, and express the transcription factor Sry-Box Transcription Factor 11 (*SOX11*) [9]. cMCL constitutes 80-90% of MCL cases diagnosed [10]. These cases tend to be aggressive and require rapid treatment. In contrast, non-nodal MCL (nnMCL) is commonly an indolent disease arising from B cells that have undergone germinal center education, *IgHV* somatic hypermutation, and express minimal *SOX11*. These patients are often able to undergo a “watch and wait” treatment plan [11].

Histologically, cells are small to medium sized and monomorphic, excluding the pleomorphic variant [7, 12]. Neoplastic cells have little cytoplasm, clumped chromatin, and prominent nuclear clefts [7]. Besides high levels of Cyclin D1 and SOX11, they will also express CD19, CD20, CD22, and CD79a [1]. They are typically negative for B cell Lymphoma 6 (BCL-6), CD10, and CD23. Their CD23 status helps differentiate this disease from another mature B cell lymphoma, chronic lymphocytic leukemia (CLL). MCL cells are typically clonal, resulting in a large expansion of kappa or lambda light chain positive B cells. Malignant cells are most commonly found in the lymphatic system and related organs including lymph nodes, bone marrow, spleen, liver, and circulating in the peripheral blood. Extranodal sites can include gastrointestinal tract, lungs, pleura, skin, and central nervous system. Diagnosis is performed through a tissue biopsy with analysis for aberrantly expanded B cells expressing high levels of cyclin D1 and/or SOX11 [1]. Additional diagnostic tests may include complete blood counts (CBCs), measurement of

serum lactate dehydrogenase (LDH) and beta-2 microglobulin, a bone marrow biopsy, and a Computerized Tomography (CT), Positron Emission Tomography (PET), or PET/CT scan [1].

1.1.b Genetic Drivers and Risk Factors

CCND1

Among the genetic players in MCL, *CCND1* and *SOX11* are the most ubiquitous. As previously stated, the t(11;14)(q13;q32) translocation key to MCL causes overexpression of the *CCND1* gene and its gene product Cyclin D1. This rearrangement attaches the *IgH* regulatory elements to the *CCND1* promoter and gene body. RNA polymerase II is then recruited to the regulatory element and the open gene body is transcribed [13]. It is of note that the hypomethylated and hyperacetylated status of the *CCND1* promoter is also observed in normal B cells. While normal B cells express only cyclin D2 and cyclin D3, this suggests that the activating regulatory element is essential and sufficient to induce Cyclin D1 overexpression in B cells [13, 14].

There are rare cases of *CCND1* negative MCL in which *CCND2* or *CCND3* is commonly overexpressed [15]. While each of these cyclins are typically cell type specific, there are studies showing the ability for one cyclin to compensate for the loss of another [16, 17]. These proteins are key in controlling cell cycle through protein and transcriptional level control. On the protein level, Cyclin D1 binds to Cyclin Dependent Kinase 4 (CDK4) or Cyclin Dependent Kinase 6 (CDK6), activating them to phosphorylate retinoblastoma protein (pRB). A secondary set of phosphorylation by Cyclin E/Cyclin Dependent Kinase 2

(CDK2) halts pRB's cell cycle inhibiting functions, promoting progression through G1-S phase. Cyclin D1 also plays a role in hormonal response at the nucleus, binding androgen receptors, estrogen receptors, and thyroid receptors [18]. Both basal and ligand induced transactivation were found to be under the control of Cyclin D1 [18]. Inside the nucleus, this protein also represses Signal Transducer and Activator of Transcription 3 (STAT3) transcription factors, and epigenetic modifiers including histone acetyltransferases (HATs), histone deacetylases (HDACs) and p300 independent of CDK4 [18]. The presence of Cyclin D1 in the cytoplasm has been associated with higher levels of migration and invasiveness, seen more often in the blastoid variant of MCL [19]. Interestingly, despite the significance of *CCND1* to MCL diagnosis, and the evidence in numerous cancers of oncogenic function [18], overexpression of *CCND1* alone does not induce lymphomagenesis in murine models of MCL [20, 21]. This finding correlates with the observation from Lecluse et al. that 7% of their healthy individuals had circulating B cells with the t(11;14) break but no apparent adverse effects over the course of many years [22].

SOX11

A second key gene in MCL biology is *SOX11*, which is highly expressed in the majority of MCL cases but not in normal mature lymphocytes [23, 24]. *SOX11* expression is also specific to MCL, among other B cell malignancies [23, 24]. This predominantly fetal transcription factor is part of a family of 20 *SOX* genes which influence transcription. They are essential in regulating stemness and terminal differentiation of many cell

types [25]. SOX11 has been shown to induce conformation changes in the DNA, facilitating the action of other transcriptional complexes and potentially acting as a pioneer factor [26]. SOX11 may contribute to MCL pathogenesis by activating paired box 5 (PAX5), a protein key to B cell development, that blocks terminal B cell differentiation, maintaining a more plastic phenotype [27]. Another potential mechanism is SOX11 amplification of the WNT canonical signaling pathway [28], a known player in MCL tumorigenesis [29, 30]. Kuo et al. demonstrated the oncogenic function of SOX11 in their E μ -SOX11-EGFP mouse model [31]. This B cell specific overexpression of SOX11 resulted in aberrant B cell expansion with an MCL-like phenotype [31]. One mechanistic effect of SOX11 overexpression was a hyperactivation of B cell receptor (BCR) signaling which could be counteracted with the bruton's tyrosin kinase (BTK) inhibitor, ibrutinib [31].

Secondary Hits

Due to the observation that Cyclin D1 overexpression does not cause MCL, a second hit hypothesis has been proposed. Clear candidates for the two hits has been difficult to identify due to the high mutational burden and large inter-tumor heterogeneity of MCL [9, 32-34]. This variation is more pronounced in cMCL, which more closely resembles naïve B cells, including their methylation status, and tendency toward chromosomal instability [35-37]. The continued addition of oncogenic events results in over 90% of MCL cases displaying highly altered genomes [35, 38]. There are several major groups of genes for which secondary hits belong, including DNA damage (Ataxia Telangiectasia Mutated [*ATM*], Tumor Protein 53 [*TP53*]), CDK kinase regulators

(*CCND1*, cyclin-dependent kinase inhibitor 2A [*CDKN2A*]), and epigenetic modifications (Histone-lysine N-methyltransferase 2D [*KMT2D*], BCL-6 corepressor [*BCOR*]). The most common are discussed below.

Among the secondary hits observed in MCL, mutations in *ATM* are the most common, with Hill et al. finding 43.5% of cases mutated in their meta study [32, 39]. This percentage increases with disease progression to 57.6% [32]. This mutation is also enriched in MCL compared to other lymphomas [37, 40]. *ATM* functions as a DNA damage repair checkpoint, regulating many proteins including Tumor Protein 53 (p53), Breast Cancer gene 1 (BRCA1), and Checkpoint Kinase 2 (CHK2) [41]. Mutated or deleted *ATM* correlates with a high number of chromosomal alterations but not with a differential survival statistic [39].

Tumor Protein 53 (*TP53*) is another key gene in the DNA damage response commonly mutated in MCL. *TP53*, the gene for p53, is called the “guardian of the genome” for its ability to halt cell cycle progression when DNA damage occurs. Beyond simple inactivation, mutations in *TP53* have been shown to support the growth and proliferation of cancer cells [42]. Hill et al. found *TP53* to be mutated in about a quarter of all MCL cases as baseline (26.8%) [32]. Similarly to *ATM*, the percentage of mutated *TP53* increases to 43.0% of cases with disease progression. Mutated *TP53* is associated with cMCL and is a negative prognostic factor [43, 44].

RB Transcriptional Corepressor 1 (*RBI*), whose gene product pRB was discussed previously as a binding partner to the Cyclin D1/CDK4/6 complex, also prevents cell cycle progression through the binding and inactivation of E2F proteins. This gene was also found

to be mutated in about a quarter of all MCL cases at baseline (24.3%) but showed no increase with disease progression [32]. Mutations to this gene likely synergize with overexpressed *CCND1* to further activate the E2F proteins.

c-myc, an oncogene that controls almost 15% of all cell growth regulating genes, was found to be mutated at a high frequency at diagnosis but not enriched after disease progression (20.6%, 11.2%) [32]. This mutational status could play a role in prognosis as well as predicting response to the BTK inhibitor, ibrutinib [45, 46].

Deletion of *CDKN2A* results in the loss of multiple proteins, including p16 (INK4A) and p14 (ARF). p16 binds to CDK4 and CDK6 and prevents cell cycle progression while p14 binds and stabilizes p53. Deletion of this gene is enriched in aggressive cases of MCL and leads to poorer outcomes [43, 47, 48]. p16 knockout mice develop spontaneous lymphomas supporting the importance of this gene to tumorigenesis [49].

Epigenetics

Epigenetics, the change in gene expression due to factors other than the nucleic acid sequence, is another key driver of MCL. Techniques such as Chromatin Immunoprecipitation sequencing (ChIP seq), Assay for Transposase-Accessible Chromatin with high throughput sequencing (ATAC seq) or bisulfite sequencing provide information about what regions of the genome are open vs. closed, promoted vs. repressed, and associated with one another. A DNA methylation study from Quierós et al. showed that the methylome of MCL samples could be used to identify two clusters, one more

closely resembling germinal center inexperienced B cells and the second germinal center educated, more differentiated cells [50]. Cluster one was also identified to be globally hypomethylated when compared to naïve B cells, a proposed cell of origin, suggesting greater promotion of numerous genes [50]. Overall, MCL genomes are significantly hypomethylated compared to healthy samples; however, similarly to genetic profiles in MCL, epigenetic profiles have a high level of inter-sample variability [50, 51]. These epigenetic changes from normal B cells have been associated with the expression of key oncogenes, including *CCND1* from the *IgH* juxtaposition and actions on non-translocated alleles [52], *SOX11* from novel enhancer association [50], and *CDKN2B* through hypermethylation of its promoter [51].

Environmental and Hereditary Risk Factors

The risk factors for MCL are not well defined due to the relatively small number of cases, and limited studies on MCL specifically. Grouped NHL studies have implicated factors such as BMI, smoking, and alcohol intake, though these factors have not been validated in MCL-specific studies [53, 54]. This is similarly true for factors such as immune suppression and viral infections (Epstein Barr Virus, T cell leukemia/lymphoma virus, Hepatitis B virus etc.). A common factor with other NHLs is family history; a hematological malignancy among first-degree relatives is associated with a 2 to 2.3-fold increased risk in developing MCL [54, 55]. Whether this is due to a genetic predisposition, shared environmental exposures, or a combination is not known. Interestingly, Smedby et al. reports a negative association with a history of hay fever (OR = 0.63, 95%

CI = 0.48 to 0.82) [54]. With the addition of genetic sequencing to diagnostic panels and access to larger data sets, these factors should become more defined in the future.

1.1.c Staging and MIPI Score

Ann Arbor

Staging of MCL was historically done using the Ann Arbor Staging System, a system also used for other non-Hodgkin lymphomas and originally designed for use with Hodgkin lymphomas (**Table 1**) [56, 57]. Stage I is defined by the presence of disease in a single lymphatic site or localized extranodal site. Stage II is diagnosed when the disease has spread to two or more lymph node regions on the same side of the diaphragm or one lymph node region and one site or organ outside of the lymphatic system. Stage III and IV are the most common diagnoses of MCL, making up >80% of initial diagnoses. These stages are recognized when the disease has spread to lymph node regions on opposite sides of the diaphragm or spread to distal sites in extra lymphatic tissues respectively. Added to the numeric staging are additional classifications: A – No symptoms, B – Fever, drenching night sweats, unexplained loss of >10% of body weight within the preceding six months, E – Involvement of a single extranodal site that is contiguous of proximal to the known nodal site (for stages I-III), X – Bulky disease, and S – Splenic involvement [57].

Stage	Description
I	Involvement of a single lymphatic site (i.e., nodal region, Waldeyer's ring, thymus, or spleen) (I); or localized involvement of a single extralymphatic organ or site in the absence of any lymph node involvement (IE).
II	Involvement of two or more lymph node regions on the same side of the diaphragm (II); or localized involvement of a single extralymphatic organ or site in association with regional lymph node involvement with or without involvement of other lymph node regions on the same side of the diaphragm (IIE).
III	Involvement of lymph node regions on both sides of the diaphragm (III), which also may be accompanied by extralymphatic extension in association with adjacent lymph node involvement (IIIE) or by involvement of the spleen (IIIS) or both (IIIE,S).
IV	Diffuse or disseminated involvement of one or more extralymphatic organs, with or without associated lymph node involvement; or isolated extralymphatic organ involvement in the absence of adjacent regional lymph node involvement, but in conjunction with disease in distant site(s). Stage IV includes any involvement of the liver or bone marrow, lungs (other than by direct extension from another site), or cerebrospinal fluid.

Table 1-1: Ann Arbor staging of lymphomas

Details for each stage of MCL as developed by Carbone et al. and updated by Lister et al.

Reproduced from PDQ Cancer Information Summaries [58]

Lugano

In response to updated imaging modalities, the Lugano classification system was published by Cheson et al. in 2014 (**Table 2**) [59]. This classification system includes guidelines regarding FDG-PET and PET/CT imaging which are more sensitive and specific than previous methods of CT scanning and gallium scanning [60]. While the Ann Arbor system was designed to direct radiation therapy whereas Lugano takes into account

additional factors to classify patients with the variety of treatment options available today. Lugano has two main categories, limited (I/II) or advanced disease (III/IV) with stage II with bulky disease falling into either category depending on additional risk factors. The designation of A (no B symptoms) or B (B symptoms present) was removed as these criteria has no prognostic value and does not change the course of treatment in the majority of cases. The designation of X for bulky disease was also removed in favor of the greatest diameter of the largest mass.

Stage	Involvement	Extranodal Status
I	One node or a group of adjacent nodes	Single extranodal lesions without nodal involvement
II	Two or more nodal groups on the same side of the diaphragm	Stage I or II by nodal extent with limited contiguous extranodal involvement
*II B	II as above with “bulky” disease	N/A
III	Nodes on both sides of the diaphragm; nodes above the diaphragm with spleen involvement	N/A
IV	Additional noncontiguous extralymphatic involvement	N/A

Table 1-2: Lugano Classification of Lymphoma Stages

Table of Lugano classification details for the staging of lymphomas. Stage I and II are considered limited while stages III and IV are considered advanced. Stage II B could fall into either category depending on histology and other prognostic factors. Reproduced from Cheson et al. [59].

MIPI

While useful in describing the extent of disease and directing treatments, neither staging system provides prognostic value on their own [62]. In order to provide a prognosis, clinicians use the MCL International Prognostic Index (MIPI) [62]. First published by Hoster et al. in 2008, this index uses age, performance status, (LDH) level, and leukocyte count to classify patients as low risk (LR), intermediate risk (IR), or high risk (HR) [62]. Immunohistochemical staining of marker of proliferation Ki-67 (AKA KI-67) identifies the relative number of cells with strong nuclear signal, which is associated with proliferation. This signal has been shown to be an independent risk factor and can be included in this score (MIPI-c or MIPI-b) marginal improvement (R coefficient 0.9554, $P < 0.001$) [62]. For ease of use, there is also the simplified MIPI score, which uses points from 0 to 3 for each of the four metrics and sums them for a score between 0 and 11 [62].

There is potential for additional improvements on prognostic ability by taking into consideration factors such as *TP53* expression, time to disease progression, cytology, and the presence of minimal residual disease [63, 64]. One such effort by Clot et al. used a gene expression assay to distinguish between cMCL and nnMCL, which showed significant prognostic value [44]. They also determined that survival plotted by *TP53* status or copy number alternation provided similarly significant prognostic value, suggesting that oncogenic drivers may provide a more valuable prognosis than disease subclass [44]. Factors such as CNS involvement [7] also lend a poor prognosis. Some factors that do not provide prognostic value include, sex, Ann Arbor (Stage III vs. Stage IV), bone marrow

involvement, number of extranodal sites, number of nodal sites involved and albumin level [53].

1.1.d Current Treatments

Wait and Watch

The course of treatment for MCL varies based on aggressiveness of the disease, effect of previous treatments, and fitness of the patient. In some cases of nmMCL, treatment is often stalled for months or even years with limited repercussions [11, 61-64]. This option is appropriate in cases where the disease shows positive prognostic markers such as Ki-67 staining less than 30%, a maximum tumor diameter of less than 3cm, normal serum LDH levels, normal Beta-2 microglobulin levels, no B symptoms, and a non-blastoid histology [1, 63]. A wild type *TP53* gene and low MIPI score also support the “watch and wait” approach [1].

Frontline therapy

For newly diagnosed patients who require treatment, an induction phase is completed first. For fit patients who are autologous stem cell transplant eligible, a regimen of cytarabine, a DNA damaging agent, in addition to rituximab, an anti-CD20 antibody, is used to clear the bulk of the disease [63]. Older or less fit patients are typically given bendamustine, an alkylating agent, and rituximab [63]. Between 2011 and 2021, this was the most common front line therapy with 42% of new diagnosed MCL patients receiving this combination [69]. Multidrug regimens such as R-CHOP (rituximab/cyclophosphamide/doxorubicin/vincristine/prednisone), R-DHAP

(rituximab/dexamethasone/cytarabine/platinum) and VR-CAP (bortezomib/rituximab/cyclophosphamide/doxorubicin/prednisone) are also commonly used [63, 70]. These combine immunotherapy (rituximab) DNA damaging agents (cyclophosphamide, doxorubicin, cytarabine, platinum), proliferation preventing agents (vincristine) and/or proteasome inhibitors (bortezomib). Steroids such as prednisone or dexamethasone are added to reduce inflammation and manage side effects. There are several more variations on these combinations in phase 2 and phase 3 trials, including the non-chemotherapeutic option of rituximab and lenalidomide, an immunomodulatory agent [9, 71]. All of these induction protocols result in systemic dosing of chemotherapeutics, resulting in high frequencies of adverse events (AEs) and increased morbidity. Targeted therapies currently used as second line therapies, such as BTK inhibitors or the BCL-2 inhibitor venetoclax, are being explored as front-line agents with promising results [69, 72].

Stem Cell Transplant

The only potentially curative treatment available to MCL patients is autologous or allogenic stem cell transplant (ASCT) [7]. This involves collecting healthy hematopoietic stem cells from the blood or bone marrow, using high dose chemotherapy to attempt to eliminate all remaining cancer cells, and finally, replacing the immune system by reintroducing the collected stem cells. This process is physically difficult, with a wide range of side effects due to chemotherapy (nausea, fatigue, changes in taste or smell, problems sleeping) as well as long term deficits in immune response to infection [65]. The

high dose chemotherapy can act as a carcinogen resulting in secondary cancers or post-transplant lymphoproliferative disorder (PTLD) [66]. Allogenic stem cell transplant carries the extra risk of graft vs host disease where the donor stem cells create an immune system that sees the host as foreign and attacks [65].

Due to these limitations, even among younger fit patients (<65 years of age), only a quarter of patients will undergo this therapy [67]. Taking into consideration all cases this percentage makes up only about 10% of diagnoses [67]. Autologous transplant is recommended after initial consolidation, but allogenic transplant is an option for fit patients with relapsed or refractory (R/R) MCL [68]. The benefits of ASCT are not clear. Martin et al. found that ASCT recipients had no significant difference in time to next treatment or overall survival [67]. This was also described in the meta study by Liu et al. where ASCT provided a PFS advantage (HR 0.74 [0.47, 0.87]) but a very limited OS advantage (HR 0.77 [0.65, 0.92]) [69]. This is contrary to what Kumar et al. found where ASCT doubled the median OS (71.1 vs 158.5 months) [64]. Because multiple factors including fitness of patient, number of previous treatments, and the effect of high dose chemotherapy are difficult to differentiate from the effect of ASCT, additional work is needed to determine the true benefit of ASCT.

BTK Inhibitors

Currently there are four targeted therapies approved for the treatment of MCL though only for cases of R/R MCL [78]. They are all bcr-tl tyrosine kinase inhibitors (ibrutinib, acalabrutinib, zanubrutinib, pirtobrutinib) and were approved for use between

2013 and 2023. These compounds block the activation of BTK, a kinase vital to the BCR signaling pathway, by covalently binding to cysteine 481, and causing cell death [79]. Ibrutinib also binds BMX Non-Receptor Tyrosine Kinase (BMX), IL2 Inducible T Cell Kinase (ITK), and Epidermal Growth Factor Receptor (EGFR) among others at low nanomolar concentrations [79]. Acalabrutinib shows significant improvement over ibrutinib in this regard, showing a three times greater inhibition of BTK compared to the next binding target [79]. Beyond the four compounds that have been approved by the FDA, there are at least three additional compounds with active clinical trials (NCT04830137, NCT01479842, NCT03162536).

These inhibitors have been used to great success in another mature B cell lymphoma, chronic lymphocytic leukemia (CLL) [80] leading to their investigation in MCL. As ibrutinib was approved first, the most data have been collected on this agent. Single agent ibrutinib was able to achieve an overall response rate (ORR) of 66% in a pooled cohort of the PCYC-1104-CA, MCL2001, and MCL3001 clinical trials [81]. OS still remained at 25 months and similar to other studies, having relapsed on more than one line of therapy was a negative prognostic marker [81]. Response to ibrutinib, having stable disease (SD), a partial response (PR), or a complete response (CR) also significantly impacted prognosis of PFS (4 months, 17 months, not reached) and OS (10 months, 25 months, not reached) [81]. Acalabrutinib was able to improve these numbers with an ORR of 81% and a CR rate of 43%. Pirtobrutinib showed similar ORR during the BRUIN phase I/II study with the advantage of showing robust response in BTKi pre-treated MCL [82].

These responses are tempered with the fact that 25% or more of patients will discontinue due to toxicities [70]. In a study performed by Sharman et al., over four years of monitoring, ibrutinib dosing was discontinued in 84% of their population with progression of disease and toxicity being the two dominant reasons [71]. BTK inhibitors have improved the prognosis and treatment options for MCL patients but as a single agent, they are not curative nor applicable in all cases.

Novel Targeted Agents

During the course of treatment of MCL the requirement for second, third, or more lines of treatment leads to a poorer prognosis. While the average OS for patients on their first line of therapy is 116.3 months, their second line reduces that to 41.1 months, their third to 25.2 months and it continues to worsen from there [68]. These statistics show the urgent need for additional treatment strategies that produce robust and long-lasting results.

At the time of writing, there are over 400 active clinical trials for non-Hodgkin lymphoma and over 100 active trials for R/R MCL registered on clinicaltrials.gov, showing the breadth of options for further lines of treatment. Novel targeted therapies for MCL make up 86 of these trials (**Appendix A, Figure 1-1**) and range in targets from signaling pathways to epigenetic regulators.

BCL-2 inhibitors make the largest share of targeted agent trials with a single inhibitor, venetoclax, being included in 11 active trials. This interest is driven by the approval of venetoclax for the treatment of another mature B cell lymphoma, CLL [84]; the strong safety profile, and promising early results [85]. Following the success of BTK

inhibitors, they are currently the second most investigated target among clinical trials, commonly used in multidrug regimens or in combination with a second novel agent. Other trends include targeting the PI3K/AKT pathway, epigenetic enzymes, and cell cycle regulators.

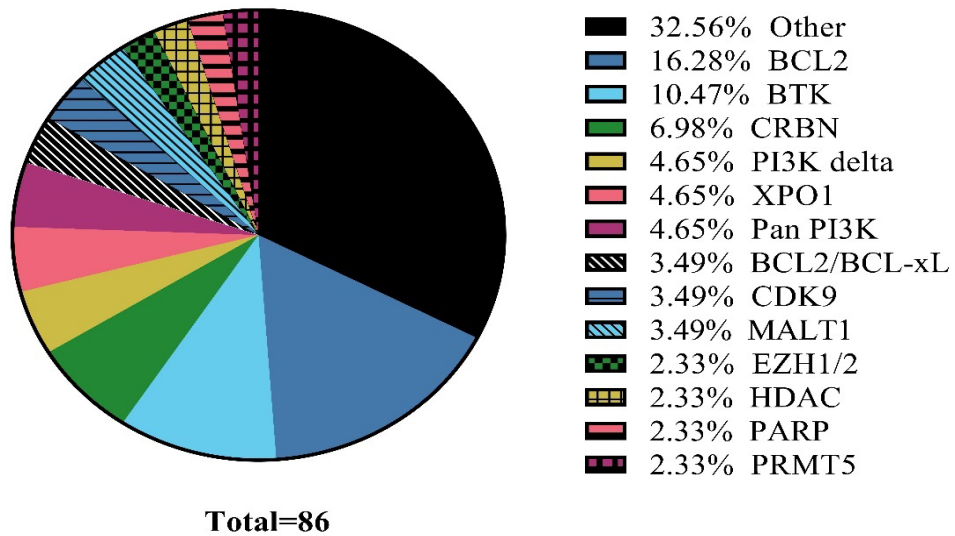


Figure 1-1: Pie chart of targeted agent clinical trials by target.

Biologics and Immunotherapy

Immunotherapy has a long history in MCL with the first antibody, rituximab, being approved by the FDA for use in R/R NHLs in 1997 [72]. This anti-CD20 antibody is one of the most common treatments for MCL patients with over 50% of patients receiving rituximab-containing regimens for their first line of therapy, and an additional 30% of patients receiving it for their second line [73]. Post consolidation or ASCT, 65% and 35% of patients, respectively, received rituximab maintenance therapy [73]. This work has been

expanded to additional anti-CD20 antibodies, as well as other disease targeting antibodies such as anti-CD19, and anti-CD79b (**Appendix B, Figure 1-2**). Antibodies are also being tested to block immunosuppressive marks such as PD-1, PD-L1, and TGIT. Bi- and tri-specific antibodies that physically connect T cells with lymphoma cells make up over 20% of the current trials.

Cellular based therapies are also under investigation. Chimeric antigen receptor (CAR) cells are genetically modified T or NK cells with high affinity for a lymphoma antigen such as CD19 or CD20. These cells can be made from the patient's cells (autologous) or from another source (allogenic). Autologous CAR cells have the advantage of a low risk of rejection as the antigens match perfectly. However, this technique takes time to harvest cells, modify them, expand them, and transfuse them back into the patient as well as requiring the patient to have a sufficient number of cells to harvest. Allogenic techniques hope to speed up this process by providing "off the shelf" options with major antigen matching.

The anti-CD19 CAR T cell product, brexucabtagene autoleucel, was the first CAR cell therapy approved for R/R MCL in 2020 [74]. This approval was based on the results of the ZUMA2 trial, where R/R MCL patients having previously received BKT inhibitors were given a single infusion of brexucabtagene autoleucel. The ORR was 85% with 12.3 months of observation [88], later updated to 91% with 35.6 months of follow up [89]. The CR of 68% was very encouraging though the median duration of response of 28.2 months showed this treatment is not curative. This avenue continues to be explored with almost 20% of all immunological trials using an experimental anti-CD19 CAR T cell

product. Targets are also expanding to CD20 as well as multiple target CAR T cells such as anti-CD19/CD20 or the anti-CD19/CD20/CD22 trispecific product being tested at The Ohio State University (NCT05418088).

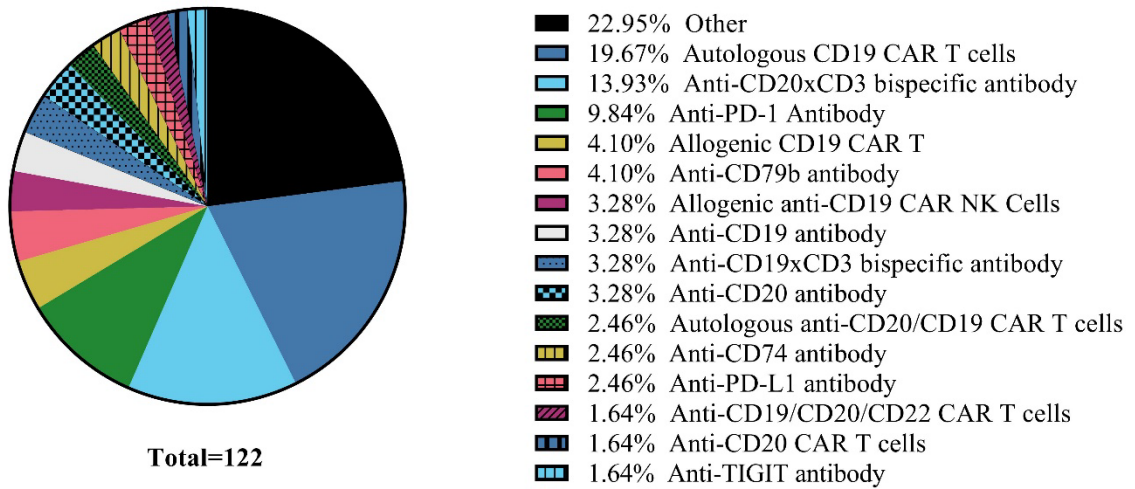


Figure 1-2: Pie chart of immunotherapy based active clinical trials

CAR NK are being tested as a promising allogenic option with reductions in AEs associated with CAR T cells (cytokine storm, immune effect cell-associated neurotoxicity syndrome [ICANS]) [75]. These cells can be produced from multiple sources including cord blood, induced pluripotent stem cells, or immortalized cell lines [75]. While CD19 is the only target being explored [75] (**Appendix B**), we will likely see NK products targeting additional oncogenic targets in the near future.

Other Approaches

Additional approaches include CLR131, a conjugated radioisotope to a phospholipid ether. This treatment works with the theory that cancer cells have a higher

level of lipid rafts in their cell membrane and will therefore incorporate more phospholipid drug conjugate than healthy cells [76]. Betalutin uses a similar concept, where the anti-CD37 murine antibody, lilotomab, is conjugated to p-SCN-Bn-DOTA (satetraxetan), which chelates the beta-emitting isotope lutetium-177 [77]. This concept is being tested in phase 1 clinical trials (NCT02952508, NCT01796171).

Another approach has been to introduce biologically active immune cells such as AB-101 or GDA-201 which are non-genetically modified ADCC enhanced NK cells [78, 79]. This treatment hopes to restore a functioning innate immune response to a cancer by using allogenic NK cells in concert with a secondary biologic [78]. The Mayo clinic is using the same theory to support their clinical trial combining the anti-PD1 antibody pembrolizumab and cryosurgery with autologous dendritic cell therapy that have been educated against the patient's cancer (NCT03035331).

1.1.e Prognosis and outcomes

Front line therapies currently have a median PFS ranging from 16.6 months with R-CHOP to 109.2 months with R-CHOP with rituximab, dexamethasone, cytarabine, and platinum followed by ACST [67]. This wide range is due to multiple factors including late median age of diagnosis, where aggressive chemotherapy and stem cell transplantation are often not realistic options due to the genetic and molecular heterogeneity of MCL, and resistance to standard immuno-chemotherapy regimens [80]. As mentioned previously, each line of therapy correlates to a poorer prognosis, as each relapse or non-response indicates a more aggressive disease [64]. The current average OS of patients with MCL is

approximately 5-6 years [81, 82] and for patients who progress on ibrutinib, survival remains at a dismal 3-8 months [82, 83]. Newer options in the immunotherapy space are encouraging, showing utility in heavily pre-treated cases and high levels of ORR but have failed to be curative [84]. Short of salvage immuno-chemotherapy followed by a stem cell transplant, relapse is virtually universal and for the most part, MCL is considered incurable [85].

1.2 PRMT5

1.2.a Protein Structure and Function

Protein Arginine Methyltransferase 5 (PRMT5) is one enzyme in the PRMT family. The first of this family, PRMT1, was identified in 1996 by Lin et al. using yeast and mammalian cell lines [86]. These proteins are highly conserved with homologs found in humans, yeast, and even rice plants [87, 88]. There are currently nine members of this family identified, where each protein shares the ability to transfer a methyl group to an arginine amino acid. Type 1 PRMTs (PRMT1, PRMT2, PRMT3, PRMT4, PRMT6, and PRMT8) catalyze two sequential methylations resulting in an asymmetric dimethylation of arginine (ADMA). Type 2 PRMTs (PRMT5, PRMT9) transfer two methyl groups in a symmetric dimethylation (SDMA), while the sole type 3 PRMT (PRMT7) is only able to transfer a single methyl group resulting a mono-methylation (MMA) [89]. This family utilizes the methyl donor S-adenosyl-L-methionine (SAM) to transfer the methyl group onto the target arginine. The enzymes of each type are not equally responsible to the formation of methylation; PRMT1 is responsible for the majority of ADMA [90] while PRMT5 is responsible for the majority of SDMA [91, 92].

PRMT5 was originally described as a binding partner of Jak2 in a yeast screen performed by Pollack et al. in 1999 [93]. It was added to the PRMT family and renamed to PRMT5 after Rho et al. identified its methyltransferase abilities [94]. They also identified that PRMT5 complexes, describing dimer and tetramer structures [94]. Crystallization has revealed that PRMT5 forms a dimer with the cofactor methylosome protein 50 (MEP50)

and these dimers homo-oligomerize to tetramers [95]. This complex is able to interact with many different proteins including histones; transcription factors such as p53 and E2F1; signaling receptors such as EGFR; and spliceosome proteins [88, 96].

While the PRMT family performs similar enzymatic roles, they are not redundant in many cases [97]. This is true of PRMT5 and PRMT9, where PRMT9 has a high specificity for an amino acid sequence only present in one protein (SF3B2) [92], whereas PRMT5 is considered a promiscuous protein as it binds over 100 different proteins [98, 99]. There are also differential expressions based on tissue type and stage of development. PRMT5 is essential for fetal development as PRMT5 knock out embryos are not viable [100]. The essential enzymatic effects are cytosolic and are required for the proliferation of embryonic stem cells [101]. According to the Human Protein Atlas, PRMT5 can be found highly expressed in adult tissues including the brain, reproductive organs, and lower digestive tract as well as lower expression in lymphatic systems and upper digestive tract [102, 103]; however, these results should be further validated, as no expression was detected in the bone marrow [103], despite evidence that PRMT5 is essential for the maintenance of hematopoietic stem cells [104]. PRMT5 expression is essential for the maturation and development of lymphocytes including B cell development and germinal center reactions [105] as well T cell proliferation [106, 107]. T cell differentiation and response is also influenced by PRMT5 expression, though the science is not settled with CD8⁺ T cell response reported as decreased or not effected by PRMT5 inhibitors [107, 108].

The cellular functions of PRMT5 are diverse, ranging from transcriptional regulation to cell cycle control. The methylation marks on histones are a classic example of epigenetic regulation where SDMA on some arginine residues (H2aR3, H4R3, H3R8)

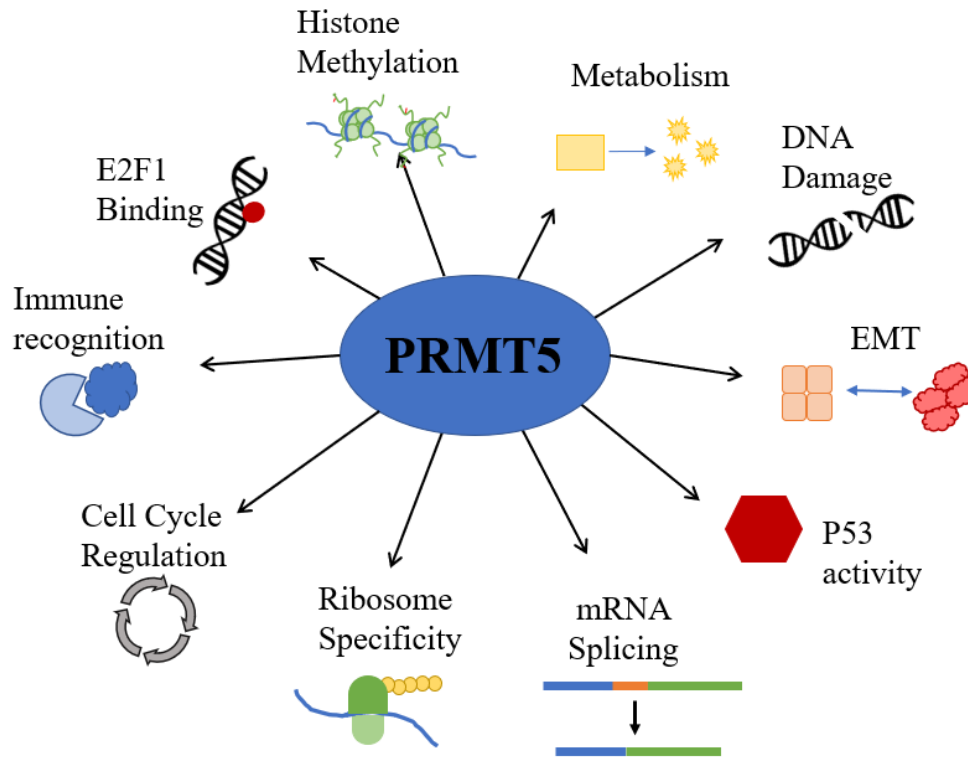


Figure 1-3: A diagram of the roles of PRMT5

The roles of PRMT5 include but are not limited to methylation of histones, control of metabolism, supporting DNA damage repair, promotion of epithelial-mesenchymal transition, influencing the actions of p53, regulation of mRNA splicing, influencing ribosome specificity, regulation of cell cycle, reduction of immune recognition, and promotion of E2F1 binding.

results in transcriptional repression, whereas methylation of H3R2 enhances the binding of WD repeat domain 5 (WDR5) and promotes transcription [96, 109]. Transcriptional regulation also comes from the methylation of transcription factors such as p53 and E2F1. The addition of SDMA has many effects, including transcriptional activation, decrease of protein half-life, enhancing DNA binding, and repressing recruitment all of which effects the target genes of the methylated protein [96]. PRMT5 activity in the nucleus can also affect DNA damage responses including activation of p53, increased activity of RAD9 Checkpoint Clamp Component A (RAD9), and Tyrosyl-DNA Phosphodiesterase 1 (TDP1), and enhanced recruitment to damage foci of Flap Structure-specific Endonuclease 1 (FEN1) [96].

The cytosolic activities of PRMT5 include modulation of splicing, translation, and growth factor signaling. The spliceosome, which is responsible for splicing mRNA before translation, is comprised of small nuclear RNAs (snRNA), numerous small nuclear Ribonucleoproteins (snRNP), and non-snRNP components. snRNPs will complex with seven SM proteins (B/B1, D1, D2, D3, E, F, and G) to form a ring-like core. PRMT5 facilitates this initial binding of SM proteins to the UsnRNAs through physical and enzymatic actions [110]. PRMT5 also influences alternative splicing regulators such as Serine and Arginine Rich Splicing Factor 1 (SRSF1) [111] and Zinc Finger Protein 326 (ZNF326) [112].

Translation of genes with an internal ribosome entry site (IRES) are regulated by PRMT5 through the methylation of Heterogeneous Nuclear Ribonucleoprotein A1 (hnRNP A1) which promotes the interaction of IRES containing mRNA with this protein [113].

These transcripts include key oncogenic proteins such as Myc and Hypoxia Inducible Factor 1 Subunit Alpha (HIF1a) [113]. PRMT5 methylation of eIF4e also promotes the translation of these transcripts [114].

PRMT5 control of signaling has been described with the suppression of EGFR and extracellular signal-regulated kinase (ERK) signaling [115], response to Tumor Necrosis Factor alpha (TNF α) stimulation through methylation of homeobox A9 (HOXA9) [116], response to Interferon gamma (INF γ) signaling through multiple pathways [117-119], support of androgen receptor (AR) transcription [120], and production of IL-2 [121]. PRMT5 also controls cell cycle regulation primarily through transcriptional control of key genes such as CDK4, CDK6, cyclin D1 and pRB which specifically accelerate the G1 to S transition [122]. Metabolic signaling is also influenced by PRMT5. Tsai et al. showed that PRMT5 depletion in hepatic cells caused a significant depletion in circulating blood sugar and a tempered response to glucagon, likely due to reduced transcription of key metabolic genes [123].

Overall, PRMT5 is an essential protein for embryonic development and hematopoietic stem cell maintenance. This enzyme can be found throughout the cell and plays many roles, from transcriptional regulation to supporting splicing fidelity. Many of these roles have been co-opted by malignant cells, resulting in oncogenesis and aggressive cancers, as discussed below.

1.2.b PRMT5 in Cancer

PRMT5 is overexpressed in numerous cancers, including B and T cell lymphoma, multiple myeloma, metastatic melanoma, neuroblastoma and glioblastoma, germ cell tumors, ovarian cancer, nasopharyngeal cancer, breast cancer, colorectal cancer, and gastric cancer (reviewed in [124-126]). This overexpression has been tied to oncogenesis [127-130], as well as the survival and aggressiveness of cancer [127, 131, 132]. PRMT5 overexpression has significant prognostic value, being associated with later stage cancers and poor OS and PFS across many cancer types [133, 134]. Similar to PRMT5 importance for embryonic viability, PRMT5 has been shown to be vital for cancer stem cell pluripotency and survival in glioblastoma [135], breast cancer [136], and chronic myeloid leukemia (CML) [137].

Among hematologic malignancies, overexpression of PRMT5 in Mantle Cell Lymphoma was determined to be the result of dysregulated micro RNA expression where low levels of miR-92b and miR-96 increased PRMT5 expression [138]. PRMT5 was first shown to be essential to B cell lymphomagenesis by Alinari et al. using Epstein Barr virus positive cancers as a model system [127]. Interestingly during this study, a positive feedback loop was identified, where PRMT5 cooperates with a repressive complex to methylate and silence miR-96 therefore promoting additional PRMT5 transcription [127]. These findings were corroborated in CLL [139], though miR-4518 was implicated in gliomas [140], suggesting a tumor type specific regulation.

Hing et al. also showed the importance of PRMT5 for blood cancers with their Eμ-PRMT5 model, which resulted in spontaneous CLL like cancers as well as additional

spontaneous B cell, T cell, and myeloid abnormalities [130]. These mice showed a significant reduction in OS with the majority of the mice monitored presenting with a spontaneous hematological abnormality [130]. In an adoptive transfer transgenic model, PRMT5 co-expressed with constitutively nuclear mutation of Cyclin D1 in murine bone marrow cells resulted in an aggressive T cell leukemia/lymphoma [141].

Alternative splicing can have a great influence on cancer, as shown by the alternative splicing of MDM4 Regulator of p53 (MDM4) that occurs when PRMT5 is inhibited. With reduced splicing fidelity, MDM4S, a shorter isoform becomes more common, resulting in a reduction of MDM4 protein and activation of p53 [142]. This axis has also been observed in melanoma [143], breast cancer [144], and lymphomas [144]. This shows how PRMT5 expression is key to inhibiting the pro-apoptotic functions of p53.

Oncogenic metabolism is regulated by PRMT5, as shown by Qin et al. in their study on pancreatic cancer, where PRMT5 deletion led to lower ¹⁸F-FDG uptake in an *in vivo* model while overexpression led to higher glucose uptake and lactate production *in vitro* [145]. Similar results were seen in colorectal cancer with decreased glycolysis after treatment with a PRMT5 inhibitor [146]. Effects on lipid metabolism were recently described by Yuan et al., with PRMT5 influencing metabolic proteins directly as well as regulated metabolic genes [147].

Epithelial-mesenchymal transition is the process by which an epithelial-like cancer cell can gain mesenchymal-like properties, resulting in increased mobility and invasion, resulting in additional metastases. PRMT5 was found to support this process in pancreatic cancer through the EGFR/AKT/ β -catenin pathway [134].

In summary, PRMT5 over expression has been observed in solid and hematological cancers, often with prognostic value. The functions PRMT5 plays in development, including protecting plasticity and promoting expansion, are also seen in cancer with support for cancer stem cells and expansion of cancer.

1.2.c PRMT5 inhibitors

Given the role of PRMT5 in cancer, PRMT5 inhibitors have been an area of focus since the crystal structure of PRMT5:MEP50 was published in 2012 [95]. Two of the first compounds, CMP5 [127] and EPZ015666 [148], would either act as the pharmacophore or be used directly in clinical trials. CMP5 was licensed to Prelude Therapeutics, who then developed the PRT382/PRT543 and PRT808/PRT811 class of compounds which have been tested in clinical trials, whereas EPZ015666 was acquired by GSK and brought directly to trial (**Appendix A**). While there are only two clinical trials open specifically for MCL with PRMT5 inhibitors (NCT03573310 and NCT05528055), there multiple inhibitors from various classes that have been produced and could be tested (**Table 1-3**).

Name	Company	Stage	Citation
EPZ 015666 (GSK3235025)	GSK	Clinical	10.1021/acsmedchemlett.5b00380.
Pemrametostat (GSK3326595)	GSK	Clinical	10.1093/annonc/mdz244
AMG193	Amgen	Clinical	10.1200/JCO.2022.40.16_suppl.TPS3167

Continued

Table 1-3: Current PRMT5 inhibitors in clinical trials or published as tool compounds

Note: * Pan PRMT inhibitor ** PRMT5, PRMT7 inhibitor. Many compounds are reviewed for structural similarities and general class in Fu et al. [149].

Table 1-3 continued

Name	Company	Stage	Citation
JNJ-64619178	Janssen	Clinical	10.1016/j.annonc.2020.08.651
PF-06939999	Pfizer	Clinical	10.1158/1535-7163.MCT-21-0620
TNG908	Tango	Clinical	10.1158/1538-7445.AM2022-3941
SCR-6920	Jiangsu Sincere	Clinical	NCT05528055
PRT811	Prelude	Clinical	10.1158/1538-7445.AM2020-2919
PRT543	Prelude	Clinical	10.1182/blood-2021-150938
MRTX1719	Mirati	Clinical	10.1021/acs.jmedchem.1c01900
LLY-283	Eli Lilly	Tool	10.1021/acsmchemlett.8b00014
EPZ015866 (GSK 3203591)	GSK	Tool	10.1021/acsmchemlett.5b00380.
PRT382	Prelude	Tool	10.1038/s41467-022-35778-1
PRT808	Prelude	Tool	
AMI-1*	Academic	Tool	10.1002/cmdc.200900459
11-9F	Academic	Tool	10.1038/s42003-022-03991-9
43g	Academic	Tool	10.4155/fmc-2021-0244.
3039-0164	Academic	Tool	10.3390/molecules27217436
CMP5	Academic	Tool	10.1182/blood-2014-12-619783.
DC_C01	Academic	Tool	10.1039/C7OB00070G
17	Academic	Tool	10.1021/acs.jmedchem.7b00587
DS-437**	Academic	Tool	10.1021/ml500467h
PF-06829927	Pfizer	Tool	10.1016/j.celrep.2020.01.054
C9	Academic	Tool	10.1371/journal.pone.0181601
P1608K04	Academic	Tool	10.1039/C7MB00391A
P1618J22	Academic	Tool	10.1039/C7MB00391A
4b14	Academic	Tool	10.1016/j.bmcl.2018.10.026
P5i-6	Academic	Tool	10.1111/cbdd.12881
5 and 19	Academic	Tool	10.1016/j.bioorg.2018.08.021
PJ-68	Academic	Tool	10.1172/JCI85239
HLCL-61	Academic	Tool	10.1038/leu.2015.308
HLCL-65	Academic	Tool	10.4049/jimmunol.1601702
A, B, and C	Academic	Tool	10.3390/ijms23094806
T1551	Academic	Tool	10.3389/fphar.2018.00173
BRD0639	Academic	Tool	10.1021/acs.jmedchem.1c00507
C_4	Academic	Tool	10.1007/s10822-019-00214-y
9, 10, 11, 12	Prelude	Tool	10.1021/acsmchemlett.9b00074

Continued

Table 1-3 continued

Name	Company	Stage	Citation
34 and 72	Merk	Tool	10.1021/acs.jmedchem.0c02083
9-1	Merk	Tool	10.1016/j.bmcl.2018.03.087
Candesartan cilexetil	N/A	Approved for other uses	10.1016/j.gendis.2022.04.001
Cloperastine hydrochloride	N/A	Approved for other uses	10.1016/j.gendis.2022.04.001

There are also additional trials oriented toward precision medicine and open to Methylthioadenosine Phosphorylase (MTAP) negative cancers (NCT05094336 and NCT05245500). MTAP is a crucial enzyme to the methionine salvage pathway and without expression, there is a buildup of the SAM precursor (methylthioadenosine) MTA. This metabolite competes with SAM for PRMT5 binding, resulting in additional sensitivity to PRMT5 inhibitors [150, 151].

There are several classes of PRMT5 inhibitors both in clinical trials and as tool compounds including substrate, SAM, or dual competitive; complex inhibitors; covalent inhibitors; dual target inhibitors; and PROTAC inhibitors some of which fall into multiple classes [149]. EPZ 015666 (GSK3235025), one of two PRMT5 inhibitors reported in 2015, is a substrate competitive inhibitor [148], meaning the compound competes with arginine residues that could be demethylated. The clinical compound Pemrametostat (GSK3326595) also falls into this class of PRMT5 inhibitors. CMP5, the second inhibitor reported in 2015, is a dual substrate and SAM competitive inhibitor [127] as it blocks both the SAM and arginine pockets to prevent PRMT5 enzymatic activity. The clinical

compounds JNJ-64649478, PRT543, and PRT811 all fall into this category. Compound 17 from Mao et al. is an example of a SAM competitive inhibitor as shown by its non-competitive inhibition when used with the substrate specific EPZ015666 [152].

The complex inhibitors move past the SAM or substrate pocket to target PRMT5 binding partners. In 2019, Dr. Lin from Prelude Therapeutics and colleagues reported the discovery of a new class of PRMT5 inhibitors that would covalently bind PRMT5 at C449, inhibiting the PRMT5:MEP50 complex [153]. MRTX1719 targets PRMT5 specifically in MTAP deleted cancers, as it inhibits the activity of the PRMT5:MTA complex but not the PRMT5:SAM complex [154]. Another method of inhibiting complexes is displayed with BRD0639, which covalently blocks the PRMT5 binding motif, preventing the interaction of PRMT5 with its adaptor proteins such as Methylosome Subunit pICln and RIO kinase 1 (Riok1) [155].

Also in 2015, the first Type II specific, dual inhibitor was produced. DS-437 selectively inhibits both PRMT5 and PRMT7, thereby reducing all SDMA in a cell. Another dual inhibitor was published by Al-Hamashi et al, this one targeting PRMT4 and PRMT5, opening the possibility of co-targeting a type 1 and type 2 PRMT with specificity [156].

Among the synthesized PRMT5 inhibitors, Prabhu et al. found that two regulatory approved compounds Candesartan cilexetil (Can) and Cloperastine hydrochloride (Clo) showed inhibitory activity against PRMT5 [157]. Can has been approved by the FDA for hypertension while Clo has been approved by the EMA for cough treatment. These two compounds had competitive enzymatic IC₅₀s at 33 μ M and 27 μ M, respectively [157]. They

also demonstrated *in vitro* and *in vivo* activity against pancreatic ductal adenocarcinoma, colorectal cancer, and breast cancer [157].

Proteolysis targeting chimera (PROTAC) compounds target specific proteins for degradation thereby resulting in a more similar effect to genetic knockdown compared to chemical inhibition. Shen et al. developed two such chimeric agents by linking EPZ015666 to a von Hippel-Lindau (VHL) E3 ligase ligand, (S,R,S)-AHPC-Me (VHL-2) [158]. Compound 15 showed significant reductions in PRMT5 expression, as well as downstream activity as determined by SDMA levels [158].

The numerous PRMT5 inhibitors and other targeting compounds show a wide range of enzymatic activity, specificity, and potential toxicities, showing some of the challenges with reaching FDA approval for PRMT5 inhibitors. That being said, the numerous studies showing the anti-cancer efficacy of these inhibitors provide hope for the potential of these agents to reduce proliferation, sensitize cancer to combination treatments, and reduce cancer stem cells.

1.3 BCL-2 Family Proteins

1.3.a Class and Function

The B cell Lymphoma 2 (*BCL-2*) gene was first described in 1985 as being present in a common translocation in follicular lymphoma (FL) and was then determined to suppress apoptosis [159]. Since then, 12 core members of the BCL-2 protein family have been identified; these core proteins share structural similarities to BCL-2, either tertiary or predicted secondary. This count increases up to 25 members when proteins with limited sequence homology such as the BCL-2 homology 3 (BH3) only proteins are included [160]. **Table 1-4** shows the most referenced BCL-2 family proteins and their role in the intrinsic apoptotic balance. Almost all members of this family share the BH3 domain motif (with the exception of BFL-1 and BCL-B), though they may also share BH1, BH2, and BH4 domains [159]. They are predominantly found in the cytosol or the outer membrane of the mitochondria, except Bcl-2-Interacting Killer (BIK), which is localized to the endoplasmic reticulum [161]. The family consists of four major subclasses of proteins: 1) anti-apoptotic proteins that bind and block the activity of effector proteins; 2) pro-apoptotic effector proteins that are able to oligomerize and create pores in the mitochondria, releasing cytochrome C and triggering apoptosis; 3) pro-apoptotic activators that interact with effectors; and 4) pro-apoptotic sensitizers that sequester anti-apoptotic proteins (**Table 1-4, Figure 1-4**).

This balance of pro- and anti-apoptotic signals is dependent on levels of protein expression, localization, signaling and interaction between proteins. BCL-2-associated X (BAX) is an example of the importance of localization where it is typically found in the

Protein	Role
BCL-2	Anti-apoptotic
BCL-xL (BCL2L1)	Anti-apoptotic
BCL-W	Anti-apoptotic
BFL-1 (BCL-2A1, or A1)	Anti-apoptotic
BCL-B (BCL-2L10)	Anti-apoptotic
MCL-1	Anti-apoptotic
BAX	Pro-apoptotic (effector)
BAK	Pro-apoptotic (effector)
BOK (MTD)	Pro-apoptotic (effector)
BID	Pro-apoptotic (activator)
BIM (BOD)	Pro-apoptotic (activator)
PUMA (BBC3)	Pro-apoptotic (activator)
BAD	Pro-apoptotic (sensitizer)
BMF	Pro-apoptotic (sensitizer)
NOXA (PMAIP1)	Pro-apoptotic (sensitizer)
HRK (DP5)	Pro-apoptotic (sensitizer)
BIK (BLK or NKB)	Pro-apoptotic (sensitizer)

Table 1-4: Table of primary BCL-2 Family proteins

cytosol but is trafficked or allowed to remain on the mitochondrial membrane during apoptosis [162]. BCL-2 proteins are present throughout the endoplasmic reticulum, nuclear envelope, and outer mitochondrial membrane and function to inhibit BAX oligomerization [163]. Upregulation of B cell lymphoma-extra large (BCL-xL) through the multiple transcription factors [164] or myeloid cell leukemia-1 (MCL-1) through decreased ubiquitination and degradation can lead to cell survival [165]. Upregulation of BAX, which is typically stable in its expression [159], through c-MYC [166] or p53 [167] regulation

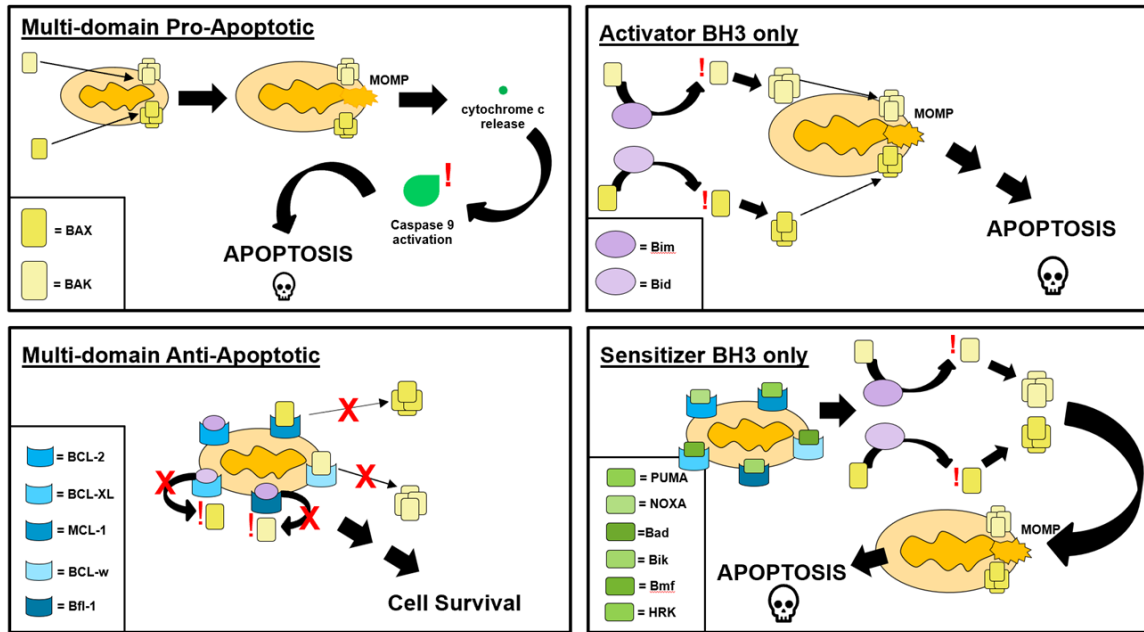


Figure 1-4: Diagram of major BCL-2 family proteins indicating their subclass and binding affinities

Top left: Multi-domain Pro-Apoptotic or effector proteins include BAX and BAK which homo-oligomerize and create pores on the mitochondria leading to cytochrome c release, caspase 9 activation and apoptosis. Top right: Pro-apoptotic activator proteins include Bim and Bid which promote the homo-oligomerization of the effector proteins. Bottom left: Multi-domain anti-apoptotic proteins include BCL-2, BCL-xL, MCL-1, BCL-w and BFL-1. These proteins bind effector or activator proteins increasing the apoptotic threshold or sensitizer proteins, releasing activators and effectors. Bottom right: Sensitizer BH3 only proteins include PUMA, NOXA, Bad, Bik, Bmf, and HRK. These proteins block the activity of the anti-apoptotic proteins and support apoptosis. Reproduced with permission from Claire Hinterschied 2023.

has the opposite result and tips the balance toward apoptosis. Signaling can come in many forms from DNA damage signaling in the case of NOXA and p53 upregulated modulator of apoptosis (PUMA) to Bcl-2 Interacting Mediator of cell death (BIM) and BCL2 Associated Agonist Of Cell Death (BAD) activation with growth factor deprivation [159].

The interactions between these proteins are numerous and varied, as can be demonstrated through BH3 profiling (**Figure 1-5**). By using peptides of the key BH3 domains, Certo et al. were able to determine relative affinities for each activator or sensitizer to the anti-apoptotic proteins [168]. This study revealed that despite the similarities in sequence, the peptides had unique binding affinities with two, NOXA and Activator of apoptosis harakiri (HRK), only binding one anti-apoptotic member of the

	BID	BIM	BIDM	BAD	BIK	NOXA A	NOXA B	HRK	BNIP	PUMA	BMF
BCL2	66 (6)	<10	-	11 (3)	151 (2)	-	-	-	-	18 (1)	24 (1)
BCLXL	12 (9)	<10	-	<10	10 (2)	-	-	92 (11)	-	<10	<10
BCLW	<10	38 (7)	-	60 (19)	17 (12)	-	-	-	-	25 (12)	11 (3)
MCL1	<10	<10	-	-	109 (33)	19 (2)	28 (3)	-	-	<10	23 (2)
BFL1	53 (3)	73 (3)	-	-	-	-	-	-	-	59 (11)	-

Figure 1-5: Table of half maximal effective concentration (EC50) of BH3 only peptides binding to anti-apoptotic truncated peptides

Values are listed in nM with greyed boxes being greater than 1 μM. Reproduced from "A Laboratory Guide to BH3 Profiling" from the Letai lab. BIDM = mutation of BID
 BNIP3 = BH3 only related pro-apoptotic protein

BCL-2 family. These differentials would become key when attempting to target specific anti-apoptotic proteins with BH3 mimetics.

1.3.b BCL-2 Proteins in Lymphoma

As demonstrated by the first description of BCL-2 dysregulation in FL [169], BCL-2 proteins play a key role in many lymphomas [170, 171]. Shortly after the discovery of BCL-2 Fanidi et al., described how BCL-2 supported the oncogenic functions of c-MYC, another key protein in lymphoma, while preventing pro-apoptotic signaling from this protein [172]. This finding was supported by the E μ -bcl-2/myc mouse model that has hyperproliferation of pre-B and B cells and developed tumors faster than the classic E μ -myc model of lymphoma [173]. This result could also be obtained by deleting the pro-apoptotic protein BAX [174]. BCL-2 mutations are associated with poor prognosis in FL [175] and diffuse large B cell lymphoma (DLBCL) [176], and are used to diagnose double or triple hit lymphomas subtypes within DLBCL [177]. Expression levels of this key pro-survival protein were found to be elevated in five types of NHL, Burkitt's lymphoma, DLBCL, FL, marginal zone lymphoma, and MCL [178].

Overexpression of other pro-survival proteins such as MCL-1 and BCL-xl are also described in lymphomas and murine model of lymphoma [179-181] (Reviewed in Ref 194). Similar to BCL-2, BCL-xL overexpression is found in multiple lymphomas including DLBCL and MCL [182, 183]. In MCL, this overexpression, in combination with a BAX deletion, resulted in 300-fold resistance to the proteasome inhibitor, bortezomib [184]. MCL-1 overexpression is limited in hematological malignancies [178] but plays an

important role in cell survival when BCL-2 or BCL-xL are inhibited or deleted [185]. Detection may also be limited by the short half-life of MCL-1, which is less than one hour [186], leading to this protein being more sensitive to sample processing time than other BCL-2 family proteins.

Homozygous Bim deletions have been described in about 20% of MCL cases and in several cell lines, a genetic feature that appears to be fairly unique to MCL [187, 188]. The expression of this protein appears to have some prognostic value in MCL cases, especially when stratified by stage [189]. Alterations of the other pro-apoptotic proteins have not been as clear, with some resulting in lymphomagenesis in mice, while others resulted in no phenotype [181]. Findings in clinical samples are lacking in the literature.

The BCL-2 family of proteins is a complex network that governs apoptosis and frequently dysregulated in lymphomas [170, 171]. This provides a therapeutic target for molecular treatments in the form of BH3 mimetics.

1.3.c BH3 mimetics

BH3 mimetics interact with the BCL-2 family of proteins that are responsible for controlling intrinsic apoptosis by mediating the formation of pores on the mitochondria, leading to the release of cytochrome C and caspase cleavage. BH3 mimetics block the pro-survival signals from proteins such as BCL-2, MCL-1, and BCL-xL. These compounds are well reviewed by Diepstraten et al. [190] and a select number will be discussed here.

Venetoclax, a BCL-2 inhibitor, is a very popular choice for MCL treatment off-label with 12 active clinical trials (**Appendix A**). Two of the most closely watched

trials are venetoclax dosed in combination with ibrutinib (NCT03112174) or R-CHOP (NCT02055820) for R/R MCL. This compound has been approved for CLL by the FDA, supporting its use in mature B cell lymphomas. Single agent dosing resulted in an ORR of 75%, with 21% achieving CR, which was the highest among the various NHLs tested [191]. Dosing was very well tolerated, with some patients remaining on venetoclax for 4 years by the end of the study [191]. The combination of ibrutinib and venetoclax was able to achieve an impressive 71% CR in a small cohort of high-risk patients [192]. This led to the phase III SYMPATICO trial, which has reported an ORR of 81% with 62% of patients achieving CR [193].

MCL-1 and BCL-XL act as pro-survival proteins for MCL, though at a lower level than BCL-2 [181]. Their upregulation has been suggested as a major contributor to venetoclax resistance [194], which lends additional support to the use of MCL-1 and BCL-XL inhibitors. MCL-1 inhibitors, while showing promise in multiple hematopoietic malignancies, have yet to be used successfully due to the protein's key role in cardiac, neural, and hepatic cell survival resulting in intolerable side effects [194, 195]. Trials with AstraZeneca's AZD5991 and Amgen's AMG-176 were recently terminated, though Amgen continues to test their compound in multiple myeloma and other myeloid malignancies (NCT05209152 and NCT02675452).

BCL-XL inhibitors have similar difficulties in clinical trials due to the role BCL-XL plays in platelet health. The initial work with the BCL-2/BCL-XL/BCL-w inhibitor navitoclax [196] showed excellent reductions in disease but only at doses that also caused high levels of thrombocytopenia [197]. To work around these limitations, new

formulations of BCL-2/BCL-XL inhibitors have been designed [198, 199] as well as targeted delivery systems for MCL-1 and BCL-2/BCL-XL inhibitors [200-202]. The effective cancer killing properties of these agents show great potential and suggest a need for ways to reduce dosing or otherwise minimize side effects.

1.4 Mouse Models

1.4.a Mouse Models of Lymphomas

Mouse models for MCL are made up of cell line derived xenografts (CDXs), patient derived xenografts (PDXs), and transgenic (tg) models. Each carries its own benefits and drawbacks. CDXs are easily generated from cell lines used *in vitro* such as CCMCL1 and Granta-519, show consistent pathology from experiment to experiment, and are derived from human cells. These are excellent for drug screening studies or other research that requires a speedy and consistent model. PDXs share many of the same benefits as CDXs, with the additional benefit of reducing the time the cells are cultured or passaged between the patient sample and the experiment. PDXs do have the drawback that developing these models can be time consuming and expensive, failing up to a third of the time [203]. Another consideration is that expansion of these models requires additional mice rather than additional cell culture. The drivers of cancer for both models could be varied and potentially change over time. The process of creating a PDX or passaging a cell line through a mouse provides selective pressure that is difficult to control for. For both of these models, human MCL cells are engrafted into immunocompromised NOD.Cg-Prkdcscid Il2rgtm1Wjl/SzJ (NSG) mice systemically via tail vein or subcutaneously on a flank. Disease burden can be measured through flow cytometric analysis of circulating human cells or measurements of tumor volume.

Tg models provide the benefits of a simple genetic profile and the immunocompetent environment lacking in CDX or PDX models. These models are

typically produced on a C57Bl/6 background or slight variations on this strain (**Table 1-5**). Spontaneous murine models may take years to develop full blown lymphoma or leukemia and the penetrance is likely to be less than 100%. Creating a cohort large enough to have temporally controlled groups to test therapeutics on is very difficult. Some of these challenges can be overcome by adoptive transfer protocols where disease cells are harvested from a spontaneous donor and transplanted into a healthy or irradiated immunocompetent mouse. With the next generation of cancer treatments focusing on immunotherapy, the presence of a functioning immune system is vital for this pre-clinical research. These models take the longest time to produce.

1.4.b Mouse Models of MCL

CDX and PDX models of MCL are fairly easy to come by, thanks to cell banks such as ATCC and PRoXe [204]. All commonly used MCL cell lines are tumorigenic and can be used systemically or subcutaneously as a model of MCL. PDX models can be produced from collected MCL samples or applied for from PRoXe. The lymphoma group at The Ohio State University has produced two PDX models from patients at the Comprehensive Cancer Center. PDX.AA.MCL was produced from an ibrutinib relapsed male who was 75 years of age, allowing us to model an aggressive treatment resistant MCL. The second, PDX.DA.MCL, was produced from a 71-year-old treatment naïve male and allows for exploration of potential frontline treatments.

Contrary to the availability of immune incompetent models, murine models of MCL with intact immune systems are severely lacking. The first attempts to generate a

Cyclin D1 driven cancer, a logical step for modeling MCL where *CCND1* translocation is a hallmark, were published by Bodrug et al., in 1994 [20]. Despite high levels of Cyclin D1 production driven by the E μ promoter, transgenic models overexpressing this protein failed to produce a lymphoma [20]. Lymphoma could be induced in this model with a pristane injection at one year [205], though pristane alone causes malignant expansion of B cells [206]. The FC-muMCL1 cell line was developed from a pristane induced lymphoma in a E μ -CCND1 and then adoptively transferred and cultured *ex vivo* [207]. This cell allows for engraftment into pre-conditioned C57Bl/6 mice allowing for immune studies but contains a complex karyotype with no clear driver.

Lymphomas were achieved by creating a double transgenics with the E μ -CCND1 model, starting with a cross with E μ -myc mice (**Table 1-5**) [20]. In clinical MCL, while myc aberrations provide prognostic value, they only occur in 14-20% of MCL cases [32, 36]. Other efforts with *CCND1* include a constitutively nuclear mutant of Cyclin D1 which also required a second genetic alteration such as mutations in *TP53* or *MDM2* [208], and E μ -CCND1 mice with *Bim(fl/fl)* [209]. Other efforts include overexpression of *CCND1* downstream target c-Myc and IL-14 [210], a mutant *Cdk4* [211] or a heterozygous deletion of *TP53* [212]. Another reported model utilizes *CCDN2* overexpression in all hematopoietic cells [213]. All of these models have limited representation of conventional MCL due to inconsistent disease development, unusual genetic drivers, and/or deviant pathology. The limit of currently available models shows the need for new options for both spontaneous and adoptively transferred transgenic models of MCL.

Name	Genetics	Background	Citation
myc/cyclinD1	E μ myc X E μ cyclinD1	C57BL/6J x SJL/J	[20]
E μ -D1/T286A	E μ CCND1 ^{T286A}	C57/BL6	[208]
IL-14 α \times c-Myc	E μ IL-14 α X E μ myc	C57/BL6	[210]
Ccnd2 ^{Vav}	R26-Ccnd2 ^{tg/tg} ; Vav-iCre ^{tg/+}	(E2.5 Swiss X C57BL/6) X Vav-iCre	[213]
E μ ^{CycD1} CD19 ^{CRE} Bim ^{fl/fl}	E μ CCND1 X CD19 Cre X Bim ^{fl/fl}	B6SJLF1 X B6.129P2(C)- CD19 ^{tm1(cre)Cgn/J} X C57Bl/6	[209]
Myc/Cdk4 ^{R24C}	Myc-3'RR X CMV Cdk4R24C	C57/BL6	[211]
c-myc-3'RR/p53 ^{+/-}	cMyc-3'RR X PGK-tk P53 ^{+/-}	C57/BL6 X 129/Ola	[212]

Table 1-5: Table of published transgenic murine models of MCL

Chapter 2: PRMT5 Inhibition Reactivates FOXO1 and Leads to Synthetic Lethality with BCL-2 Inhibitor Venetoclax

Modified from “PRMT5 Inhibition Drives Therapeutic Vulnerability to Combination Treatment with BCL-2 Inhibition in Mantle Cell Lymphoma” with permission.

2.1 Background and Rationale

Mantle cell lymphoma (MCL) is a CD5+/CD19+ B cell non-Hodgkin Lymphoma (NHL), defined by the t(11;14) translocation juxtaposing *CCND1* downstream of the *IgH* promoter, which results in Cyclin D1 over expression and cell cycle dysregulation. MCL comprises up to 6% of NHL cases diagnosed annually [80] and is associated with an overall poor prognosis due to multiple factors, including advanced stage of disease at diagnosis, resistance to standard immuno-chemotherapy regimens, and clinical factors [80]. Due to the late median age of diagnosis, approximately 70 years of age [214], aggressive chemotherapy and stem cell transplantation are often not realistic options [215]. Without stem cell transplant, the average overall survival of patients with MCL is approximately six years [64]. For the majority of patients who progressed on targeted agents like ibrutinib prior to the recent FDA approval of brexucabtagene autoleucel CarT therapy [216], survival remained very poor [83]. Short of salvage immuno-chemotherapy followed by a stem cell transplant, relapse is virtually universal and for the most part, MCL is considered incurable [85]. Thus, there is a major unmet need to identify new therapeutic targets and strategies that are well tolerated by less fit patients to improve prognosis and quality of life [214].

Protein arginine methyltransferase 5 (PRMT5) is a type II PRMT enzyme that modulates the activity of a wide range of proteins through symmetric-dimethylation of arginine residues (sDMA) [217]. PRMT5 is required for normal B cell development and formation of germinal centers via direct and indirect modulation of P53 and the spliceosome [105]. We and others have documented overexpression of PRMT5 and its oncogenic activity promoting the growth and survival of MCL and other lymphoid malignancies [127, 137, 138, 141, 218, 219]. The sDMA activity of PRMT5 regulates many cellular functions including alternative splicing, epigenetic control of gene expression, and survival/growth and death pathways orchestrated by P53 [220], NF κ B/p65 [127, 221], BCL-6 [222] and E2F1 [223, 224]. Inhibition of PRMT5 leads to reduced cancer cell growth [225, 226], abrogation of a stem cell phenotype [135, 136], and increased survival for *in vivo* models [144, 148, 219, 225]. These observations have led to the development of several unique classes of small molecule PRMT5 inhibitors [127, 148, 227, 228] that are currently being explored in clinical trials (NCT03886831, NCT04089449, NCT04676516, NCT05094336, and others).

Prior work has shown that PRMT5 promotes survival of lymphoma cells by epigenetically suppressing AXIN2 and WIF1, supporting the WNT- β -CATENIN pathway, and enhancing AKT activity [30]. AKT phosphorylates protein and lipid kinases, metabolic enzymes, cell cycle regulators, and transcription factors among others [229]. AKT is also known to provide pro-growth and survival signals through several pathways including DNA damage repair [230], cell cycling [231], degradation of p53 [232], and receptor tyrosine kinase signal modulation [233].

One of the direct targets of AKT is the forkhead box protein O1 (FOXO1), a transcription factor canonically known to function as a tumor suppressor [234-236] and critical for normal B cell development [237, 238]. FOXO1 has been shown to be essential for pro-B cells to advance to pre-B cells, peripheral blood B cells to traffic to lymph nodes, and to support immunoglobulin class switching to drive efficient antibody memory responses [237]. In cancer, FOXO1 regulates cell cycle [239, 240], autophagy [241, 242], and has been correlated to prognosis in multiple types of cancer [243, 244]. These functions are suppressed through the PI3K/AKT axis, where AKT phosphorylates FOXO1, preventing FOXO1's transcriptional activity and triggering export from the nucleus [235]. In lymphomas, PRMT5 supports the activity of PI3K/AKT through the sDMA of R391 of AKT [30, 245]. We hypothesized that PRMT5 inhibition may lead to interruption of this signaling pathway and restore tumor suppressor activity of downstream targets like FOXO1.

Here, we show how PRMT5 inhibition leads to the dissociation of FOXO1 and AKT, followed by the nuclear translocation of FOXO1 in MCL cells, and recruitment to the promoter regions of target genes including members of the pro-apoptotic BCL-2 family. Following PRMT5 inhibition, FOXO1 directly binds to the promoter region of BCL-2-associated X protein (*BAX*) leading to its enhanced expression and decreased apoptotic threshold of MCL cells. We hypothesized this would drive a therapeutic vulnerability to BCL-2 inhibition and demonstrate that treatment with venetoclax and a PRMT5 inhibitor leads to synergistic cell death of MCL cells both *in vitro* and *in vivo* preclinical models. Basal expression of BCL-2 was found to correlate with synergistic anti-

tumor activity of this combinatorial strategy. This study provides support for combining PRMT5 and BCL-2 inhibition in clinical trials for patients with MCL.

2.2 Methods

Cell culture, Measurement of Anti-tumor Activity, and Synergy

Nine cell lines were used in this work: Jeko, Rec-1, SP53, UPN-1, CCMCL1, Z-138, Mino, Maver-1, and Granta-519. All lines were cultured at 37° Celsius, 5% CO₂, in RPMI 1640 supplemented with 10% FBS, 1% glutamax, and 1% penicillin/streptomycin. Cell lines were validated by STR. Mycoplasma testing was performed monthly. PRT382 was supplied by Prelude Therapeutics (Wilmington, DE, USA). Venetoclax (ABT-199) was purchased from MedChemExpress (Monmouth Junction, NJ, USA). IC₅₀s, defined as a 50% reduction in percentage of live cells, were measured with Annexin V/PI staining and flow cytometry. IC₅₀s were measured at day nine for PRT382 and day three for venetoclax. Synergy was measured via MTS assay at day nine with six days of PRT382 pre-treatment and three days of combination treatment. Synergy scores and plots were calculated with the Loewe model via Combenefit [246].

Chromatin Immunoprecipitation Sequencing and q-PCR

Sample preparation, library construction and ChIP-seq were performed as described previously [247]. Briefly, cells treated with and without PRT382 were harvested after 48 hours and fixed. Nuclei were harvested and chromatin sheared via sonication before immunoprecipitation with 10 µg of anti-FOXO1 (custom raised rabbit polyclonal)

was performed at 4°C overnight. The preparation was cleaned with RNase and Proteinase K. DNA was reverse-crosslinked and extracted via NucleoSpin Gel and PCR clean-up DNA extraction kit. Libraries were generated using KAPA Hyper Prep kit and 8-cycle PCR amplified, followed by purification using 1X SPRI beads. Sequencing and post-processing of the raw data was performed at Genomics Core facility at Weill Cornell Medicine. ChIP-seq data is available on Gene Expression Omnibus (GEO) database with accession number GSE182689.

Reverse transcription was carried out on 200 ng of total RNA using the RevertAid RT kit. RT-qPCR was performed on cDNA samples using the PowerUp™ SYBR® Green Master Mix on the 7500 Fast Real-time PCR system. mRNA level of each sample was normalized to that of ACTB mRNA. The relative mRNA level was presented as unit values of $2^{-\Delta Ct}$ (=Ct of ACTB-Ct of gene). Primer sets are listed in **Appendix D**.

Western Blotting and Immunofluorescence

Cells were treated with small molecule inhibitors for up to nine days, with media changed completely every three days. Doses are listed in **Appendix C** and were chosen to maintain viability above 70% at time of collection. Cells were harvested by pelleting at 300g for 10 mins, washed with ice cold PBS, and pelleted at 300g for eight minutes at 4° Celsius. Lysates were made using RIPA buffer with phosphatase and protease inhibition cocktails. Western blots were run with 20-30ug of protein on 4-20% SDS-PAGE gels before being transferred to PVDF using the Turbo Transfer System. Blots were blocked, probed, washed, and imaged according to LiCor protocols. For immunofluorescence, cells

were fixed with paraformaldehyde and permeabilized with 0.2% TX100. Incubation with the primary antibody was performed overnight at 4° Celsius and imaging was completed with an alexa488-conjugated donkey anti rabbit IgG secondary. FOXO1 localization was determined by quantification of cells with FOXO1 enriched nuclei by view field. Additional primary and secondary antibodies are listed in **Appendix E**.

Knock Down Cell Lines

BAX and BAK1 knock down cell lines were created using two shRNA plasmids (Mission shRNA, Sigma) for each gene. Briefly, glycerol bacterial stocks were expanded and harvested for plasmid. This was transduced with a packaging and envelope plasmid into Lenti X 293T cell. Virus was produced, collected and used to transduce cells of interest. Successfully transduced cells were selected with puromycin and knock down was confirmed via rtPCR and western blot. A pLKO.1 empty plasmid SHC001 was used as a control.

In Vivo Studies

Two patient derived xenograft (PDX) and two cell line-derived xenograft (CDX) models were used in this work. The CCMCL1 CDX, PDX.AA.MCL, and PDX.IR.96069 studies were performed at The Ohio State University (OSU) under protocol 2009A0094-R4 and IACUC approval. PDX.AA.MCL was developed by the OSU Lymphoma group from an ibrutinib resistant patient sample [248] while the PDX.IR.96069 was obtained from PRoXe [204] and tested for continued ibrutinib resistance. The Granta-519 CDX flank

model was performed at Crown Bioscience on behalf of Prelude Therapeutics under their ethical guidelines. NOD.Cg-Prkdcscid Il2rgtm1Wjl/SzJ (NSG) or NOD.Cg-Prkdcscid/J (NOD SCID) mice (OSU ULAR or LC Shanghai Lingchang Bio-Technology co., LTD) were engrafted either via tail vein or on the flank with 10e6 cells. Disease burden was monitored via flow cytometry or measurement of tumor size. Mice were dosed variably with the CCMCL1 CDX (see **Appendix E**), four days on, three days off (PDX.AA.MCL and PDX.IR.96069), or daily (Granta-519 CDX) via oral gavage.

Statistics

Data was analyzed with a two-way ANOVA, Student's t test, Spearman Correlation, or log rank (Mantel-Cox) test, as applicable. To compare changes in disease burden over time, we used Generalized Estimating Equations (GEE) with autoregressive correlation structure to test the differences of slopes between groups. For this exploratory pre-clinical study, p-values were not adjusted for potential multiple comparisons. Error bars show standard deviation of the data. * P<0.05, **P<0.01, ***P<0.001, ****P<0.0001.

2.3 Results

Selective inhibition of PRMT5 with PRT382 drives MCL anti-tumor activity *in vitro* and *in vivo*

To selectively target PRMT5 activity in MCL, we utilized PRT382 (Prelude Therapeutics), a novel S-adenosyl methionine (SAM) competitive, selective small molecule inhibitor of PRMT5 enzymatic activity [130] (**Figure 2-1A, 2-1B**). *In vitro* anti-MCL activity was demonstrated in nine cell lines which showed IC50s ranging from

44.8nM to 1905.5nM (**Figure 2-1C**). *In vivo*, PRT382 demonstrated a favorable oral bioavailability and pharmacokinetic profile in mice (AUC 1175 hr*kg*ng/mL/mg at 10mg/kg) (**Figure 2-1D**). The human MCL cell line derived xenograft (CDX), CCMCL1, was used to evaluate a range of doses and schedules for evaluation of toxicity and anti-tumor activity. 10mg/kg every other day showed the lowest efficacy compared to 5mg/kg daily, likely attributed to off target gastrointestinal toxicity leading to rapid weight loss (**Figure 2-2A, 2-2B, 2-2C**). 10 mg/kg 4 days on, 3 days off (4D/3D) showed marked improvement in therapeutic anti-tumor activity over 5mg/kg daily. PRT382 delivered on a dose and schedule of 10 mg/kg 4D/3D off achieved a prolonged significant reduction in circulating disease and extended median survival from 37 days to 87 days (**Figure 2-2A, 2-2B**; $p < 0.01$). This schedule avoided dose limiting toxicities, defined as greater than 10% body weight loss in a week (**Figure 2-2C**), and provided robust anti-tumor activity. Despite the significant survival advantage, all treated mice did eventually reach early removal criteria due to MCL disease burden prompting consideration of combination strategies.

PRMT5 inhibition promotes a FOXO1-driven transcriptional program in MCL

We and others have previously reported that PRMT5 directly and indirectly supports AKT activity [30, 128]. We hypothesized that the reduced AKT activity occurring as a consequence of PRMT5 inhibition would lead to perturbation of AKT:FOXO1 interaction, FOXO1 nuclear translocation, and modulation of genes with tumor suppressor activity. Using CCMCL1 and Z-138 as representative MCL cell lines, we confirmed PRMT5 inhibition disrupted the physical interaction between AKT and FOXO1 (**Figure 2-3A**). Using immunofluorescence, we evaluated the nuclear localization of FOXO1 in

CCMCL1 and Z-138, comparing control and PRMT5 inhibited cells. Within the nuclear compartment, we saw increased levels of FOXO1 following PRMT5 inhibition (both $p < 0.001$) (**Figure 2-3B**). This observation led us to explore FOXO1 recruitment on potential target promoters.

PRMT5 inhibition promotes the expression of pro-apoptotic BCL-2 family proteins

In order to determine the downstream response of FOXO1 activation, CCMCL1 cells were treated with PRT382 for 48 hours and then processed for ChIP sequencing. Among those genes associated with FOXO1 peaks of particular interest were genes in the BCL-2 family (**Figure 2-4A**). This collection of proteins containing a BH3 motif, includes both pro-apoptotic and pro-survival proteins, where the balance of concentrations and interactions determine whether a cell enters intrinsic apoptosis. We found FOXO1 to be associated with the pro-apoptotic genes *BAX*, *BAK1*, *BIK*, and *BBC3* (**Figure 2-4A**). These genes produce either direct effectors of apoptosis as in the case of BAX and BAK1, or mediate apoptotic activity as in the case of BIK and BBC3. In support of the ChIP-seq data, we identified the presence of a FOXO1 consensus binding motif (5'-GTAAA(T/C)A-3') [249] in the *BAX* gene promoter (**Figure 2-4B**). ChIP q-PCR confirmed that FOXO1 was significantly enriched on the *BAX* gene promoter in Z-138, Maver-1 and SP53 cell lines following PRT382 treatment (**Figure 2-4C**). ChIP q-PCR on Z-138, CCMCL1, and Maver-1 cell lines also confirmed increased enrichment for FOXO1 binding to the active regulatory regions of *BAK1*, *BIK*, or *NOXA1* when PRMT5 was inhibited (**Figure 2-4D, 2-4E, 2-4F**).

Supporting the relevance of FOXO1 enrichment on these genes, qPCR showed several pro-apoptotic BH3 family members were upregulated on a transcript level after PRMT5 inhibition (**Figure 2-5A, 2-5B, 2-5C**). Similarly, immunoblot assay showed that BAX, BAK1, and BBC3 protein levels were all upregulated in multiple MCL cell lines following six days of PRMT5 inhibition (**Figure 2-6A, 2-6B, 2-6C, 2-6D**). BAX was the most frequently upregulated and had the greatest fold increase across all cell lines with PRMT5 inhibition (**Figure 2-6B**). These data show that pro-apoptotic proteins are upregulated with PRMT5 inhibition and suggests that FOXO1 regulates the expression of the key pro-apoptotic protein BAX.

PRMT5 and BCL-2 inhibition drives synergistic MCL cell death

Given the observed upregulation of pro-apoptotic proteins including BAX with PRMT5 inhibition, we looked for an agent that could capitalize on this shift in intrinsic apoptotic signaling. The protein BCL-2 binds and blocks the activity of BAX, so we chose to test venetoclax, a BCL-2 inhibitor approved for the treatment of chronic lymphocytic leukemia [250]. As a single agent, venetoclax produced IC₅₀ values below 1 μ M in four of the MCL lines tested (**Figure 2-7A**). We then evaluated the synergy of venetoclax in combination with PRT382 using the Loewe Model of Synergy computed by Combenefit ([246, 251] **Figure 2-7B, 2-7C**). Z-138 was found to be the most sensitive to the combination treatment with synergy scores reaching as high as 63.9 (**Figure 2-7B**) while other lines such as Mino and Jeko were found to be moderately sensitive. The range of sensitivities across nine MCL cell lines, as shown in **Figure 2-7B**, shows significant synergy in six of the nine cell lines tested (Synergy score 12.8 - 63.9). This led us to explore

why three lines showed resistance and whether we could determine a biomarker correlative to the degree of synergy.

BCL-2 expression is a biomarker for synergy response in MCL cells

We explored the basal expression of key proteins to determine if a correlative pattern of expression associated with the level of anti-tumor synergy observed in each cell line (**Figure 2-13A**). Baseline levels of BCL-2, BAX, FOXO1, PRMT5 and the ratio of BAX to BCL-2 expression were all correlated to Loewe synergy scores. BCL-2 expression, with Maver-1 censored as an outlier, provided the strongest correlation (Spearman's $r = 0.4524$, $p = 0.2675$) where higher expression of BCL-2 resulted in higher synergy scores (**Figure 2-8B**). FOXO1 and PRMT5 expression had negative correlations with synergy score while BAX expression and the ratio of BAX to BCL-2 resulted in positive correlations (**Figure 2-8C-F**). Clustering the cell lines by p53 status (WT or mut) showed no difference in synergy scores (**Figure 2-9A**, $p > 0.529$). Five patient samples and two MCL PDX model cells were also analyzed for basal expression of BAX, BCL-2, FOXO1, and PRMT5 (**Figure 2-9B**). BCL-2 was found to be highly expressed in all samples tested, suggesting a high level of synergy could be achieved.

PRMT5 inhibition in combination with venetoclax induces intrinsic apoptosis dependent on BAX expression

To determine the mechanism driving cell death with drug treatment, caspase 3, 8 and 9 expression was examined in cells treated with DMSO, PRT382 only, venetoclax only, or the combination. The cleavage of caspase 9, indicating intrinsic apoptosis, was

seen as early as day two (**Figure 2-10A**) while caspase 8 remained relatively unchanged showing little to no extrinsic apoptosis signaling. Corresponding with viability measurements, the greatest cleavage of caspases 3 and 9 was seen in the combo treatment cohort on day 6 (**Figure 2-10B**).

From our immunoblots, we determined that BAX was the most commonly and significantly upregulated protein among the pro-apoptotic BCL-2 family. To examine the importance of BAX for venetoclax activity and the synergistic response with combination treatment, we created BAX knock down lines with Z-138, Jeko, Granta-519, and Maver-1 using shRNA (**Figure 2-11A**). As BAK1 is also capable of triggering the mitochondrial depolarization that leads to intrinsic apoptosis, we also created shRNA knock downs using the same four cell lines (**Figure 2-11A**). Each line was treated with DMSO, PRT382, venetoclax, or the combination for four days. Annexin V/PI stain with flow cytometry was used to measure the viability of each treatment. As seen in **Figure 2-11B**, BAX knock down was protective in Z-138 ($p < 0.0001$) while both knock down of BAX and BAK1 were protective in Jeko ($p = 0.0285$, $p = 0.0102$) (**Figure 2-11C**). Granta-519 also showed a trend toward rescue with BAX knock down ($p = 0.223$) (**Figure 2-11D**) while neither protein knock down rescued Maver-1 cells (**Figure 2-11E**). The trend in Granta-519 may be due to the moderate knock down achieved in this cell line (**Figure 2-11A**).

PRMT5 and BCL-2 inhibition is synergistic *in vivo* reducing disease burden and improving survival.

One cell line derived xenograft (CDX) and two MCL PDX models were used to test the combination of venetoclax and a PRMT5 inhibitor. The CDX was a flank model

using Granta-519 cells engrafted subcutaneously. The sub therapeutic dose of 30mg/kg dosed daily via oral gavage of PRT543, the clinical PRMT5 inhibitor for which PRT382 is the tool compound, was established in this model (**Figure 2-12A**). The combination of sub-therapeutic PRT543, and sub-therapeutic venetoclax showed decreased tumor burden (**Figure 2-12B**) compared to progressive disease in the single agent cohorts. The weight loss observed in this experiment (**Figure 2-12C**) could be due to similar causes seen in the PRT382 CCMCL1 CDX experiments, and a modified dosing schedule could have limited this complication.

This CDX experiment led us to test the combination in two systemic PDX MCL models, PDX.AA.MCL developed from an ibrutinib resistant patient sample in the OSU Lymphoma Research Group [248] and PDX.IR.96069 an ibrutinib resistant model obtained from PRoXe [204]. NSG mice were engrafted with the respective cells and monitored weekly by flow cytometry for circulating huCD19+/huCD5+ cells. Once disease was detectable by flow cytometry, treatment began, four days on, three days off for both drugs (**Figure 2-13A**, see **Appendix F**). Disease burden continued to be monitored weekly by flow cytometry and examination of mice. Body weight was maintained during the course of treatment (**Figure 2-13D, 2-10C**). The control and PRT only cohorts reached a median survival of 58 days and 66 days in the AA model and 53 days and 77 days in the 96069 model (**Figure 2-13B, 2-14A**). The venetoclax only cohort in the AA model had also reached ERC with a median survival of 73 days (**Figure 2-13B**) while a median survival was not reached in the 96069 model (**Figure 2-14A**). During the course of the experiment, the combination treatment reduced the tumor burden in the peripheral blood below the level

of detection via flow cytometry (**Figure 2-13C, 2-14B**) which translated into a statistically significant survival advantage as no mice had reached ERC by the end of experiment (day 100, 104) (**Figure 2-13B, 2-14A**). These results show significant synergy between PRMT5 and BCL-2 inhibition, reducing systemic disease burden and improving survival in two MCL PDX models.

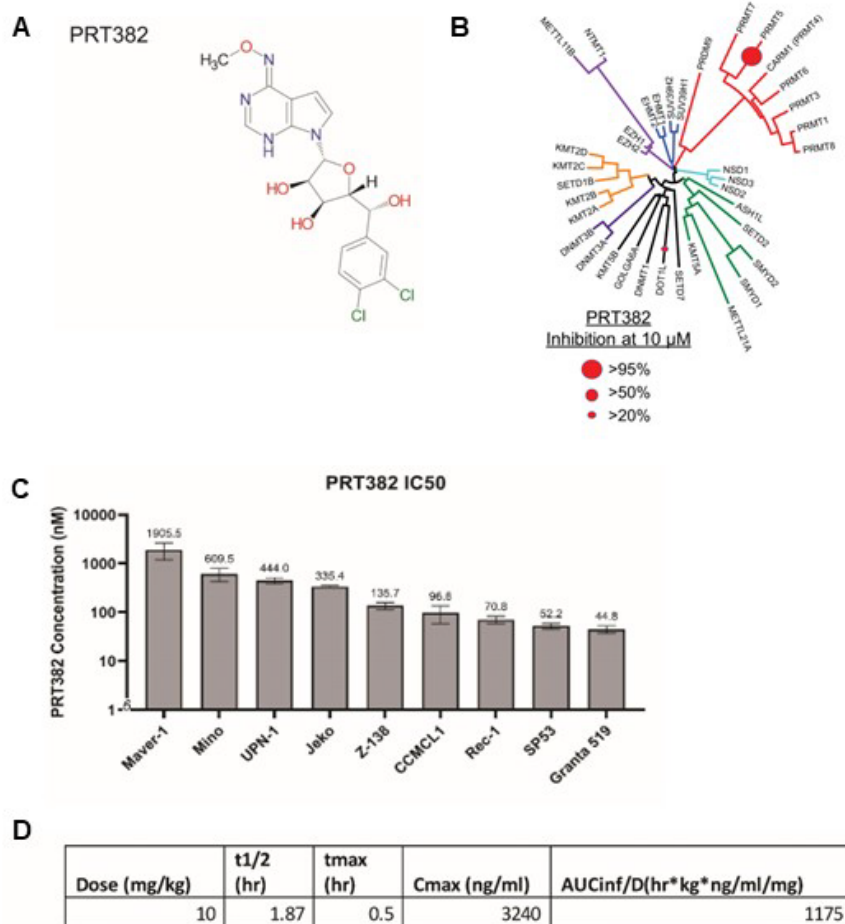


Figure 2-1: PRT382 is a selective and effective inhibitor of PRMT5

A) Chemical structure of PRT382 courtesy of Prelude Therapeutics B) Enzymatic selectivity of PRT382 including other members of the PRMT family. Figure originally published in Hing et al.. [143]. C) IC₅₀ of nine MCL cell lines as determined by the percentage of double negative cells after Annexin V/PI staining and flow cytometry after nine days of PRT382 treatment. D) Pharmacokinetic data of PRT382 dosed in mice. Data provided by Prelude Therapeutics.

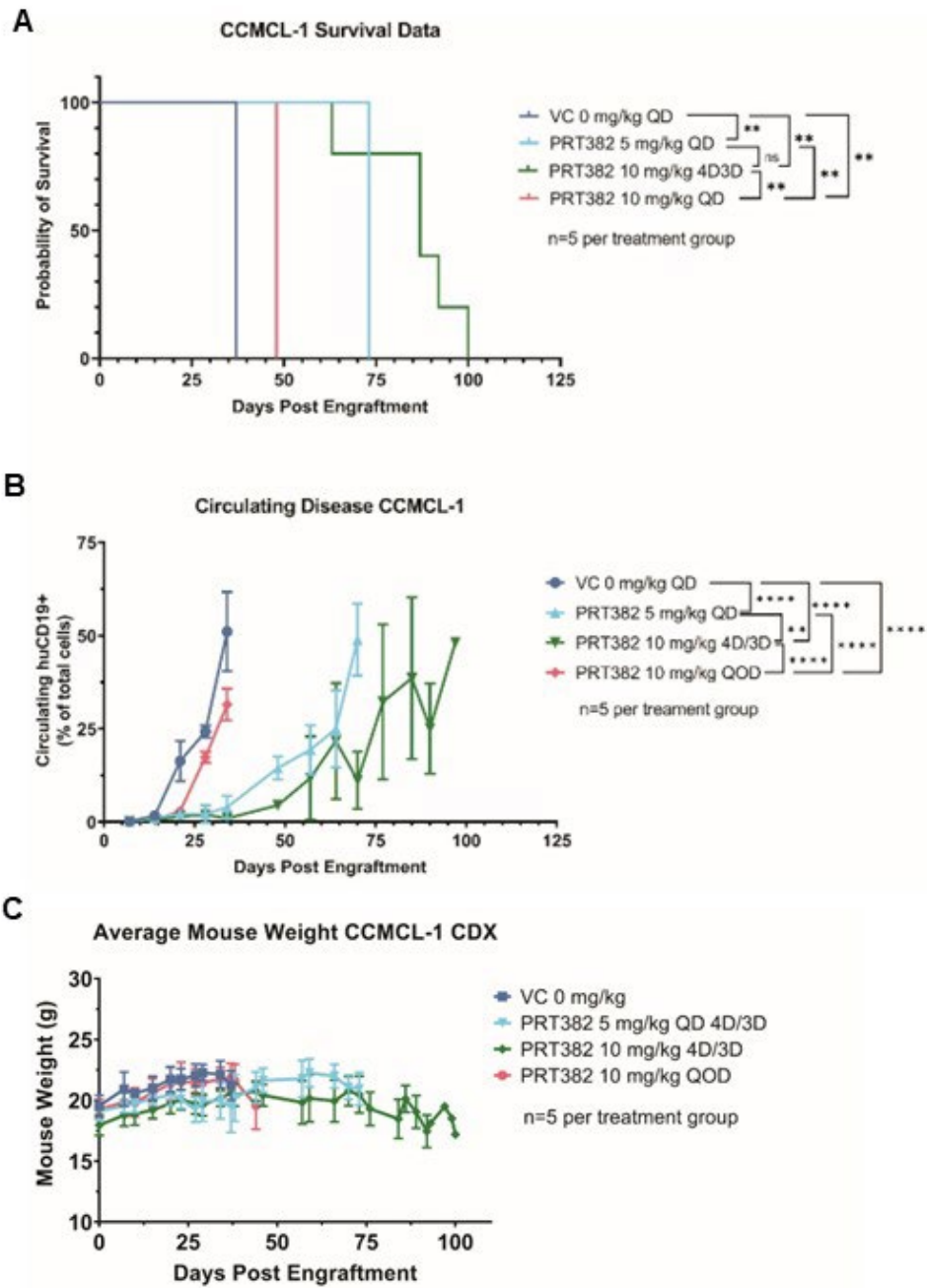


Figure 2-2: PRT382 dosing provides a survival advantage in *in vivo* model of MCL

A) Kaplan Meier of survival of the CCMCL1 CDX model of MCL treated with 5mg/kg daily, 10mg/kg four days on, three days off, or 10mg/kg daily. B) Measurement of

circulating disease as determined by the percentage of circulating lymphocytes that are huCD5/huCD19+ measured via flow cytometry. C) Weights of each group over the course of treatment. A log rank test with significance was used for A. Generalized Estimating Equations (GEE) with autoregressive correlation structure was used to compare the disease burden over time in B. * P<0.05 ** P<0.01 *** P<0.001 ****P<0.0001. Error bars show standard deviation of the data.

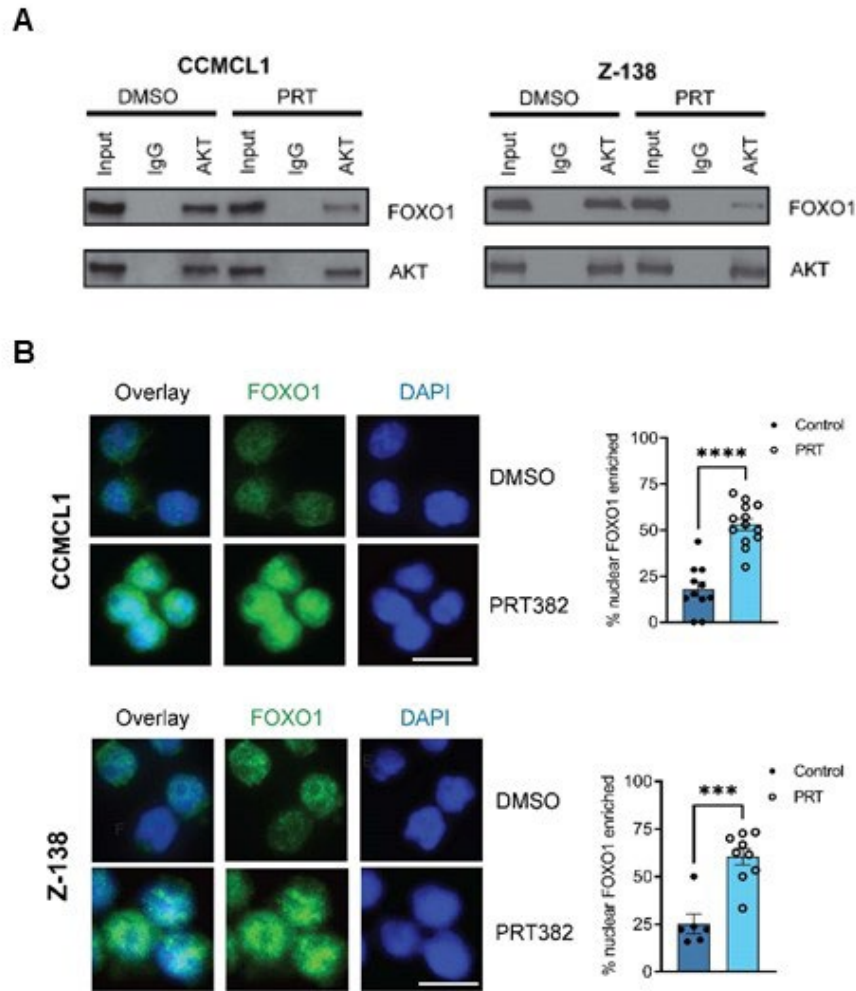


Figure 2-3: PRMT5 inhibition disrupts the AKT:FOXO1 interaction and causes FOXO1 nuclearization

A) Immunoprecipitation of AKT in CCMCL1 and Z-138 cells showing the decrease in interaction between AKT and FOXO1 with treatment with PRT382. N = 2

B) Immunofluorescence of CCMCL1 and Z-138 cell lines looking at the localization of FOXO1 after 72 hours of treatment with PRT382 or DMSO. Cells are stained with FOXO1 primary antibody and alexafluor488 conjugated donkey anti-rabbit secondary. Cells were

also stained with DAPI. Images taken on an EVOS FL Cell Auto Imaging system at 40x magnification. The percentage of cells with FOXO1 enriched in the nucleus in the microscopic field was plotted. At least six view fields were quantified for each condition. Scale bar = 10 μ M.. A student's t test was performed to show significance for B * $P < 0.05$ ** $P < 0.01$ *** $P < 0.001$ **** $P < 0.0001$. Error bars show standard deviation of the data.

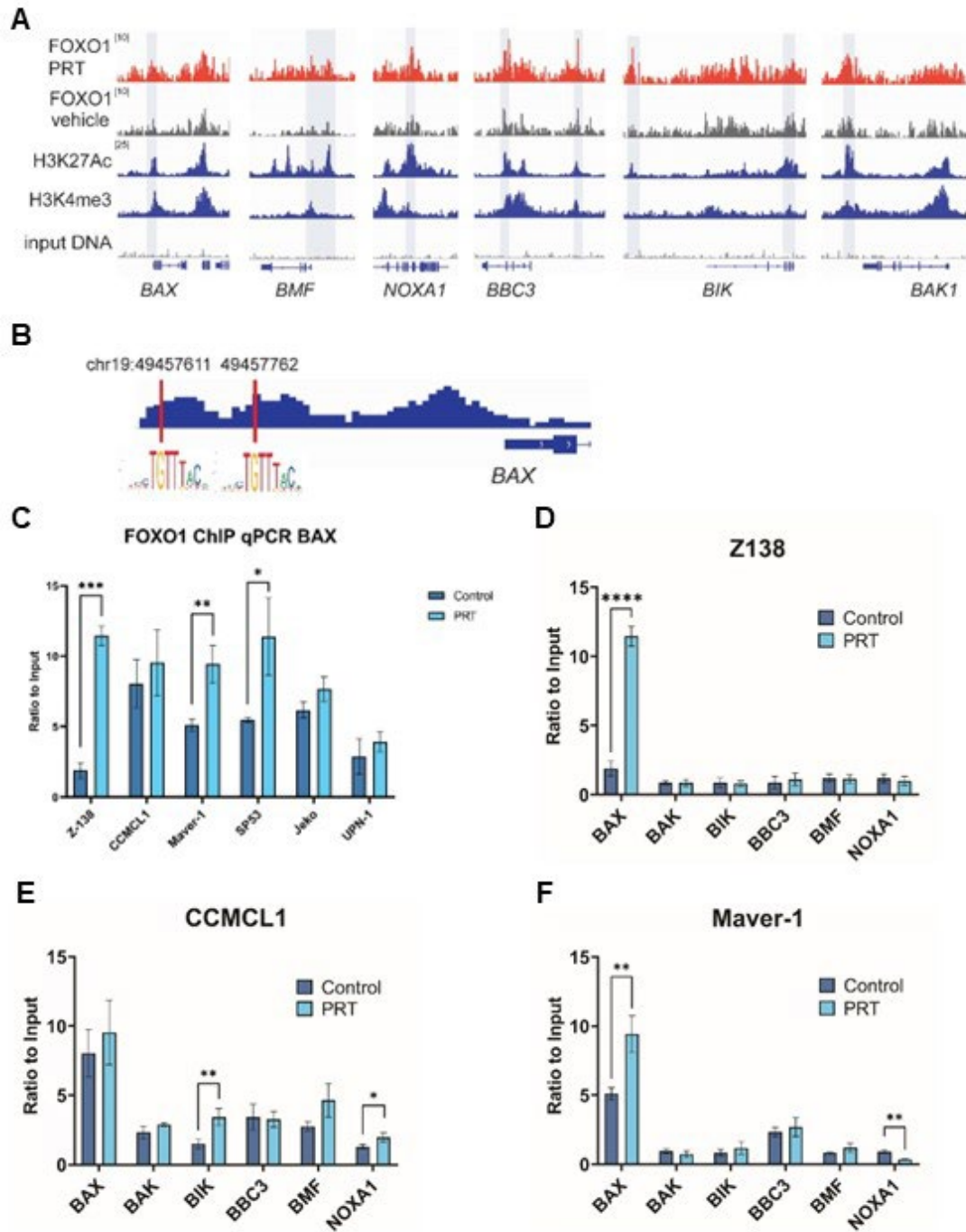


Figure 2-4: ChIP seq of FOXO1 and ChIP qPCR show *BAX* as a target of FOXO1 and significantly upregulated with PRMT5i

A) Visualization of representative ChIP-seq tracks on selected BCL-2 family genes. Analysis was performed on FOXO1 in CCMCL1 cells treated for 48 hours with PRT382 or DMSO as a control. H3K27Ac and H3K4me3 tracks show enhancer and promoter regions. IgG was used for negative control. B) FOXO1 consensus sequence was confirmed in the promoter sequences of *BAX* upstream of the gene body C) FOXO1 ChIP qPCR of *BAX* showing significant enrichment in Z-138, Maver-1, and SP53 as well as a trend in CCMCL1, Jeko, and UPN-1 (N=3). ChIP qPCR of pro-apoptotic genes BAX, BAK1, BIK, BBC3 (PUMA), BMF, and NOXA with DMSO or PRT382 treatment in D) Z-138, E) CCMCL1, and F) Maver-1. A student's t test was performed to show significance for C, D, E, and F. * P<0.05 ** P<0.01 *** P<0.001 ****P<0.0001. Error bars show standard deviation of the data.

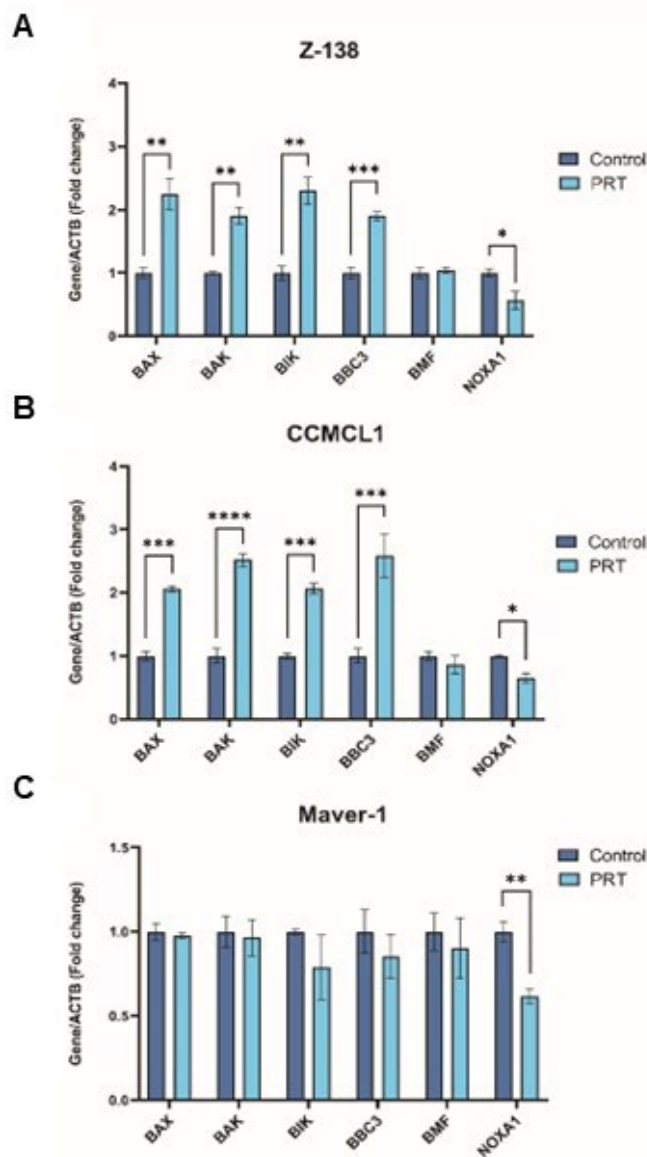


Figure 2-5: PRMT5 induces increased mRNA levels of multiple pro-apoptotic genes

qPCR measurement of the transcripts of select BCL-2 family proteins in A) Z-138, B) CCMCL1, and C) Maver-1 after PRT382 treatment (N=3). A student's t test was performed to show significance. * P<0.05 ** P<0.01 *** P<0.001 ****P<0.0001. Error bars show standard deviation of the data.

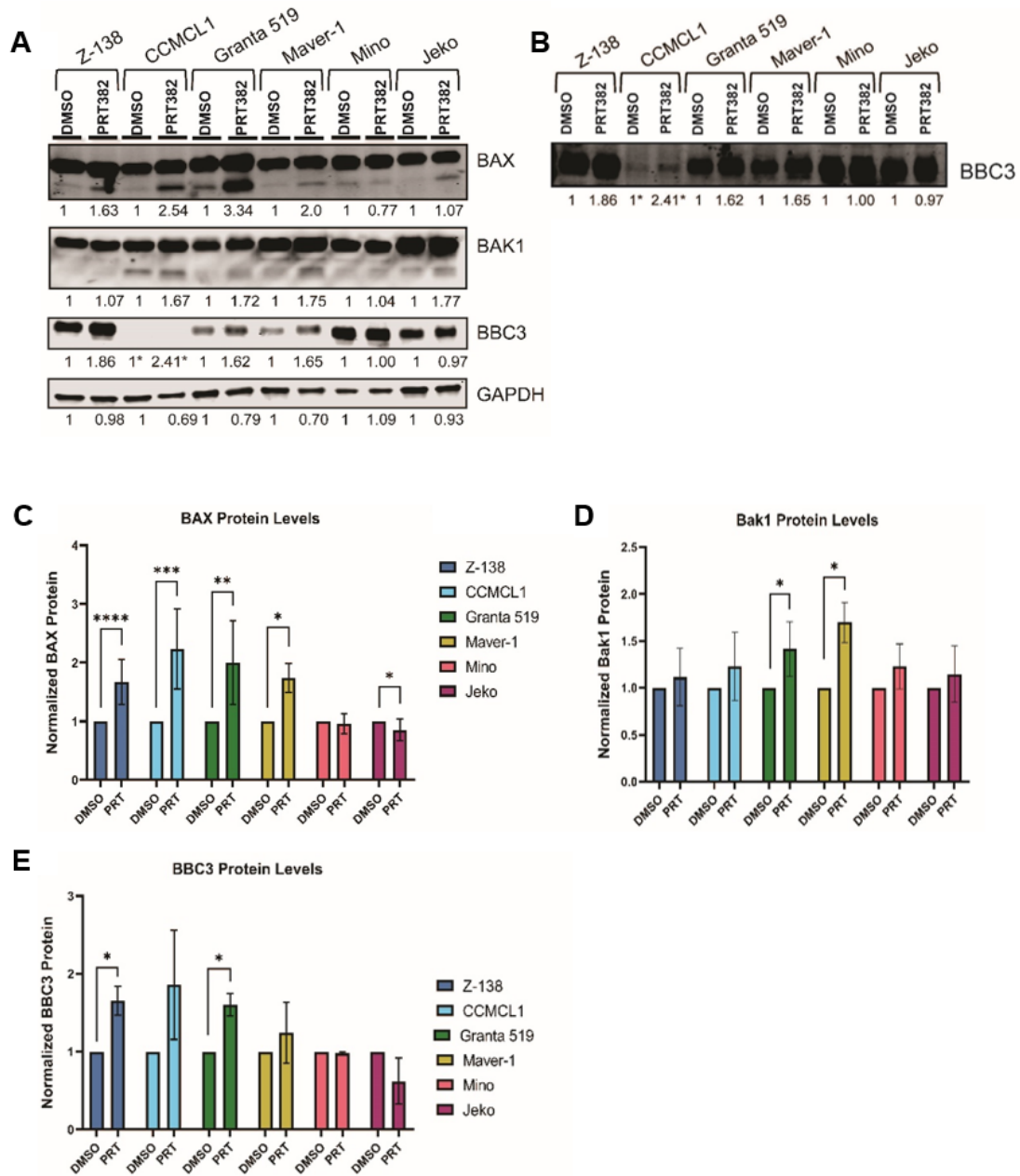


Figure 2-6: PRMT5i induces expression of pro-apoptotic BCL-2 family proteins

A) Representative western blot of six MCL cell lines after treatment with PRT382 or DMSO showing the levels of BAX, BAK1, and BBC3 including their cleaved forms.

B) An overexposed blot with BBC3 as expression in CCMCL1 is low compared to the

other cell lines. Quantification of C) BAX, D) BAK1, and E) BBC3 (PUMA) protein levels with PRT382 treatment (N>3). A student's t test was used to determine significance for C-F. * P<0.05 **P<0.01 ***P<0.001 ****P<0.0001 Error bars show standard deviation of the data.

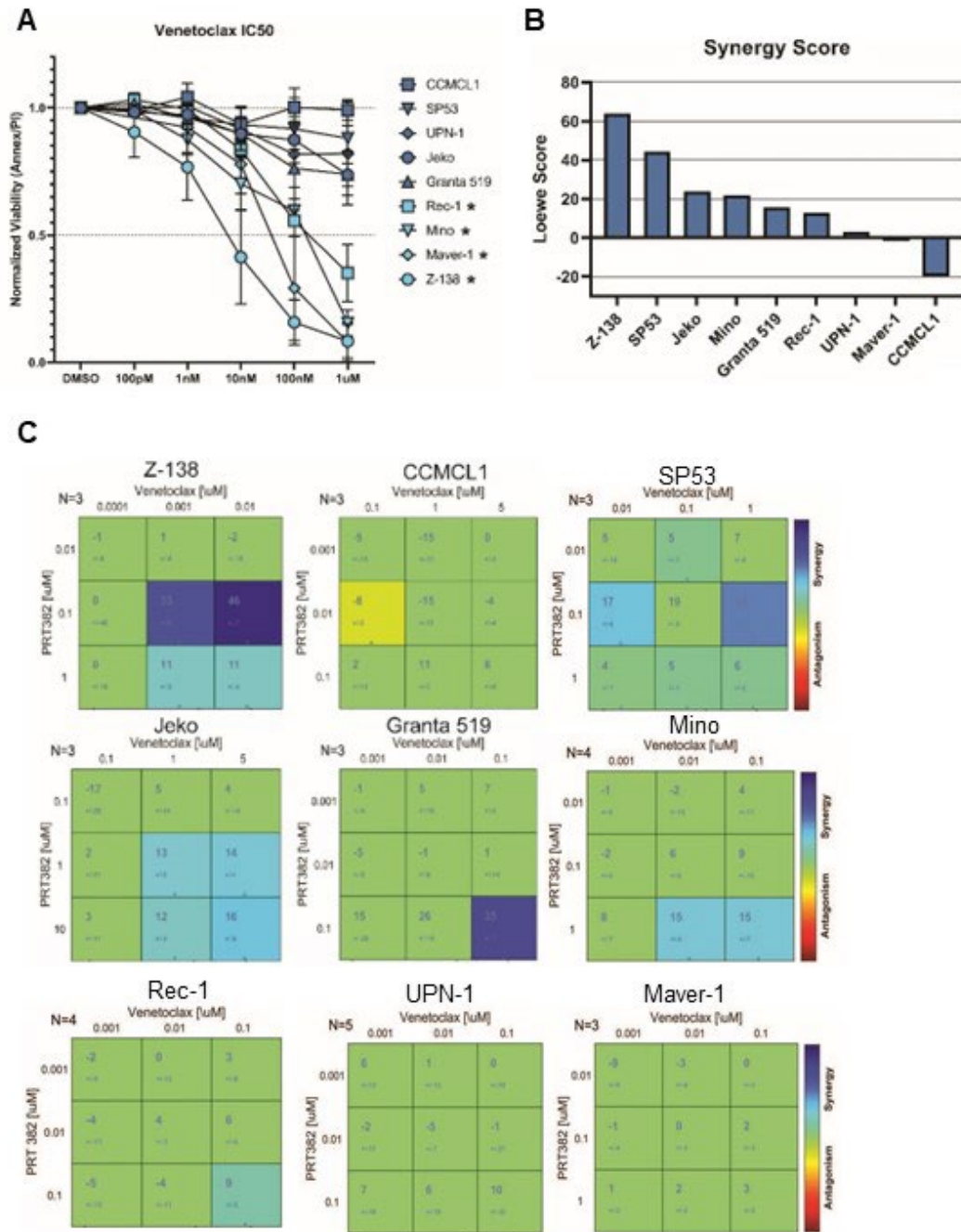


Figure 2-7: Six of nine MCL cell lines show synergistic killing with treatment with PRT382 and BCL-2 inhibitor, venetoclax

A) IC50 of nine MCL cell lines measured with annexin V/PI and flow cytometry after 72 hours of treatment with venetoclax. Cell lines with an IC50 below 1uM are starred and considered sensitive. N>3 B) 001Single synergy values calculated from at least three separate replicates for each cell line. The same levels of synergy are used as with the synergy matrices. N>3 C) Synergy matrices calculated through Combenefit [47] using the Lowe model of synergy. Values below -10 are antagonistic, -10 to 10 are additive, and values over 10 are synergistic. Significance is shown by stars at the bottom of each box. *P<0.05 **P<0.01 *** P<0.001.

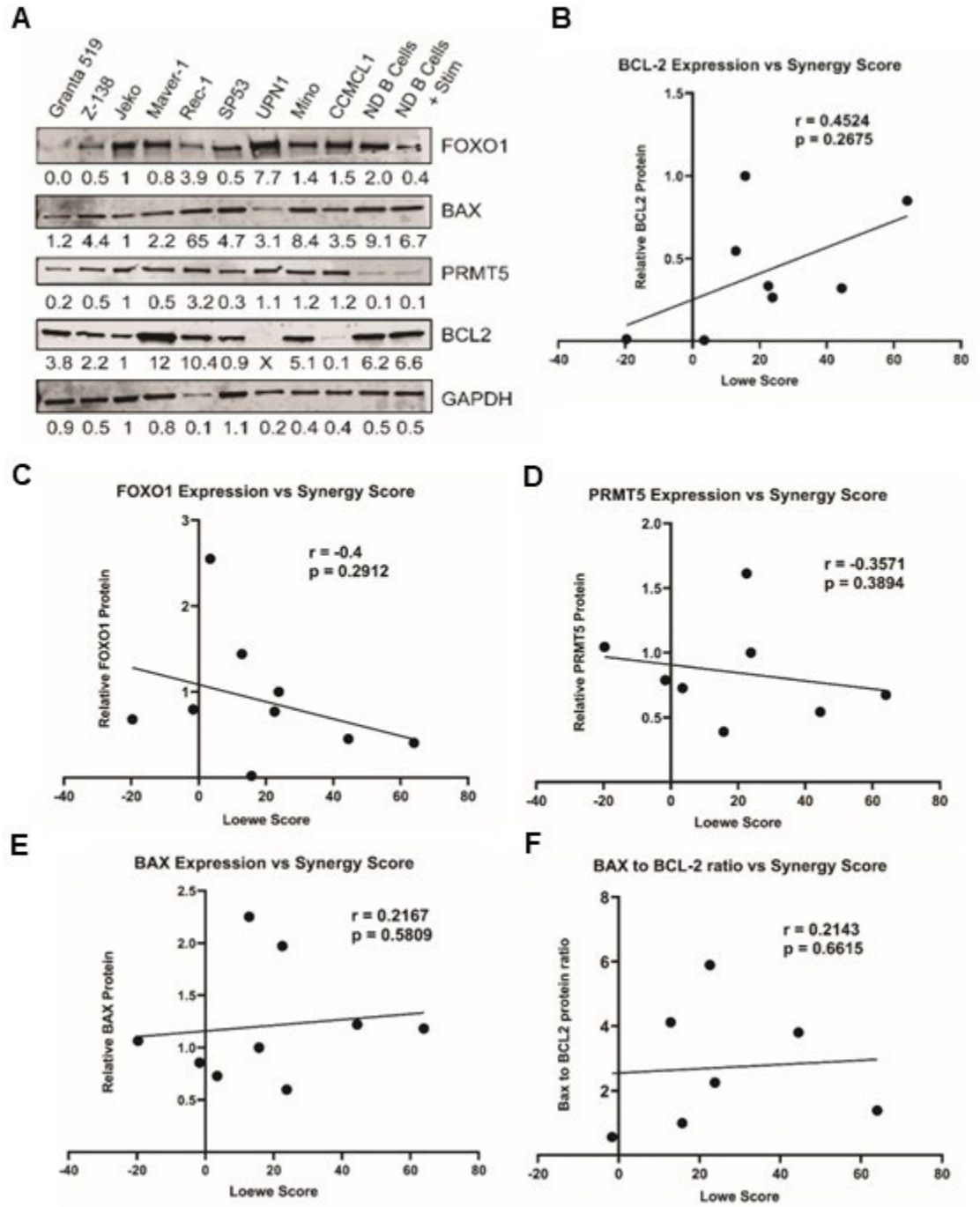


Figure 2-8: BCL-2 expression correlates to synergy score observed between PRMT5 and BCL-2 inhibition

A) Western blot showing the baseline levels of key proteins in nine MCL cell lines and normal donor B Cells (ND B cells) without and with IgG stimulation. Values are corrected by the loading control and normalized to Jeko. Note: FOXO1 expression in Granta-519 is low compared to the other cell line. See Figure 9 A for a secondary western blot. The Spearman's correlation between the baseline level of B) BCL-2 expression, C) FOXO1 expression, D) PRMT5 expression, E) BAX expression or F) BAX:BCL-2 expression ratio to Loewe synergy score as determined by Combenefit. Maver-1 was removed from the BAX analysis, CCMCL1 and UPN-1 were removed from the BAX:BCL-2 analysis, and REC-1 from the PRMT5 analysis due to outlier status (ROUT method, Q = 1%).

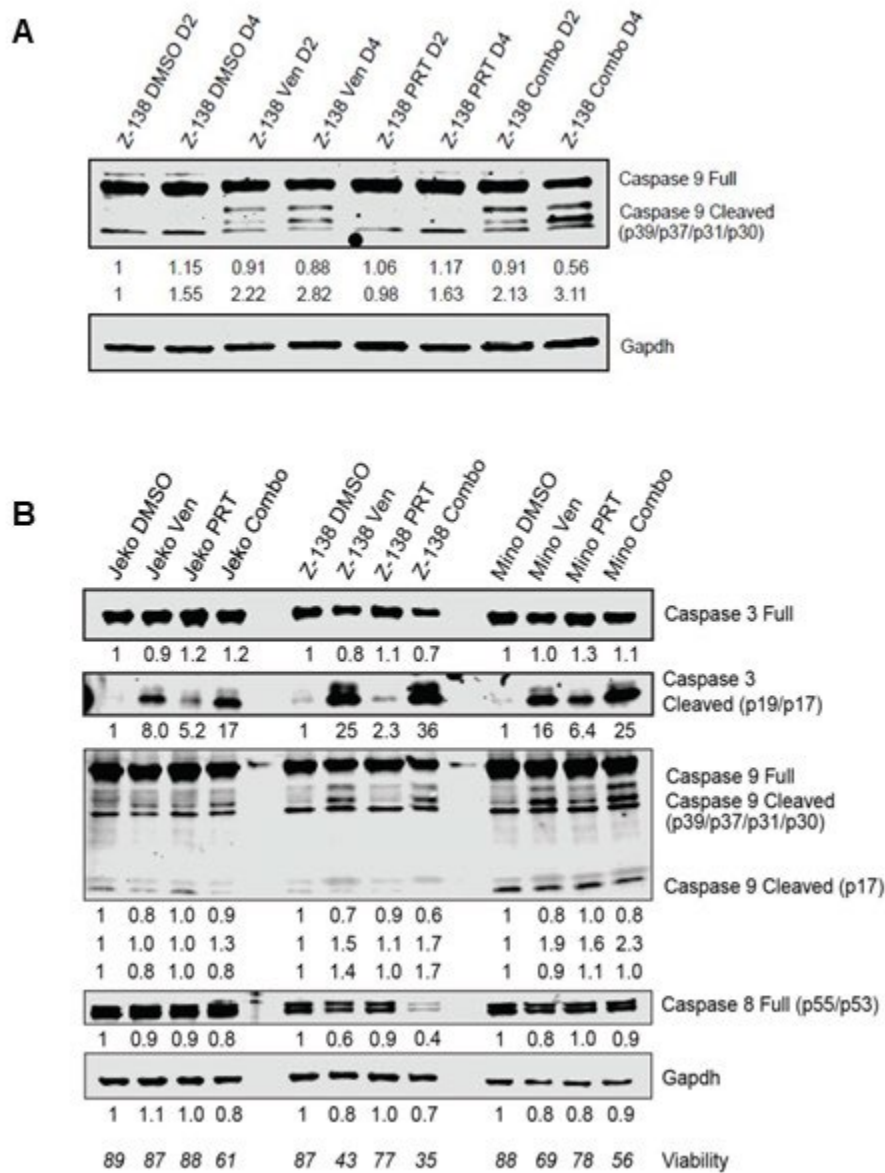


Figure 2-10: PRMT5i and BCL-2i combination therapy induces intrinsic apoptosis within 48 hours of treatment

A) Western blot of control, venetoclax, PRT382, or combination treated Z-138 cells after 48 and 96 hours of treatment blotting for caspase 9. B) Western blot showing caspase

activity with control, single agent, and combo treated Jeko, Z-138, and Mino MCL cell lines. Caspase cleavage was used as an indication of activity with caspase 8 being indicative of extrinsic apoptosis, caspase 9 of intrinsic apoptosis, and caspase 3 of general apoptosis N=2

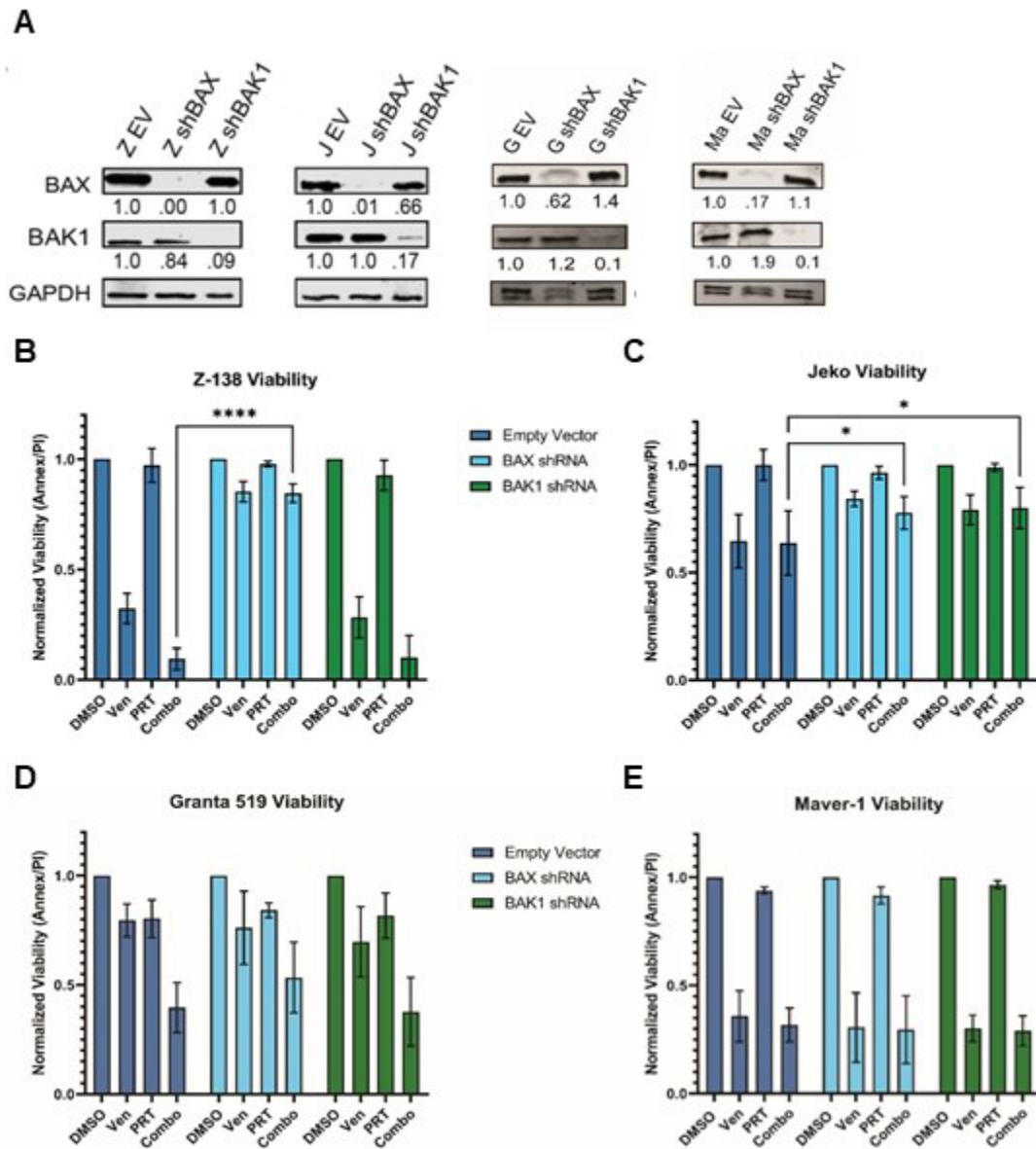


Figure 2-11: PRMT5i and BCL-2i synergy is dependent on BAX expression

A) Western blots showing the knock-down of BAX and BAK1 protein after transfection with shRNA against these transcripts in Z-138, Jeko, Granta-519, and Maver-1 cells. Values are adjusted by GAPDH and normalized to the empty vector control. Viability

of B) Z-138, C) Jeko, D) Granta-519, and E) Maver-1 knock down variants with control, single agent, or combo treatment. At least three replicates were completed, and data was measured with annexin V/PI staining and flow cytometry. A two-way ANOVA with multiple comparisons was used to determine statistical significance B-E. * $P < 0.05$
** $P < 0.01$ *** $P < 0.001$. **** $P < 0.0001$

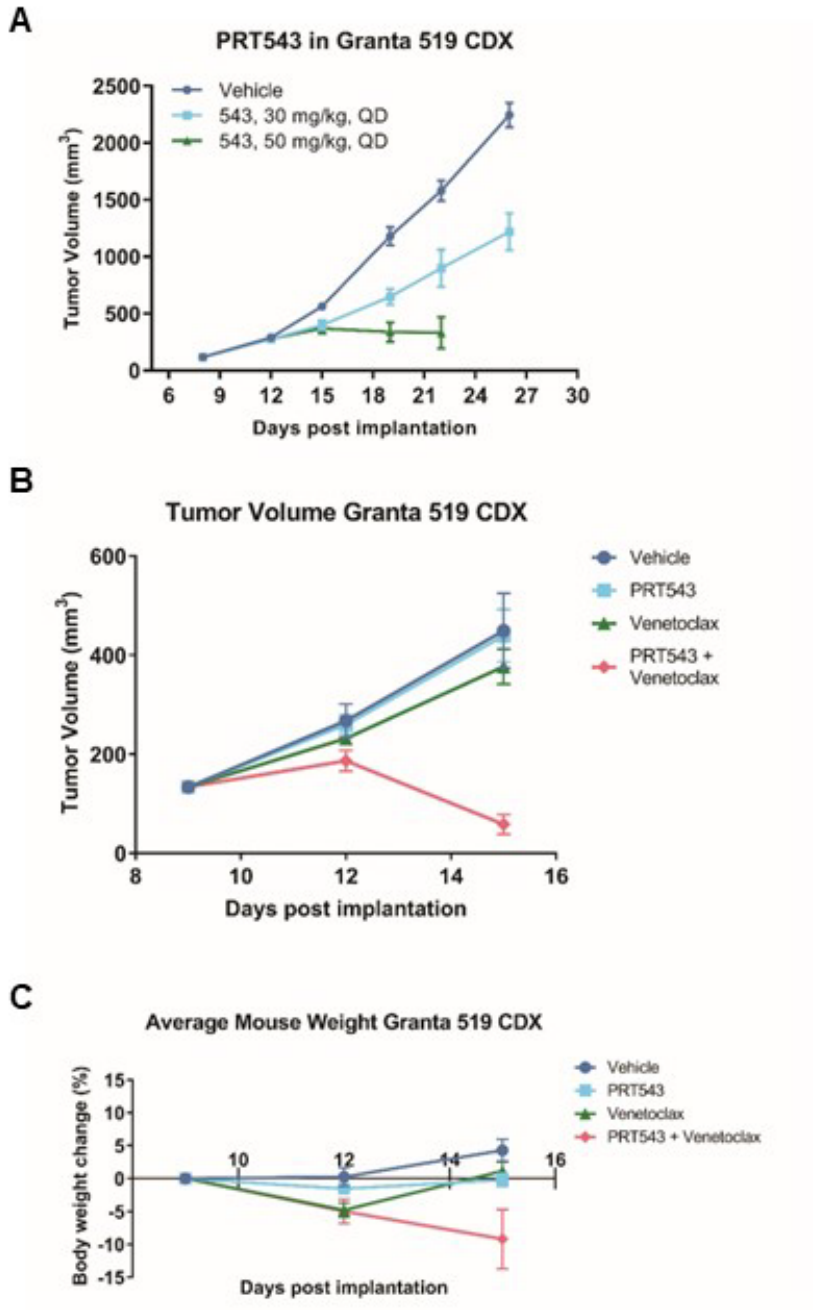


Figure 2-12: PRT543 is synergistic with venetoclax in Granta-519 CDX model of MCL

A) Tumor volume of the Granta-519 CDX model with vehicle, PRT543 at 30mg/kg daily, or 50mg/kg daily. B) Tumor volume of the Granta-519 CDX model treated with vehicles, PRT543 30mg/kg, venetoclax at sub-therapeutic dose, or the combination of the two agents daily. C) Weight of the vehicle, PRT543, venetoclax, or combination treated mice. Error bars represent standard deviation.

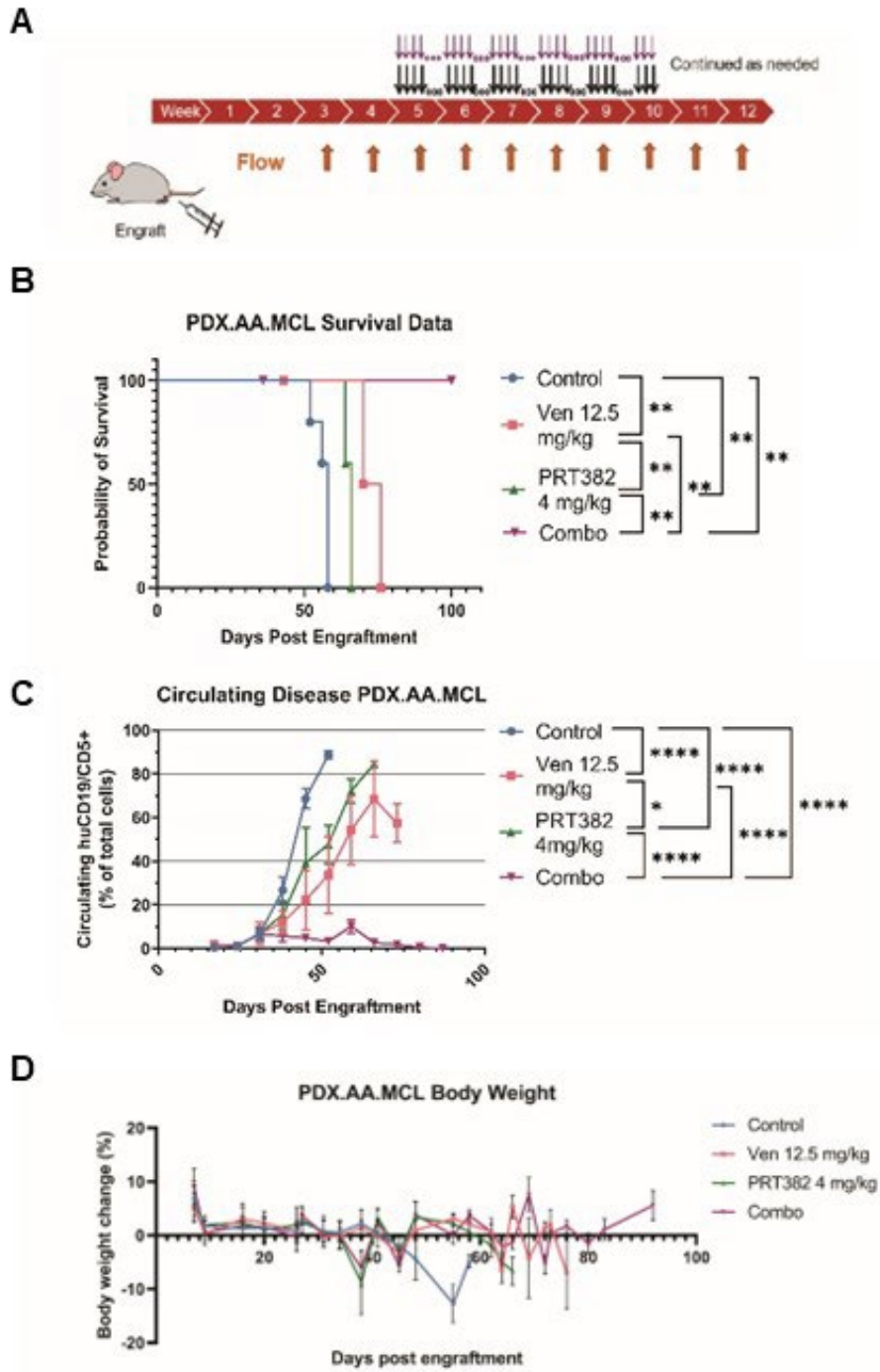


Figure 2-13: PRT382 and venetoclax are synergistic in the PDX.AA model of MCL

A) Schematic showing the setup of *in vivo* experiments. Mice were engrafted on day zero and weekly bleeds with flow cytometry were used to assess circulating disease burden. Once approximately 1% of the circulating lymphocytes were MCL cells (huCD5+/huCD19+), treatment began. Mice were treated with each single agent or the combination four days on, three days off. B) Kaplan-Meier curve showing survival of the PDX.AA.MCL model. Median survival was vehicle 58 days, PRT382 63 days, venetoclax 73 days, and the combo did not reach a median survival by experiment end of 101 days ($P < 0.0001$) C) A graph of circulating disease burden over time in the PDX.AA.MCL model measured as a percentage of huCD5+/huCd19+ cells in the lymphoid compartment. D) The body weight change from measurement to measurement of each treatment group over time. A greater than 10% change resulted in a drug holiday while greater than 20% was considered ERC. A log-rank test for trend was performed on the survival data in B. Generalized Estimating Equations (GEE) with autoregressive correlation structure was used to compare the disease burden over time in C* $P < 0.05$ ** $P < 0.01$ *** $P < 0.001$ **** $P < 0.0001$

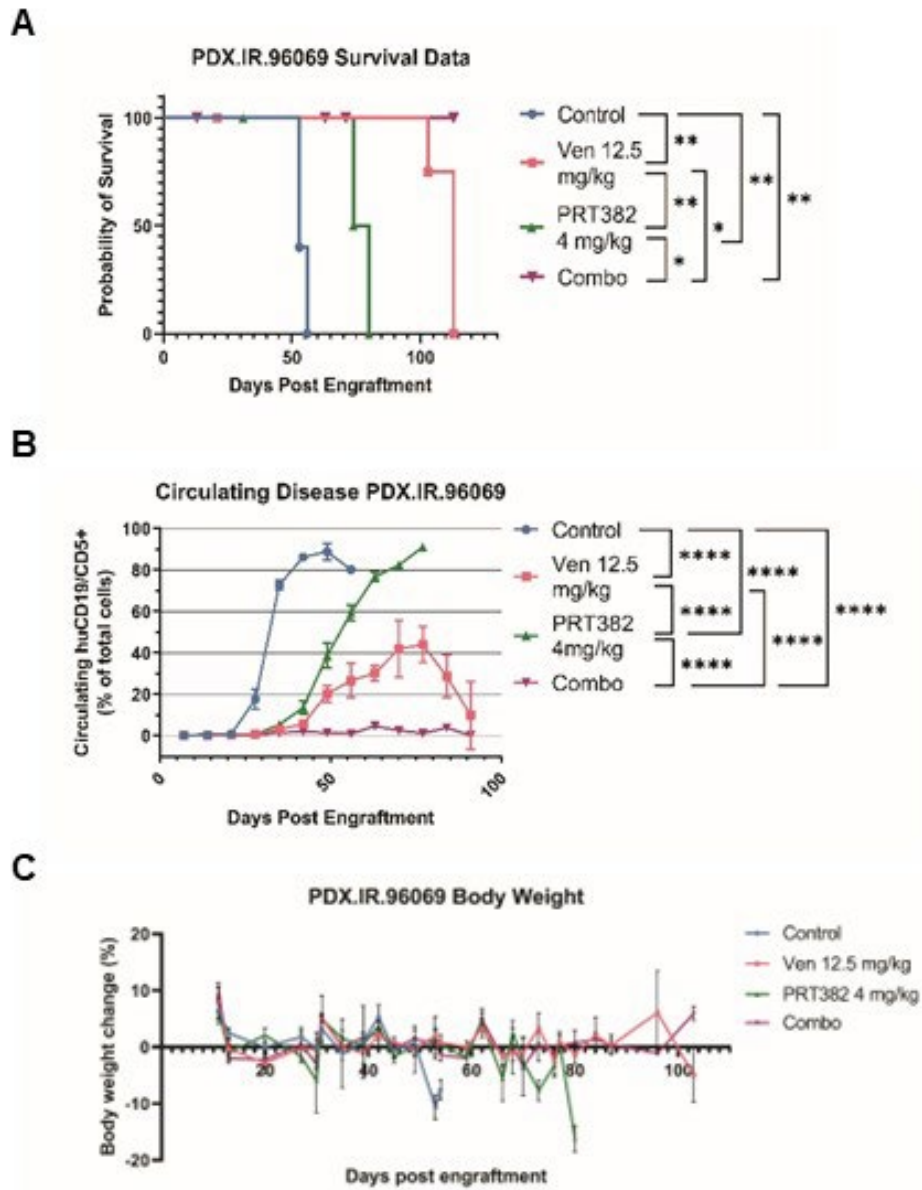


Figure 2-14: PRT382 and venetoclax are synergistic in the PDX.IR.96069 model of MCL

A) Kaplan-Meier curve showing the survival of the PDX.IR.96069 model. Median survival was vehicle 53 days and PRT382 77 days. The venetoclax and combo groups did not reach a median survival by experiment end at 104 days B) A graph of circulating disease burden

over time in the PDX.IR.96069 model measured as a percentage of huCD5+/huCd19+ cells in the lymphoid compartment. C) The body weight change from measurement to measurement of each treatment group over time. A greater than 10% change resulted in a drug holiday while greater than 20% was considered ERC. A log-rank test for trend was performed on the survival data in A. Generalized Estimating Equations (GEE) with autoregressive correlation structure was used to compare the disease burden over time in B.* P<0.05 **P<0.01 ***P<0.001 ****P<0.0001

2.4 Conclusions

The discovery of new therapeutic targets and strategies is essential for patients with MCL as this disease is currently incurable. While targeted therapies such as ibrutinib have improved outcomes for MCL patients over the last ten years, patients almost uniformly develop progressive, resistant disease and have very poor prognoses [252, 253]. Here, we describe novel mechanistic data and provide rationale for combining PRMT5 and BCL-2 inhibition for treating patients with MCL. With PRMT5 inhibitor we observed a physical dissociation of FOXO1 from AKT, freeing it from inhibition, and facilitating its nuclear translocation, where it promotes the transcription of a key BCL-2 family gene, *BAX*. This novel PRMT5-AKT-FOXO1-BCL-2 family axis was observed in multiple MCL cell lines. Modulation of this axis through the inhibition of PRMT5 created a sensitivity to the BCL-2 inhibitor venetoclax, as shown by synergistic cell death with combination treatment *in vitro* and *in vivo*.

Currently, patients who relapse on ibrutinib have few available lines of treatment and very poor prognosis [253, 254]. Of the five ibrutinib resistant cell lines assessed, three lines show synergistic cell death with PRMT5 and BCL-2 inhibition. The three murine models used for the combination studies are also ibrutinib resistant as previously determined by *in vitro* testing for Granta-519, and *in vivo* dosing for the PDX.AA.MCL and PDX.IR.96069 models [248]. Our pre-clinical data show strong evidence in support of using PRMT5 inhibition in combination with venetoclax, especially in setting of ibrutinib resistance.

With increased survival advantage and undetectable disease burden, our *in vivo* models showed impressive responses to combination treatment. This work should be continued to optimize treatment strategies and determine what, if any, remaining disease burden exists in the combination cohort. We are exploring additional treatment regimens, including increasing the dose of PRT382 and venetoclax to therapeutic levels, use of alternative PRMT5 inhibitors, and creating a reduced maintenance dosing regimen for long term survival studies.

Here we focused on the BH3 family genes that showed enrichment for FOXO1 recruitment following PRMT5 inhibition. FOXO1 ChIP sequencing following PRMT5 inhibition revealed over 2000 potential targets providing an opportunity to better understand the biologic relevance of FOXO1 to the pathogenesis of MCL. Interestingly, attempts to create FOXO1 knock down cell lines or use of a small molecule inhibitor resulted in cytotoxicity in all MCL cell lines, a counter-intuitive finding suggesting that FOXO1 is relevant for MCL survival. FOXO1 likely plays a complex role in MCL, acting as an oncogene necessary for maintaining the B lymphocyte lineage transcriptional program to promote MCL survival [255] while, in the context of PRMT5 inhibition, acting as a tumor suppressor [239, 240]. A similar dichotomy has been described by Zhao et al. in colon cancer and HeLa cervical cancer cells where cytosolic FOXO1 was essential for stress induced autophagy but also potential of inducing apoptosis [241]. Our data suggests that PRMT5 inhibition reprograms FOXO1 from an oncogene to a tumor suppressor through its transcriptional program. Further studies are needed to elucidate the context-dependent cellular roles of FOXO1 in PRMT5 driven tumors.

While we found FOXO1 to play a role in the expression of BAX, it may not be the only player at work as multiple pro-apoptotic BCL-2 family proteins were upregulated with PRMT5 inhibition and functioned independent of FOXO1. For example, the Z138 cell line treated with PRT382 showed induction of BAX, BAK1, BIK, and BBC3 at the transcript and protein level while only the *BAX* promoter was enriched for FOXO1 interaction. p53 activity while not correlative to synergy could play a role as it is known as both a target of PRMT5 and a regulator of apoptosis [144]. KLF4 has also been shown to be supported by PRMT5 activity and to repress BAX expression [132]. The increased expression seen here is likely due to promotion from FOXO1 as well as release from inhibitors like KLF4. The lack of endogenous BAX expression in MCL supports the value in increasing expression levels of this key apoptotic protein [183].

In addition to AKT and FOXO1, there are numerous other targets of PRMT5; at the time of publishing, the NCBI showed PRMT5 directly associates with over 300 proteins from which there are numerous downstream targets [256]. As we continue to unravel how PRMT5 orchestrates a malignant, resistant, and stem-phenotype in cancers, following the direct targets such as p53 or smD3 to their effectors will be important. This study shows that PRMT5 inhibition continues to be a promising target in cancer and supports ongoing PRMT5 inhibitor clinical trials. Due to the drug resistant nature of MCL, combining these novel compounds with secondary therapeutics that can take advantage of an exposed vulnerability may prove to be crucial in the treatment of MCL.

Chapter 3: PRMT5 Inhibitors and BH3 Mimetics for the Treatment of MCL

Modified from “PRMT5 Inhibition Sensitizes Mantle Cell Lymphoma to Combination Therapy with BH3 Mimetics” with permission

3.1 Background and Rationale

Mantle cell lymphoma (MCL) is a rare and aggressive B-cell malignancy which constitutes up to 6% of new non-Hodgkin lymphoma cases diagnosed annually [1]. MCL is defined by the t(11;14)(q13;32) chromosomal translocation, which places cell cycle regulator cyclin D1 (CCND1) under transcriptional control of the IGH heavy chain promoter. This mutation results in aberrant CCND1 expression and rapid cell cycle progression, supporting unchecked cell proliferation and lymphomagenesis. The average MCL patient is 70 years old at diagnosis with a 3:1 predominance in males [257]. Due to late median age of diagnosis, many patients cannot withstand aggressive treatment regimens such as immunochemotherapy and autologous stem cell transplantation [257, 258]. Although the majority of MCL patients initially respond to frontline therapies, relapse is virtually inevitable, and to date, there is no cure [258]. The average survival for MCL patients is 5 years, but for those who progress on targeted therapies such as ibrutinib, this is diminished to a bleak 3 months [259]. There is a dire need to develop novel treatment strategies that are better tolerated and improve survival outcomes in patients with mantle cell lymphoma.

Our group has identified the enzyme protein arginine methyltransferase 5 (PRMT5) as a crucial oncogenic driver in MCL [248, 260]. This type II methyltransferase catalyzes the symmetric dimethylation of arginine residues on several of proteins and histones, including P53, P65, NfKB, E2F1, H3R8, and H4R3 [88, 99, 217]. PRMT5 governs a multitude of cellular processes, including transcriptional activation and repression [99], spliceosome activity [261], protein-protein interactions, signal transduction, and subcellular compartmentalization. PRMT5 is also an essential mediator of B-cell development, facilitating germinal center expansion and preventing apoptosis upon activation [105]. Overexpression of PRMT5 has been linked to a number of cancers, including breast cancer [136], lung cancer [129], ovarian cancer [131], glioblastoma [226], and various cancers of the blood [138, 218, 219]. We have demonstrated the therapeutic potential for PRMT5 inhibition in both *in vitro* and *in vivo* MCL models, and multiple clinical trials for PRMT5 inhibitors are currently underway (NCT02783300, NCT03573310, NCT04089449).

Another hallmark of disease in many lymphomas, including MCL, is dysregulation of the intrinsic apoptotic pathway [170, 171]. This essential homeostatic mechanism is used to eliminate damaged or malignant cells from the body and is governed by the B-cell lymphoma 2 (BCL-2) protein family. These proteins can be classified as pro-apoptotic or anti-apoptotic, and they exert their function by engaging in a complex and dynamic set of binding interactions at the mitochondrial outer membrane (MOM). The sum of these interactions determines if a cell will reach its apoptotic threshold, at which point the MOM becomes permeable and the mitochondria depolarizes, triggering irreversible

cytochrome c release, caspase 9 cleavage, and eventual cell death. Malignant cells often rely on anti-apoptotic proteins for survival in the face of DNA damage and death signaling, resulting in their overexpression [170, 171]. Pro-apoptotic proteins can be further classified into effectors, activators, and sensitizers. Effectors BAK, BAX, and BIK form homo-oligomers upon activation and create pores in the outer mitochondrial membrane, resulting in membrane permeabilization, caspase 9 activation, and eventual cell death. Activators Bid and Bim complex with effector proteins to trigger their activation, inducing conformational changes necessary for homo-oligomerization. Anti-apoptotic proteins such as BCL-2, BCL-xL, MCL-1, BCL-w, and Bfl-1 promote cell survival by sequestering activators and effectors, preventing them from exerting their functions. Pro-apoptotic sensitizers interfere with this sequestration by replacing activators and effectors in binding anti-apoptotic proteins.

In our recent work, we demonstrated the therapeutic potential of combining PRMT5 inhibition with BCL-2 inhibition in preclinical mantle cell lymphoma models [260]. We showed that PRMT5 inhibition restored expression of several pro-apoptotic proteins including *BAX*, *BAK*, and *BBC3 (PUMA)*. The PRMT5 inhibitor PRT382 and venetoclax showed high levels of synergism *in vitro* and *in vivo* in two preclinical PDX models. Based on these results and the genetic heterogeneity of MCL in regard to BCL-2 family proteins, we further explored the effects of PRMT5 inhibition on apoptotic signaling and mitochondrial dynamic. In this study we show that PRMT5 inhibition restores pro-apoptotic signaling and sensitizes MCL cells to BH3 mimetics. Using six cell lines, we performed BH3 profiling, genetic analysis, and immunoblotting to create profiles of

response. These were correlated the synergy observed between PRMT5 inhibition with PRT382 and one of three BH3 mimetics (navitoclax, A852, PRT1419). These profiles were then extrapolated to PDX and primary patient samples. In support of this analysis, we saw high levels of synergy between PRMT5 inhibition and navitoclax in the PDX.AA.MCL model and between PRMT5 inhibition and the MCL-1 inhibitor PRT1419 in a Maver1 cell line derived xenograft (CDX).

3.2 Methods

Cell Culture, *In Vitro* Drugging, and Synergy Assessment

Six cell lines were used in this work, including CCMCL1, Granta-519, Z-138, UPN-1, Mino, and Maver-1. Cultures were maintained at 37 degrees Celsius in 5% CO₂ and grown in RPMI 1640 supplemented with 10% FBS, 1% penicillin/streptomycin, and 1% glutamax. All lines were validated via STR testing and mycoplasma surveillance tests were performed biweekly. PRT-382, PRT-1419 and PRT808 chow were provided by Prelude Therapeutics (Wilmington DE), and A-1331852 (Abbvie) and navitoclax (Abbott) were purchased through MedChemExpress. IC₅₀s, defined as a 50% reduction in viable cells, were assessed using Annexin V/PI staining and flow cytometry following nine-day treatment with PRT-382 and three-day treatment with PRT-1419, A-852, or navitoclax. Synergy was assessed via MTS assay following six-day pre-treatment with PRT-382 and three-day combination treatment with PRT-382 paired with PRT-1419, A-852, or navitoclax. Analyses were performed in Synergy Finder using the ZIP model of synergy.

BH3 Profiling

Plate-based BH3 profiling was performed in six cell lines at baseline and following six days of PRT-382 treatment at IC50 dose following the protocol published by the Letai Lab and Dana Farber (<https://letailab.dana-farber.org/bh3-profiling.html>). Peptides were sourced from AAPTEC and solubilized in DMSO at 10mM. Peptide sequences are as follows:

Peptide	Amino Acid Sequence (N-Term → C-Term)
hBIM	Acetyl-MRPEIWIAQELRRIGDEFNA-Amide
hBID-Y	Acetyl-EDIIRNIARHLAQVGDSMDRY-Amide
mBAD	Acetyl-LWAAQRYGRELRRMSDEFEGSFKGL-Amide
mNoxaA	Acetyl-AELPPEFAAQLRKIGDKVYC-Amide
Puma	Acetyl-EQWAREIGAQLRRMADDLNA-Amide
Bmf-Y	Acetyl-HQAEVQIARKLQLIADQFHRY-Amide
Hrk-y	Acetyl-SSAAQLTAARLKALGDELHQY-Amide
Puma2A	Acetyl-EQWAREIGAQARRMAADLNA-Amide

Table 3-1: Table of peptide sequences used for BH3 profiling

Peptide treatments were prepared at 2X final concentration in staining solution comprised of aqueous MEB buffer (150mM mannitol, 10mM HEPES-KOH, 50mM KCl, 0.2mM EDTA, 0.2mM EGTA, 0.1% BSA, and 5mM succinate, pH 7.5 +/- 0.1), 2uM JC-1 dye, 20µg/mL oligomycin, 50 ug/mL digitonin, and 10 mM 2-mercaptoethanol. JC-1, oligomycin, and digitonin stocks were prepared in DMSO at 100 µM, 20mg/mL, and 50

mg/mL, respectively. 2-mercaptoethanol stocks were prepared in water at 5M. Peptide treatments were stored at -80 degrees Celsius for up to one month and thawed prior to the addition of cells. Cells were suspended in MEB buffer at 2X final concentration, approximately 2-3e6 cells/mL, and transferred to 384 well plates containing peptide treatments. A Tecan Spark plate reader was used to detect JC-1 red fluorescence (excitation 545nm +/- 10, emission 590 nm +/- 10) at 5-minute intervals for 180 minutes as a surrogate measure for mitochondrial outer membrane permeabilization. The temperature was kept between 28-32 degrees Celsius for the duration of the assay to prevent lack of charging or rapid depolarization. BH3 profiles were generated in GraphPad via integral analysis of each kinetic trace and normalization to DMSO conditions. Further normalization involved subtraction of positive control profiles (25 µM Alamethicin) from both DMSO and peptide profiles.

Flow cytometry based BH3 profiling was performed on PDX.AA.MCL splenocytes, and primary patient PBMCs following the protocol by the Letai Lab and Dana Farber (<https://letailab.dana-farber.org/bh3-profiling.html>). Briefly, cells were thawed in a water bath at 37 degrees Celsius. They were then washed with PBS and pelleted at 300g for 10 mins and resuspended in at 10e6/ml in PBS + 1% FBS. They were stained with fixation safe live dead viability dye as well as CD5 and CD19. Stain was washed with PBS+ and cells pelleted and resuspended in MEB with 0.002% digitonin at 50,000/50µL per well in a 96 well plate. 50µL of 2X peptide treatment in MEB was added to each well. The plate was incubated at 25 degrees Celsius for 45 minutes. Cells were then fixed by adding 33uL of 4% Formaldehyde and incubated for 10 minutes at room temp. 67µL of N2

stopping buffer was then added. 40µl of the 10X CytoC stain buffer with anti-cytochrome C Fite was added and the plate was incubated at 4 degrees for at least 12 hours. 100µl of PBS was added to each well before running the samples on a cytoflex cytometer with the plate setting. Live cells staining for CD5 and CD19 were selected for quantification.

Transcriptomic and Whole Exome Sequencing

Human-CD19+ MCL cells were positively selected PDX spleens (STEMCELL Technologies Cat#17854). Whole exome sequencing (WES) of DNA from human-CD19+ B-cells of cells passaged in PDXs were performed at Nationwide Children's Hospital Genomic Core Facility. WES reads were aligned to the GRCh37 (Genome Reference Consortium Human Build 37), and data was analyzed to determine mutational variants and copy number variation (CNV).

Cell lines were treated with their IC50 concentration of PRT382 for 6 days. Total RNA was extracted using the Total RNA Purification Kit (Norgen Cat#17200) and QIAshredder Columns (Qiagen Cat#79654). RNA integrity was interrogated using the Agilent 2100 Bioanalyzer. For the RNA-sequencing, TrueSeq stranded mRNA libraries were prepared with Poly-A selection Ribodepletion library prep and sequenced using illumina NovaSeq 6000 on a S1 flow cell (paired end reads with 2X100bp). Differentially expressed genes (DEGs) were assessed using DESeq2 with pairwise comparisons between treatment and control ($q < 0.01$; $|\log_2FC| > 0.58$) ($n=3$ /group). Gene set enrichment analysis (GSEA) was used to identify significantly enriched gene sets [262].

Western Blotting

Cells were treated with small molecule inhibitors for up to nine days, with media changed completely every three days. Doses were chosen to maintain viability above 70% at time of collection. Cells were harvested by pelleting at 300g for 10 mins, washed with ice cold PBS, and pelleted at 300g for 8 minutes at 4° Celsius. Lysates were made using RIPA buffer with phosphatase and protease inhibition cocktails. Western blots were run with 20-30ug of protein on 4-20% SDS-PAGE gels before being transferred to PVDF using the Turbo Transfer System. Blots were blocked, probed, washed, and imaged according to LiCor protocols.

***In vivo* dosing and Xenograft models**

Patient derived xenograft PDX-AA was developed in our lab by tail vein engraftment of human peripheral blood mononuclear cells (PBMCs) from an MCL patient into 5–7-week-old female NSG mice (NOD.Cg-Prkdc^{scid} Il2rg^{tm1Wjl}/SzJ, RRID:IMSR_JAX:005557) as previously published [263].

The percentage of circulating disease was quantified with flow cytometry by staining for human-CD19+/CD5+ MCL cells in peripheral blood gated on the lymphoid compartment by forward scatter and side scatter dot plots (BD Biosciences Cat#555413, RRID:AB_395813; Cat#555352, RRID:AB_395756). Treatment began on day 21 for the PDX.AA.MCL model when the average circulating disease reached 1%. The PDX.AA.MCL treatment consisted of the following: A) PRT808 control high fat chow daily, B) Navitoclax vehicle dosed once weekly via oral gavage, C) PRT808 at 5mg/kg in chow given five days and vehicle chow two days D) Navitoclax at 50mg/kg given weekly

via oral gavage, or E) the combination of PRT808 chow 5/2 and navitoclax weekly. These doses had been determined to be subtherapeutic previously (data not shown).

Mice were monitored weekly for circulating disease and complete blood counts to monitor potential thrombocytopenia. Mice were sacrificed as they reached ERC defined as grossly palpable spleens impeding mobility, severely hunched posture, labored breathing, and/or 20% weight loss. Potential drug toxicity was monitored by mouse weight and treatment breaks were given if needed. Age matched unengrafted NSG mice were used as controls for flow, CBCs, and H&E.

Histopathology

Post necropsy whole mice were fixed in 10% buffered formalin. Tissues were then routinely processed for histopathology at the Comparative Pathology & Digital Imaging Shared Resource at OSU. Samples were processed on a Leica Peloris 3 Tissue Processor (Leica Biosystems, Buffalo Grove, IL), embedded in paraffin, sectioned at an approximate thickness of 4-5 micrometers, and batch stained with H&E on a Leica ST5020 autostainer (Leica Biosystems, Buffalo Grove, IL) using a routine and quality-controlled protocol.

3.3 Results

BH3 profiling uncovers varying dependence on pro-survival BCL-2 proteins

Based on our previous work describing how PRMT5 inhibition induces the expression of the pro-apoptotic protein BAX, we sought to understand how PRMT5 inhibition may shift other elements of intrinsic apoptotic balance. We used plate based BH3 profiling to explore the responses of six MCL cell lines to pro-apoptotic insults. Briefly,

cells were incubated with specific biologically active peptides of seven pro-apoptotic proteins, and JC1 dye which in healthy mitochondria complexes and fluoresces red when mitochondria are depolarized and unable to complex the dye (**Figure 3-1A**). Red fluorescence was measured over 180 minutes (**Figure 3-1B**) and depolarization due to the peptide was quantified using the area under the curve (AUC) of the sample, alamethicin treated cells, and DMSO treated cells using the formula shown in **Figure 3-1C**. Of the six MCL cells lines there was significant variation in response, due to the high genetic and molecular variability seen in this disease (**Figure 3-1D**). UPN-1 and CCMCL1 showed the most primed to undergo apoptosis showing a strong response to more of the multitargeting peptides (**Figure 3-1D**). CCMCL1 showed the greatest reliance on MCL-1 with its response to NOXA and BCL-xL with its response to HRK. This is likely due to the BCL-2 negative status of these two cell lines (**Figure 3-1E, 3-1F**). Granta-519 was the least primed cell line only showing depolarization with BMF. Z-138 and Mino showed strong depolarization in response to Bad which targets BCL-2, BCL-xL, and BCL-w. Maver1, which has a BCL-2 duplication showed, a surprising reliance on BCL-xl and MCL-1 with depolarization in response to HRK and NOXA.

PRMT5 inhibition causes mitochondria dysfunction and increased sensitivity to mitochondrial insult

We then used BH3 profiling to determine the changes in sensitivity with PRMT5 inhibition with PRT382 in MCL. Our first finding was that mitochondrial function, controlled for the number of live cells, was decreased (**Figure 3-2A, 3-2B**). Taking this

into account, we normalized the response of each treatment group to its respective DMSO and alamethicin response. **Figure 3-2C** shows the change in sensitivity with PRMT5 inhibition for the six cell lines. Four of the six lines showed increased sensitivity to most peptides, with Maver1 showing the greatest increase in sensitivity to NOXA, an MCL-1 specific insult. CCMCL1 and Mino both showed increased resistance to the majority of peptides with Mino showing strong resistance to HRK and NOXA, BCL-xL and MCL-1 specific insults respectively.

These results were supported by bulk RNA sequencing and GSEA analysis. Five of the six cell lines and a PDX model of MCL were treated with PRT382 and analyzed for changes in transcriptional signatures. The hallmark signature of apoptosis was enriched in three of the cell lines and the PDX (**Figure 3-3A, 3-3B**). Corresponding to our BH3 profiling, Mino did not have an enrichment of this pro-apoptotic signature (**Figure 3-3B**). IL2 STAT5 signaling was enriched in all samples except Z-138 which has control over BCL-xL transcription [264]. The P53 pathway, known to support transcription of pro-apoptotic genes *BAX* and *BAK1* was enriched in four of the six samples.

PRMT5 inhibition induces expression of pro-apoptotic and anti-apoptotic BCL-2 family proteins

To better understand the shift in apoptotic signaling seen with BH3 profiling and genetic pathway analysis, we interrogated the expression of pro-apoptotic activator Puma and sensitizers Bad, HRK, and Noxa (**Figure 3-4A, 3-4B**). CCMCL1 and UPN-1 showed relatively low level of expression of NOXA though had the highest level of upregulation

with PRMT5 inhibition. CCMCL1 also upregulated Puma two-fold. Bad upregulation was seen in UPN-1, Mino, and Maver1 with a decrease in Z-138 while HRK expression remained relatively stable.

Anti-apoptotic proteins were also upregulated with PRMT5 inhibition (**Figure 3-5A, 3-5B**). BCL-2 expression was elevated in Granta-519 and Mino while BCL-xL was elevated primarily in Granta-519. MCL-1 was the more commonly upregulated with striking upregulation in Z-138.

PRMT5 inhibition is synergistic with BH3 mimetics in MCL cell lines

Based on the dysregulation of the BCL-2 family proteins seen in MCL, and the changes observed, we chose to test three BH3 mimetics for synergistic combinations with PRMT5 inhibition. Navitoclax is a pan BCL-2, BCL-xL, and BCL-w compound that was tested in clinical trials for CLL and other hematological malignancies [265]. Z-138, Mino, and Maver-1 showed IC50s below 100nM for this compound (**Figure 3-6A**), a response predicted by their sensitivity to the Bad peptide (**Figure 3-1D**). Granta-519 also showed a cytotoxic response at higher doses while CCMCL1, and UPN-1 did not respond. A-1331852 (A852) is a highly selective BCL-xL tool compound. Only Z-138 showed an IC50 below 100nM though Mino, CCMCL1, and UPN-1 also showed a dose dependent response (**Figure 3-6B**). Granta-519 and Maver1 did not respond. The third mimetic tested was PRT1419, a clinical MCL-1 inhibitor from Prelude Therapeutics [266]. CCMCL1 was the only cell line with an IC50 below 100nM though UPN-1, Mino, Z-138, and Maver1 all had dose dependent responses (**Figure 3-6C**).

Synergy was then tested for each cell line and each compound using 1.25X, 1X, 0.75X, and 0.5X of the IC50 for PRT382 and the BH3 mimetics and calculated using the ZIP model [267]. The high scoring combination is shown in **Figure 3-7A-F** and the overall score is shown in **Figure 3-7G**. Scores above 10 are considered synergistic. All the cell lines tested had subset of doses that exceeded the minimum synergy score for at least one compound (data not shown) but CCMCL1, UPN-1, and Granta-519 did not show overall synergy with any of the three compounds tested. The lack of synergy from CCMCL1 and UPN-1 mirrors previous results we saw when testing PRT382 and venetoclax (See Chapter 2). Granta-519 was the least primed cell line as determined by BH3 profiling (**Figure 3-1D**), suggesting these agents are not a good candidate for this cell line. Mino showed the highest levels of synergy with A852. Maver1 showed synergy with A852 and PRT1419, while Z-138 showed synergy with Navitoclax and PRT1419. The synergy seen with PRT1419 could be correlated to the increased sensitivity seen with PRMT5 inhibition to the NOXA peptide (**Figure 3-2C**). Mino's response to A852 did not correlate to any increased sensitivity with PRMT5 as this cell line became less primed with treatment (**Figure 3-2D**). Understanding this strong synergy merits more work.

iBH3 profiling of PDX and primary samples

iBH3 or flow based BH3 profiling uses surface staining, and anti-cytochrome c antibodies to determine the amount of depolarization in a select populations of cells (**Figure 3-8A**). This is optimal for mixed samples such as PBMCs. PDX.AA.MCL cells harvested after vehicle or PRT382 treatment were profiled (**Figure 3-8B**). PRMT5 inhibition increased

apoptotic priming and pan BCL-2, BCL-xL, and BCL-w insult as shown by increased depolarization with Bim and Bmf (**Figure 3-8B**).

Two patients were also profiled with two distinct responses. Patient 1 was poorly primed and showed minimal response to most peptides (**Figure 3-8C, 3-8D**). With the greatest response to Puma, this patient is most likely to be responsive to BCL-xL and MCL-1 inhibition. The second patient was highly primed and showed the greatest response to pan sensitizers that included BCL-2, BCL-xL, and BCL-w indicating an agent like navitoclax would be very effective for this patient (**Figure 3-8C, 3-8D**).

PRMT5 inhibition and BH3 mimetics are synergistic in vivo

Based on our iBH3 profiling and genetic pathway analysis, we decided to test the pan BCL-2, BCL-xL, and BCL-w inhibitor with the PRMT5 inhibitor PRT808 in our PDX.AA.MCL model of ibrutinib resistant MCL. Mice were engrafted systemically and treatment started on day 21 when the average percentage of circulating lymphocytes that were huCD5+/huCD19+ was 1%. The PRMT5 inhibitor PRT808 was dosed in chow provided ad lib for Wednesday-Monday and control chow was provided on Monday and Tuesday. Navitoclax was dosed via oral gavage once weekly on Wednesday. Mice were monitored weekly for circulating disease and thrombocytopenia, a known toxicity of navitoclax. The single agent groups had improved survival outcomes compared to the control group (median survival of 54 vs 65 vs 75 days, $p < 0.01$ for all comparisons) (**Figure 3-9A**) as well as slowed disease progression as determined by flow cytometry (**Figure 3-9B**). The combination of PRT808 and outperformed all the groups in survival (median survival of 93 days, $p < 0.01$ for all comparisons) and circulating disease (**Figure 3-**

9A, 3-9B). Thrombocytopenia was detected in the diseased mice, but did not significantly affect the navitoclax only, or combination group more than the other cohorts (**Figure 3-10A**). The decrease in platelets tracked closer to disease progression, worsening as circulating disease progressed.

We noted that the circulating disease in the combination group remained low, even as the mice reached ERC, prompting us to look at organ infiltration. Hematoxylin and eosin (H&E) staining was performed on a mouse receiving navitoclax control (908) and a combination treatment mouse (963) (**Figure 3-11A-C**). The disease progression in the control mouse resulted in decreased bone integrity in the skull (**Figure 3-11A**), as well as disease in the liver (**Figure 3-11B**) and kidneys (**Figure 3-11C**). The combination treatment mouse showed less disease progression in the liver and kidneys as well as normal bone structure, but saw significant disease infiltration to the meninges and brain. This suggests that the drug combination continued to be effective at reducing the circulating MCL as well as reducing organ infiltration but was unable to prevent spread to the CNS causing the mice to reach ERC.

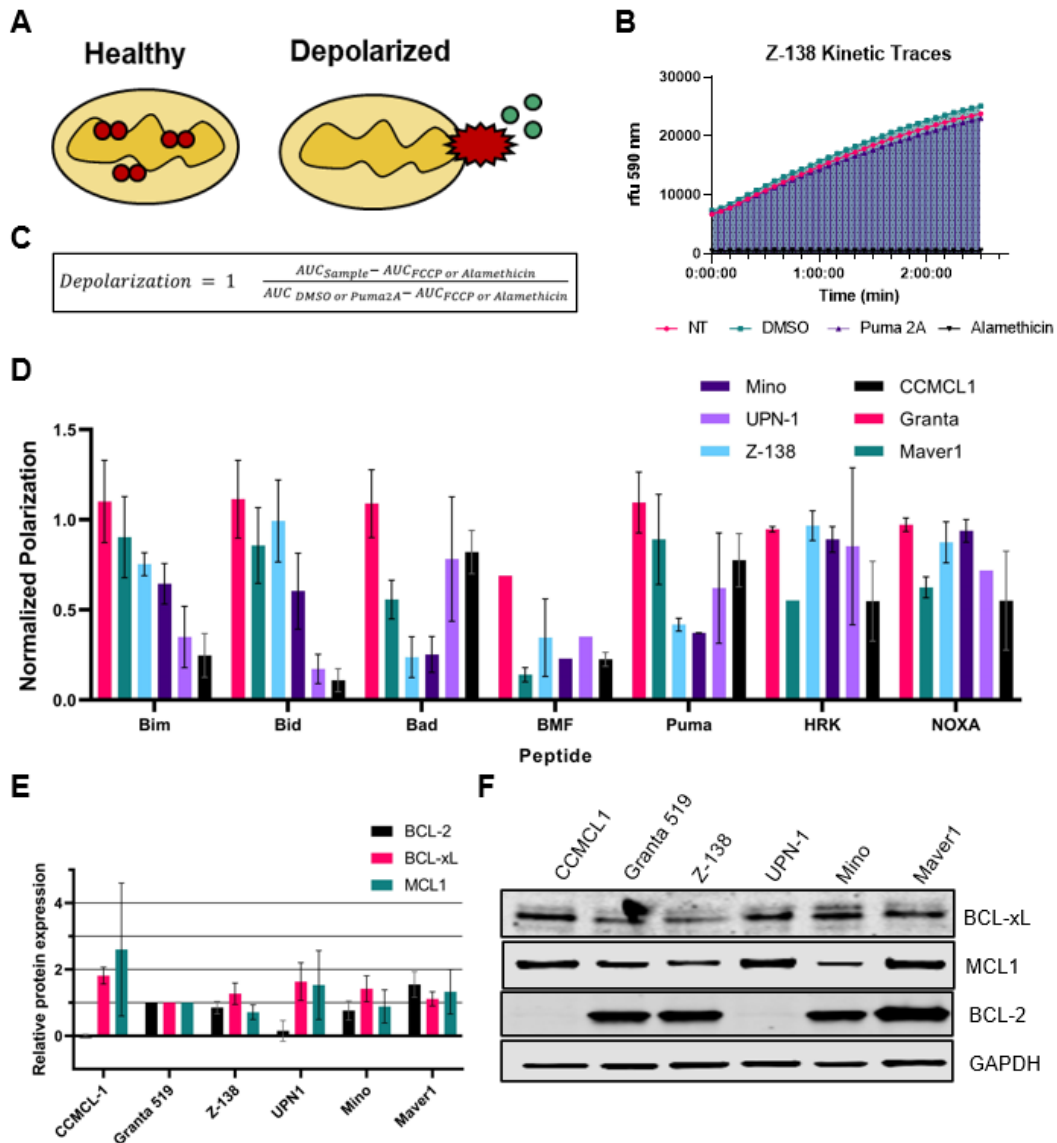


Figure 3-1: BH3 profiling reveals varied response to mitochondrial insult across MCL cell lines

A) Diagram of how JC1 fluoresces red in polarized, healthy mitochondria and green when mitochondria become depolarized. B) Kinetic trace of JC1 stained cells treated with no treatment (NT), DMSO, the biologically inactive peptide Puma 2A, or the pore forming alamethicin as a positive control. C) The formula used to quantify depolarization.

D) Normalized polarization of six MCL cell lines to seven pro-apoptotic peptides representing the proteins Bim, Bid, Bad, BMF, Puma, HRK, and NOXA. N>2

E) Quantified baseline protein expression of three key anti-apoptotic proteins BCL-2, BCL-xL, and MCL-1. F) Representative western blot of the proteins in E. Error bars represent standard deviation.

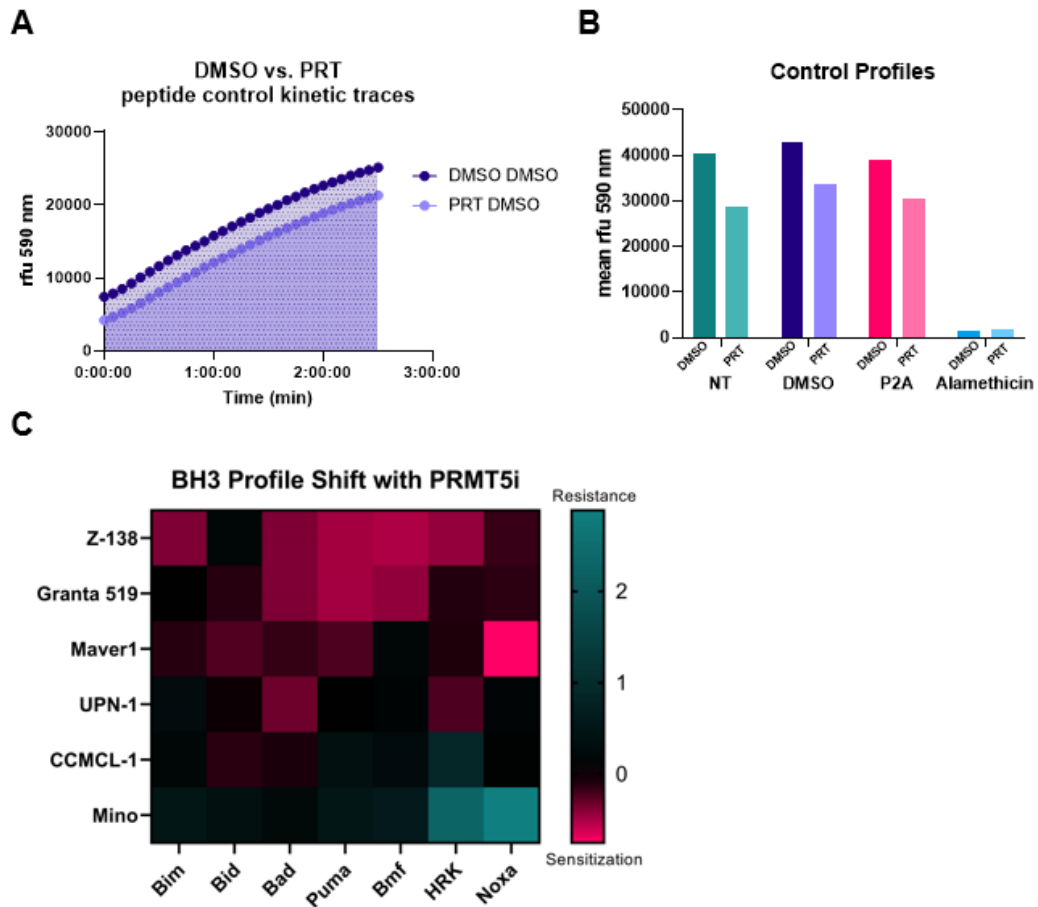


Figure 3-2: PRMT5 inhibition reduces mitochondria function and shifts response to mitochondrial insult

A) Kinetic trace of cell culture with DMSO or PRT382 and then treated with the DMSO condition for BH3 profiling. B) AUC of DMSO or PRT382 treated cells with the control conditions of BH3 profiling. C) Heat map showing shift in sensitivity the peptides as measure by BH3 profiling. Resistance means less depolarization with PRT382 treatment while sensitization shows more depolarization.

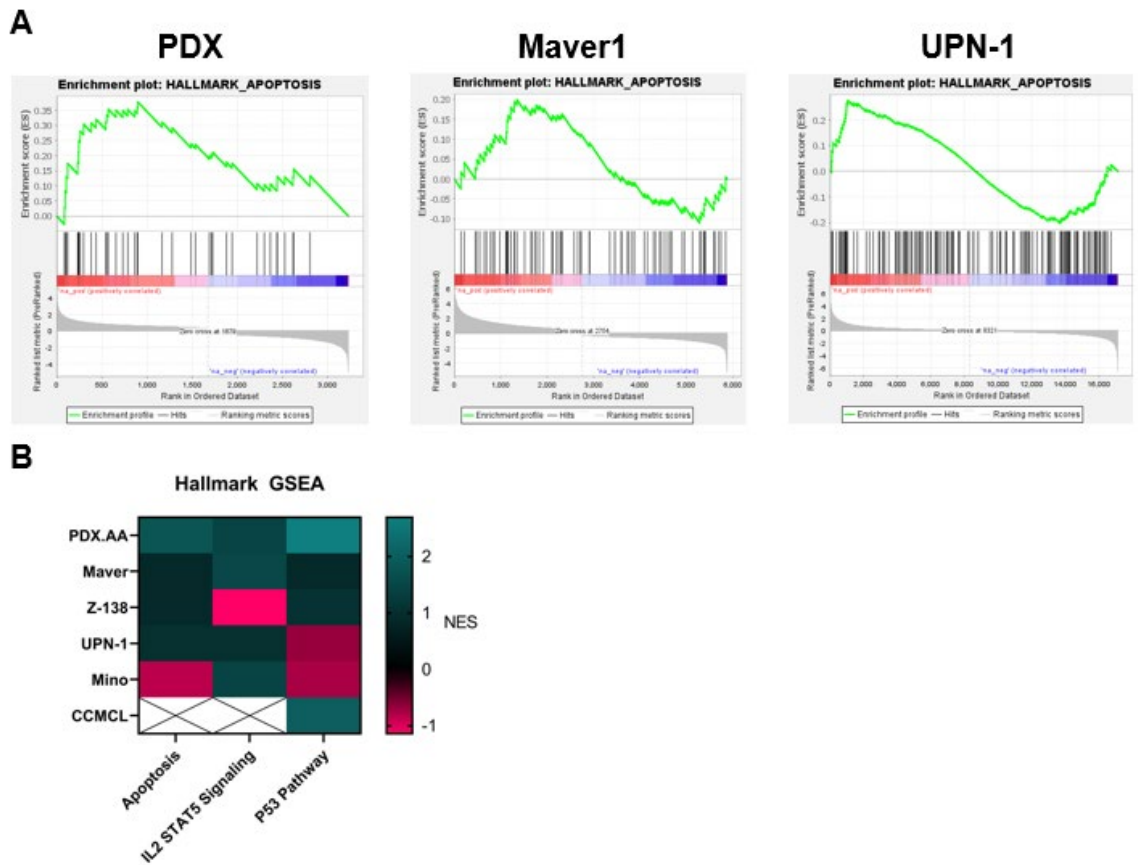


Figure 3-3: PRMT5 inhibition upregulates pro-apoptotic transcriptional profiles

A) GSEA plots of the hallmark apoptosis gene set for PDX.AA.MCL, Maver1, and UPN-1 treated with PRT382 showing upregulation in this gene set. B) Heat map of normalized enrichment score (NES) for PDX.AA.MCL and five MCL cell lines for hallmark gene sets Apoptosis, IL2 STAT5 Signaling, and P53 pathway.

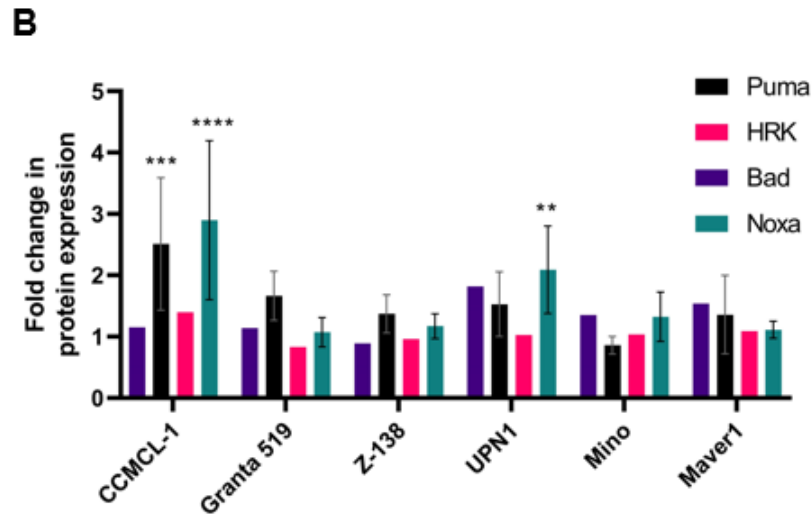
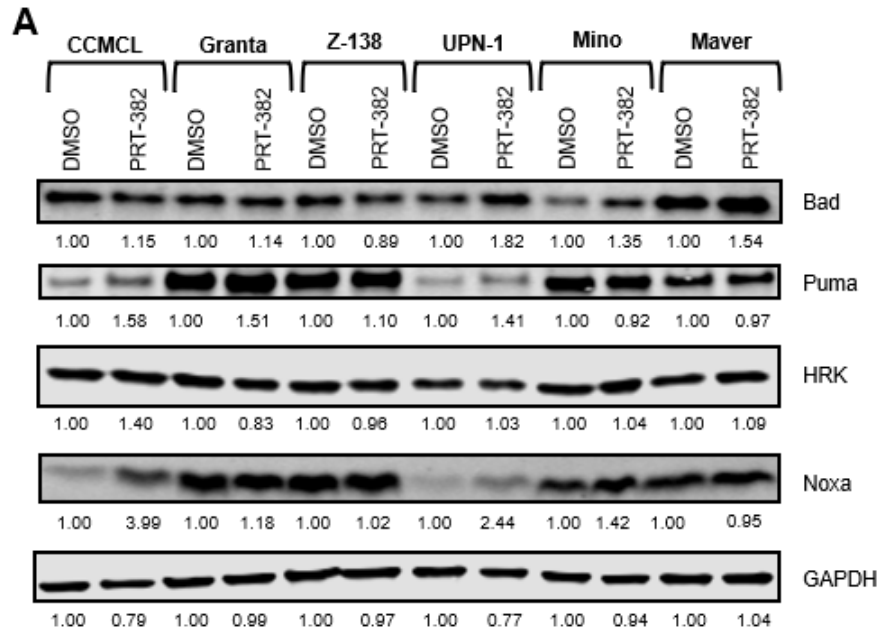


Figure 3-4: PRMT5 inhibition upregulates the expression of pro-apoptotic activator and sensitizers in MCL cell lines

A) Representative western blot showing changes in expression of Bad, Puma, HRK, and Noxa with six days of PRT382. B) Change in protein expression with PRMT5 inhibition for Puma and Noxa. Significance was determined with 2-way ANOVA with

Šídák's multiple comparisons test. * $P < 0.05$ ** $P < 0.01$ *** $P < 0.001$ **** $P < 0.0001$ Error bars show standard deviation.

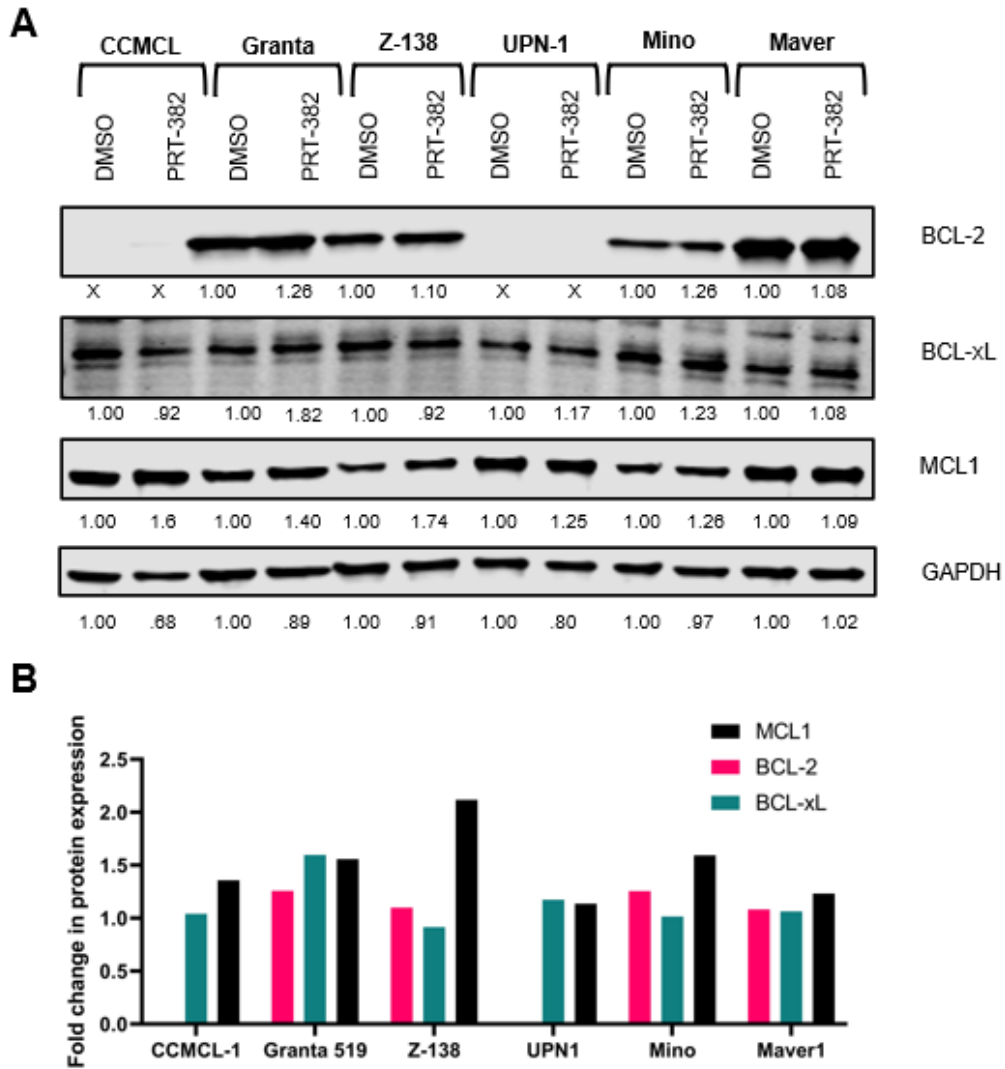


Figure 3-5: PRMT5 inhibition increases expression of anti-apoptotic BCL-2 family proteins

A) Representative western blot of anti-apoptotic proteins BCL-2, BCL-xL, and MCL-1 following six days of PRT382 treatment. B) Quantification of protein expression, N = 2 for BCL-xL and MCL-1.

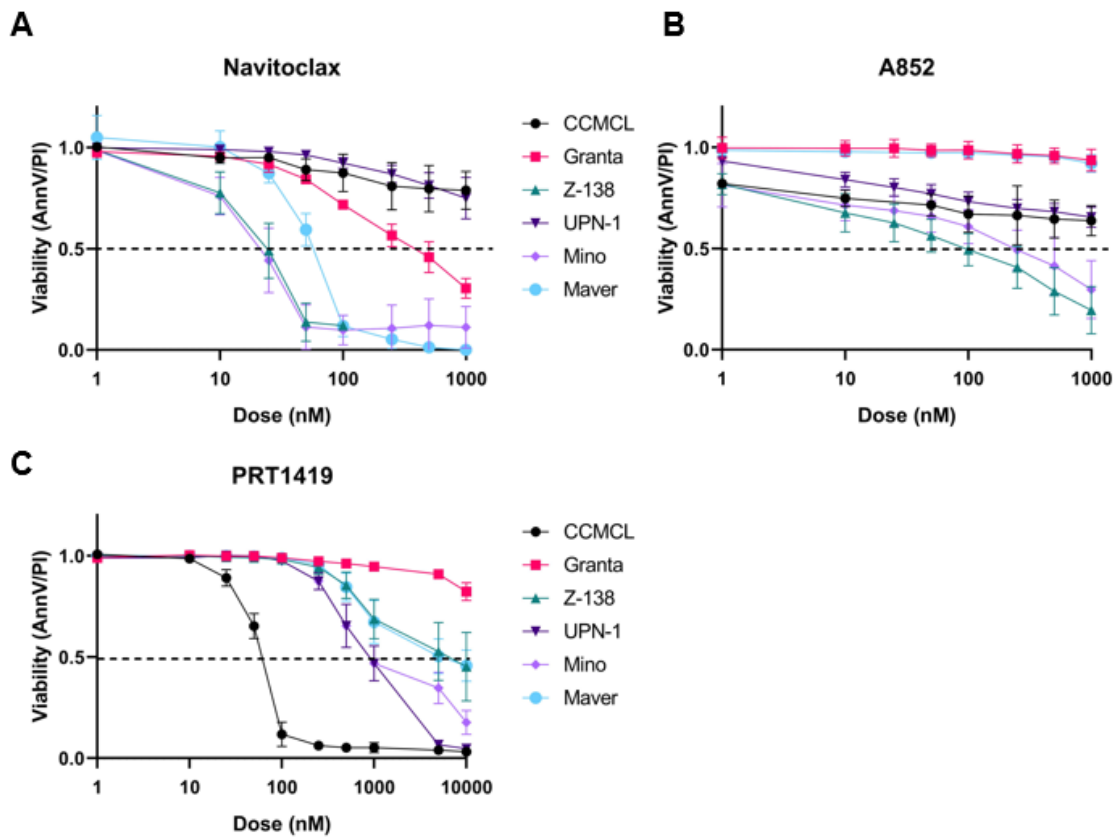


Figure 3-6: IC50s of navitoclax, A852, and PRT1419 for MCL cell lines

IC50s measured via annexin V/PI staining and flow cytometry after 72 hours of treatment for A) navitoclax, B) A852, and C) PRT1419. Error bars show standard deviation.

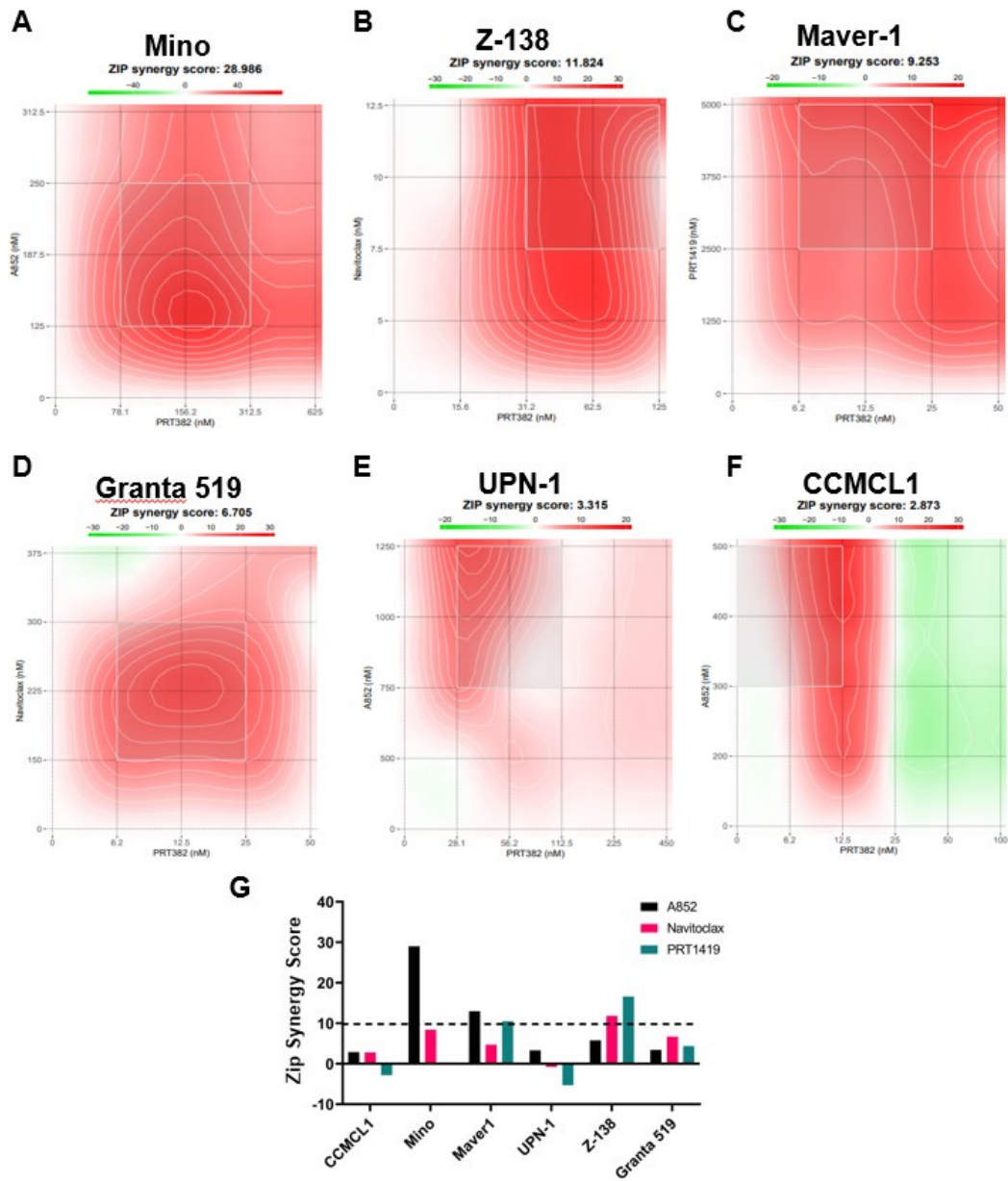


Figure 3-7: PRT382 and BH3 mimetics synergize in MCL cell lines

Synergy plots from Synergy Finder of the high score combination for A) Mino, B) Z-138, C) Maver1, D) Granta-519, E) UPN-1, and F) CCMCL1 using the ZIP method of synergy

[267]. Red areas show synergy while green show antagonism. Scores over 10 are considered synergistic. G) Overall score for PRT382 and BH3 mimetic.

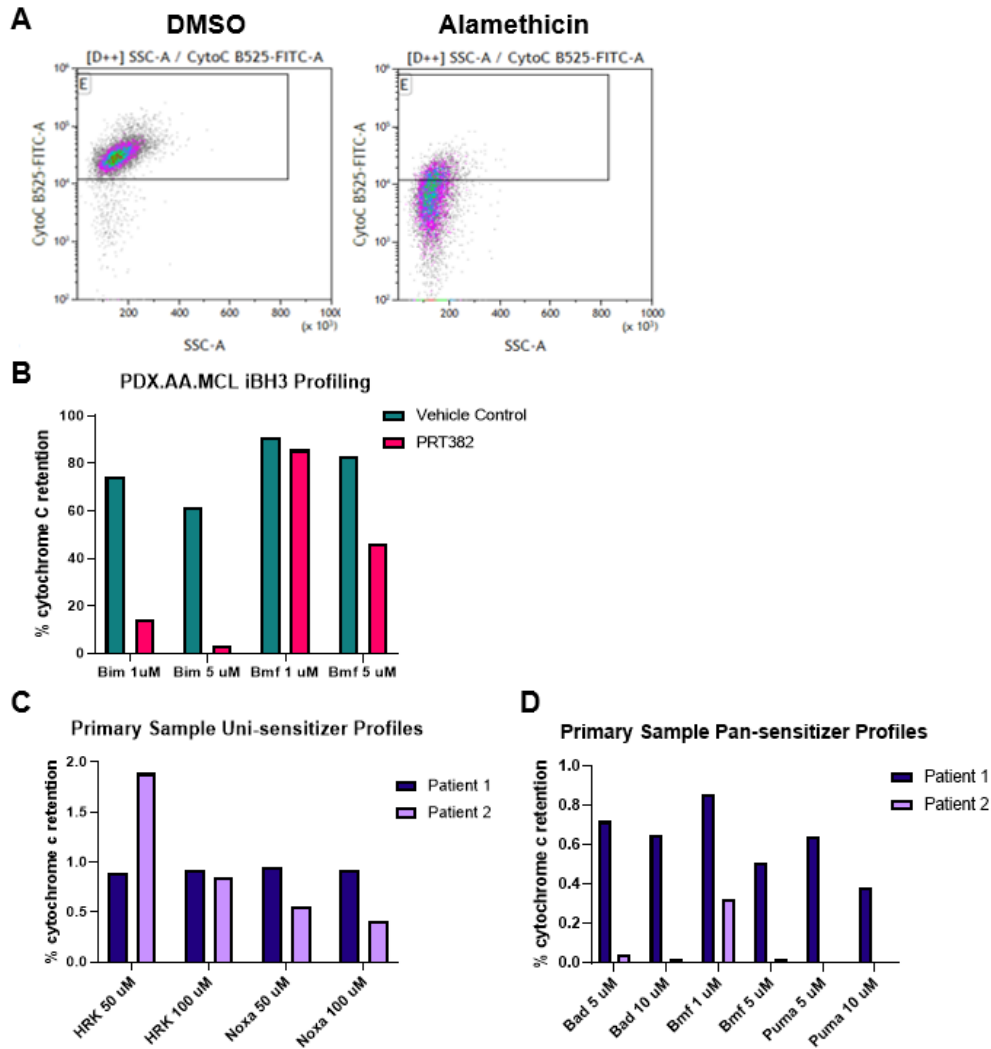


Figure 3-8: iBH3 profiling of PDX and primary MCL cells

A) Flow plots of cytochrome C in Fitc and SSC showing the decrease in cytochrome C retention with the positive control alamethicin compared the negative control DMSO. B) Quantification of cytochrome c retention in PDX.AA.MCL cells from a vehicle control mouse or a mouse treated with PRT382 for Bim and Bmf treatment. Quantification of cytochrome retention for two primary MCL patient samples after C) HRK and Noxa or D) Bad, Bmf, and Puma.

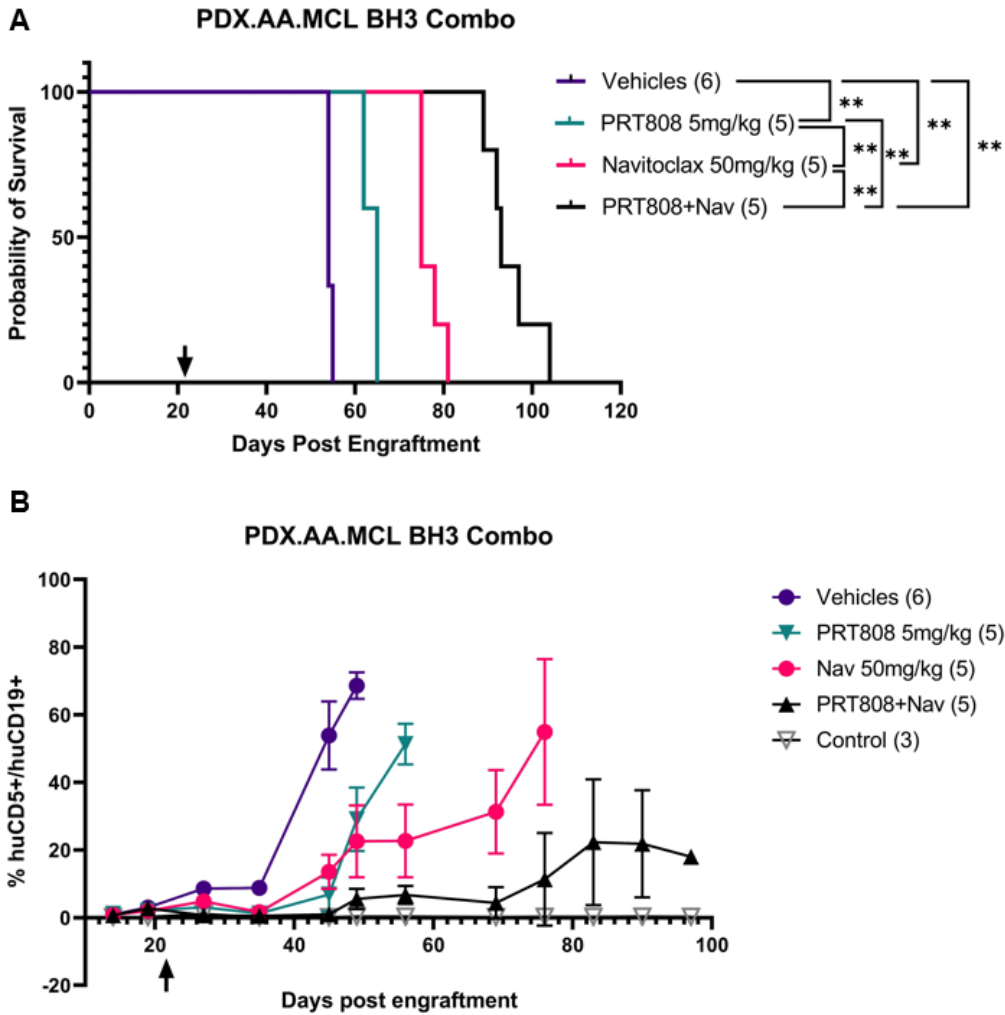


Figure 3-9: PRT808 and navitoclax are synergistic *in vivo*

A) Kaplan Meier of the survival of PDX.AA.MCL model with treated with vehicle, PRT808 at 5mg/kg, navitoclax at 50mg/kg, or PRT808 with navitoclax. Average survival was vehicle 54, PRT808 only 65, navitoclax only 75 days or combination 93 days. * $P < 0.05$ ** $P < 0.01$ *** $P < 0.001$ Significance was determined with a log-rank test. B) Circulating huCD5+/huCD19+ cells over time in the PDX.AA.MCL combination study. Error bars represent standard deviation.

A

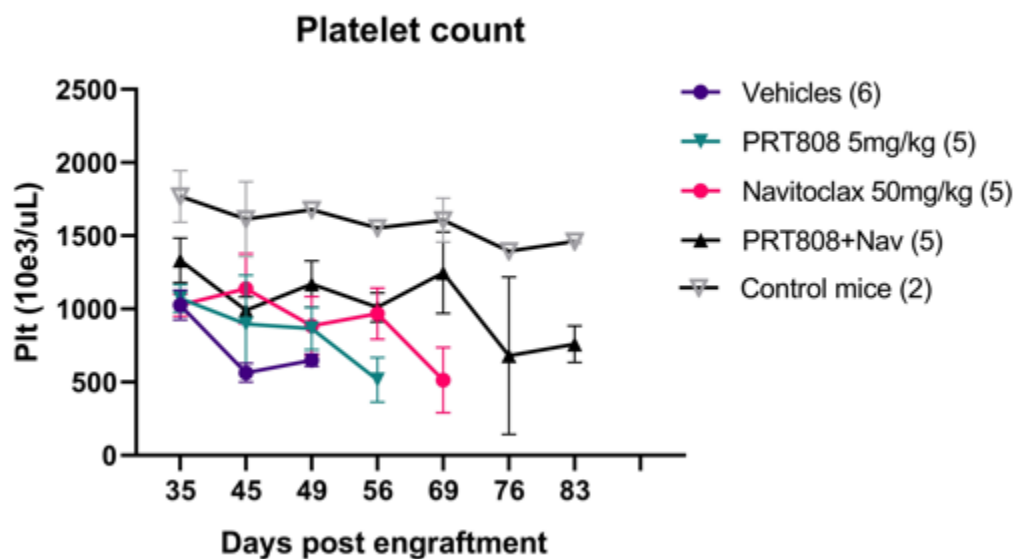


Figure 3-10: Platelet count for PRT808 and navitoclax combination treatment *in vivo* experiment

A) Platelet count per μL as determined by CBCs in the PDX.AA.MCL model in the PRT808 and navitoclax combination experiment. Control mice are unengrafted NSG mice. Error bars show standard deviation.

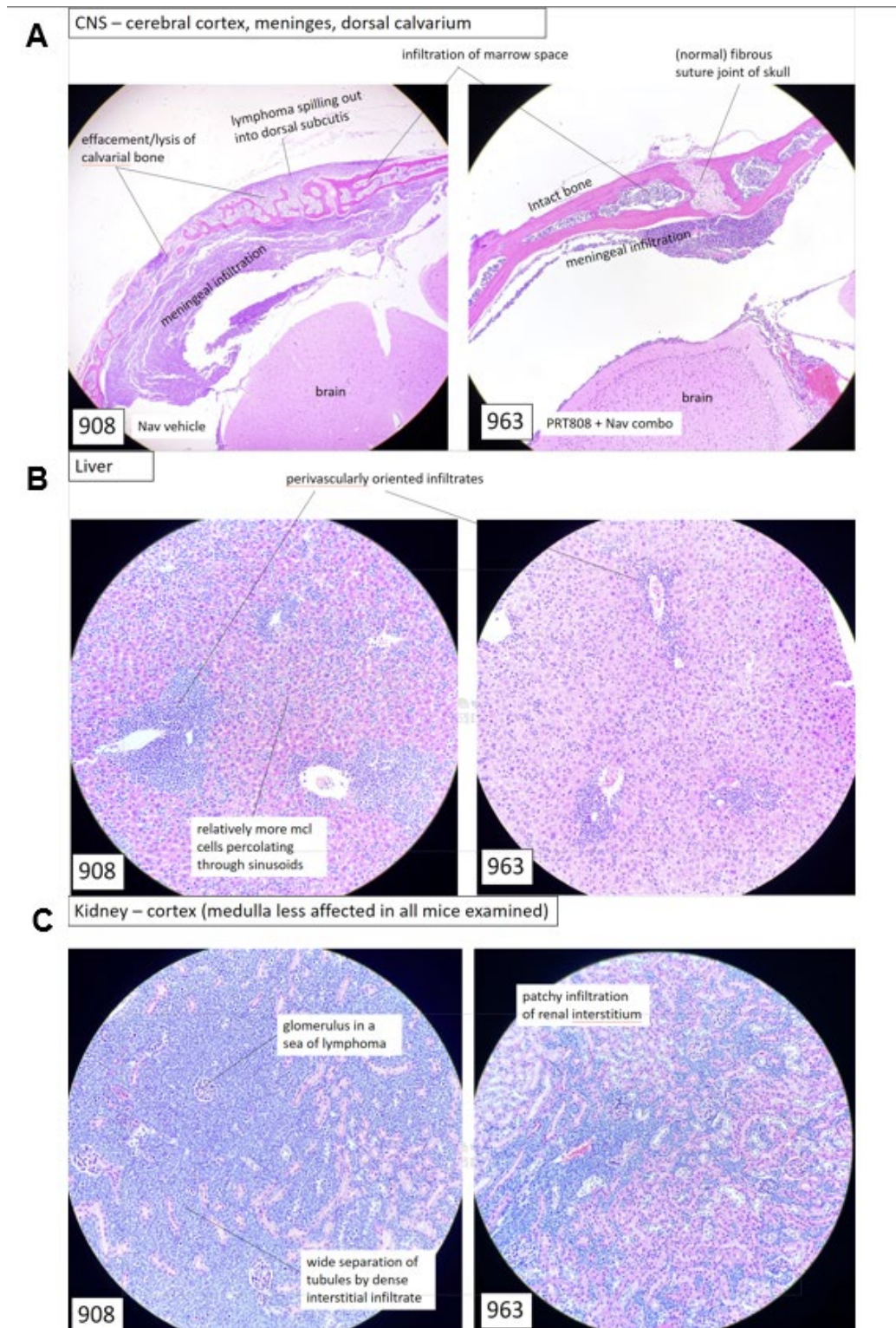


Figure 3-11: H&E of PRT808 and navitoclax combination *in vivo* experiment

H&E of a control mouse (908) or a PRT808+navitoclax treated mouse (963) from sample acquired at ERC. Images of A) central nervous system (CNS), B) liver, and C) kidney with pathologist notes shown here.

3.4 Conclusions

At the time of publication, MCL is considered incurable highlighting the need for novel therapeutic targets and treatment strategies. While targeted therapies such as ibrutinib have improved outcomes for MCL patients over the last ten years, patients almost uniformly develop progressive, resistant disease and have very poor prognoses [252, 253]. PRMT5 inhibitors are currently in clinical trials for the treatment of heme malignancies but preliminary data has suggested that they may not be optimal as a monotherapy. This has led us to explore the effects of PRMT5 inhibition on the intrinsic apoptotic pathway through BH3 profiling, genetic pathway analysis, and immunoblots. We were able to determine that while mitochondrial dysfunction and apoptotic priming varies by cell line, PRMT5 inhibition increased sensitivity to mitochondrial insult in five of six MCL cell lines. This change in threshold supported the use of BH3 mimetics in combination with PRMT5 inhibition. Navitoclax, A852, and PRT1419 showed synergistic responses with PRT382 in multiple cell lines. BH3 profiling of PDX cells suggested that navitoclax and PRMT5 inhibition would be synergistic which was confirmed by our *in vivo* study with our PDX.AA.MCL model of ibrutinib resistant MCL. Here we have shown rapid profiling by BH3 profiling may reveal optimal clinical strategies for combining PRMT5 inhibition with BH3 mimetics.

BH3 profiling revealed varying degrees of apoptotic priming and sensitivity to mitochondrial insult. Granta-519 was an interesting outlier in its resistance to apoptosis as this is the only EBV positive cell line we tested. EBV is known to immortalize B cells through multiple survival pathways including upregulation of the pro-survival BCL-2

family of proteins [268, 269]. Mino also proved to be an outlier, showing resistance to mitochondrial insult with PRMT5 inhibition. The cause of this, and whether it correlates to strong synergy as seen with PRMT5 inhibition and A852 in Mino was not readily apparent based on our sequencing and protein studies. More focus on the BCL-xL pathway in this cell line or testing in additional cell lines may reveal a mechanistic explanation.

Given the positive response we have seen, this work merits expansion to additional MCL models as well as other hematological malignancies such as the mature B cell cancer chronic lymphocytic leukemia (CLL) and diffuse large B cell lymphoma (DLBCL). The BH3 mimetic and BCL-2 inhibitor venetoclax is already FDA approved for use in CLL showing the potential for BH3 mimetics to be used clinically for B cell cancers [250]. Navitoclax, a pan BCL-2, BCL-xL, and BCL-w inhibitor was tested in clinical trials for hematological malignancies but eventually shelved due to on target thrombocytopenia. This pan inhibition proved to be very effective with PRMT5 inhibition in our study and we were able to manage thrombocytopenia by reducing the dose and timing of navitoclax. This could be a model for clinical dosing in combination trials and warrants more exploration. Another possibility would be the use of platelet sparing BCL-2/BCL-xL inhibitors such as LP-118 [198] and AZD0466 [199].

In support of our previous work with PRMT5 inhibition and BCL-2 inhibition, this study shows that PRMT5 inhibition and BH3 mimetics synergize in *in vitro* and *in vivo* models of MCL. The exploration of three BH3 mimetics allows for options as not all patients will respond to all combinations. Venetoclax resistance has been described in MCL with the cancer relying on upregulation of BCL-xL and/or MCL-1 to avoid apoptosis [194].

Knowing PRMT5 inhibition synergizes with multiple BH3 mimetics will allow for quick and effective modifications to treatment plans to target the correct mitochondrial dysfunction.

We believe that PRMT5 inhibitors used in combination with second targeted therapies such as BH3 mimetics will provide an effective avenue of treatment for MCL patients, especially those who have relapsed on BTK inhibitors and have poor prognoses. This pre-clinical work supports clinical trials with PRMT5 inhibitors and BH3 mimetics currently under study.

Chapter 4: E μ -SOX11CCND1 Murine Model of Mantle Cell Lymphoma

Modified from “E μ -SOX11CCND1: A Novel Immunocompetent Murine Model of Mantle Cell Lymphoma” with permission

3.1 Background and Rationale

Mantle cell lymphoma (MCL) is a CD5⁺/CD19⁺ B cell non-Hodgkin Lymphoma (NHL), defined by the t(11;14) translocation juxtaposing the *CCND1* gene downstream of the *IgH* promoter. Among western countries MCL comprises 3-10% of adult onset NHLs [257] and is associated with a poor prognosis due to multiple factors including extranodal disease, advanced stage of disease at diagnosis, and resistance to standard immune-chemotherapy regimens [80]. Due to the late median age of diagnosis, approximately 70 years of age [214], aggressive chemotherapy and stem cell transplantation are often not realistic options [215]. The average overall survival of patients with MCL is approximately 6 years [81] and for the majority of patients who progress on targeted agents like ibrutinib, survival remains at a dismal 3-8 months [83]. Short of salvage immuno-chemotherapy followed by a stem cell transplant, relapse is virtually universal and for the most part, MCL is considered incurable [85].

There are two WHO categories for MCL diagnoses: 1) conventional or classical MCL (cMCL) derived from naïve per-germinal center B cells with unmutated *IGHV*, overexpression of SOX11, and nodal disease with aggressive disease and 2) non-nodal, or indolent MCL (nnMCL) from antigen experienced B cells, lacking SOX11 expression, and

with a more stable disease course [257]. nnMCL is relatively rare, making up less than 10% of diagnosed MCL cases [270, 271] and these patients are often able to undergo a “watch and wait” treatment plan [11].

As MCL treatment moves toward immunotherapy, with the approval of Tecartus (brexucabtagene autoleucel) anti-CD19 CAR T cells for the treatment of relapsed or refractory (R/R) MCL in 2020 [74], murine models of aggressive cMCL that can be used for pre-clinical research are highly desirable. Traditionally used models such as cell line derived xenografts (CDXs) and patient derived xenografts (PDXs) use immunodeficient mice and are not useful for understanding the effects of immunotherapy or immunomodulatory agents on the host immune system and malignant cells.

Murine models of MCL with intact immune system are severely lacking. The first attempts to generate a Cyclin D1 driven cancer were published by Bodrug et al., in 1994 [20]. Despite high levels of Cyclin D1 production driven by the E μ promoter, transgenic models overexpressing this protein fail to produce a lymphoma [20]. Lymphomas were achieved by creating a double transgenic with E μ -myc crossed with E μ -CCND1 mice. In clinical MCL, while myc aberrations provide prognostic value, they only occur in 14-20% of MCL cases [32, 36]. Lymphoma could also be induced with a pristane injection at one year [205], though pristane alone causes malignant expansion of B cells [206]. Other efforts with *CCND1* include a constitutively nuclear mutant of Cyclin D1 which also required a second genetic alteration such as mutations in *TP53* or *MDM2* [208], and E μ -CCND1 mice with *Bim*(fl/fl) [209]. Other efforts include over expression of *CCND1* downstream target c-Myc and IL-14 [210], a mutant *Cdk4* [211] or a heterozygous deletion of *TP53* [212].

Another reported model utilizes *CCDN2* overexpression in all hematopoietic cells [213]. All of these models have limited representation of true MCL due to inconsistent disease development, unusual genetic drivers and/or deviant pathology.

Here we describe a novel murine model of MCL, the E μ -SOX11CCND1 mouse model. This model utilizes two key MCL drivers *CCND1* and *SOX11* on the mature B cell specific promoter, E μ , to cause aberrant B cell expansion and spontaneous MCL like lymphoma on a C57Bl/6 background. Disease cells from a spontaneous mouse were adoptively transferred in two healthy C57Bl/6 creating a model of MCL that can be used for therapeutic studies with systemic or subcutaneous engraftment. Both models can be used for tumor microenvironment studies as shown by our analysis by spectral flow cytometry of blood, spleen, subcutaneous tumor, and bone marrow. This model is resistant to ibrutinib and venetoclax, sensitive to PRMT5 inhibition, and can be utilized for CAR T experimentation.

3.2 Methods

Mouse model

All animal experiments were carried out according to the guidelines of the Icahn School of Medicine at Mount Sinai and The Ohio State University Institutional Animal Care and Use Committee in compliance with the federal and institutional regulations.

To study the cooperation between *CCND1* and *SOX11*, we crossed *SOX11* transgenic mice (E μ -SOX11-IRES-GFP) with the E μ CCND1 mice (a kind gift from S. Katz, Yale University) [16]. E μ -SOX11 transgenic mice were generated as described before [17]. Briefly, the BstBI/BciVI digested pE μ SV-SOX11-IRES-eGFP vector

containing mouse SOX11 full-length sequence was injected into fertilized oocytes from C57Bl/6J animals (Jackson Laboratory). Mice were screened for the presence of the SOX11 and CCND1 genes by genotyping of tail DNA by quantitative PCR (Transnetyx).

Flow Cytometry

Colonies of E μ -CCND1, E μ -SOX11, and E μ -SOX11CCND1 mice were monitored at least monthly by cheek bleed and flow cytometry using the antibodies listed in **Table 4-1**. 25 μ L of mouse blood was stained with a master mix for at least 30 mins and lysed with RBC lysis buffer. Samples were washed with 2mL of PBS and resuspended in 200 μ L. Samples were run on a Fortessa cytometer. The percentage of CD45+ cells that were CD19+ and CD5+/CD19+ were quantified using Kaluza for analysis.

Marker	Fluorochrome	Volume (μ L) / test	Supplier (clone)
CD45	BV510	1	BD (30-F11)
CD5	PE	0.5	Invitrogen (53-7.3)
CD19	PE-cy7	1	Invitrogen (1D3)
CD11b	APC	1	Invitrogen (M1/70)
CD3	APC-cy7	1	BD (145-2C11)
GFP	N/A	N/A	Inherent

Table 4-1: Table of flow cytometry antibodies used to monitor disease progression in transgenic colony

Flow cytometry of adoptive transfer model during creation and during further therapeutic studies utilized the same protocol as above and the flow panel shown in **Table 4-2**.

Marker	Fluorochrome	Volume (uL) / test	Supplier (clone)
GFP	N/A	N/A	inherent
CD19	Alexa Flour 700	0.625	BD (1D3)
CD5	BV421	0.5	BD (53-7.3)
CD45.1	PE	0.5	Biolegend (A20)
CD45.2	APC	0.5	Biolegend (104)

Table 4-2: Table of flow cytometry antibodies used to monitor disease progression in the adoptive transfer model

Spectral flow cytometry was performed on blood, spleen, and tumors from SOX11CCND1 mice untreated or treated with PRT382 for nine days, daily. Briefly, cells were thawed as before, washed, and resuspended at 10^6 /mL. At least 1×10^6 cell per condition was used. Cells were stained with live dead blue, blocked with murine anti-CD16/CD32, and surface stained using the panel in **Table 4-3**. Single color controls and FMOs were performed with spleens from normal C57Cl/6 mice or disease cells as necessary due to the expression of GFP in the malignant cells. Controls were run within one week of the experiment. All samples were run on the Cytex Aurora cytometer and cleaned with Spectroflo from Cytex. UMAPs, TSNEs, and histograms were all generated in Cytobank.

Marker	Fluorochrome	Volume (uL)	Supplier (clone)
Live Dead	Live/Dead Blue	1	Fisher (L23105)
CD40	BUV661	2.5	BD (3/23)
CD23	BUV737	2.5	BD (B3B4)
CD19	BUV805	2.5	BD (1D3)
CD86	BV421	5	BD (GL1)
Ly-6C	Pac Blue	2.5	BioL (HK1.4)
CD4	BV510	2.5	BD (RM4-5)
CD25	BV605	10	BD (2A3)
CD68	BV650	10	Thermo (FA-11)
Ly-6G	BV711	2.5	BD (1A8)
PD-L1	SB780	1.25	eBio (B7-H1)
GFP	N/A	N/A	Fisher (16-10A1)
CD3	PerCP-Cy5.5	5	eBio (145-2c11)
PD-1	PE	0.5	eBio (J43)
CD11b	PE-Cy5	1.25	eBio (FA-11)
NK1.1	PE-Cy7	1.25	eBio (M1/70)
CD80	APC	2.5	Fisher (16-10A1)
CD11c	AF700	5	BD (HL3)
CD8	APC-Cy7	2.5	BD (53-6.7)

Table 4-3: Spectral flow panel with marker, fluorochrome, volume per test and catalog number

Colors indicate laser that each portion of the panel corresponds to.

Adoptive Transfer

The adoptive transfer model was created by using malignant CD5+/CD19+ cells isolated from the lymph node of an E μ -SOX11CCND1. These were engrafted via tail vein into three C57Bl/6 mice that had been irradiated with 2Gy 24 hours prior. Splenocytes were isolated from the mouse that reached ERC first and passaged into another cohort of irradiated C57Bl/6 mice. This process was repeated once more with a reduction in cell number. Passage four and on were not irradiated. Passage one – three used CD45.1 to better differentiate the CD45.2 disease cells. Mice were engrafted either by tail vein or subcutaneously using 1:1 cell:Matrigel solution deposited on the flank.

Histopathology

Post necropsy whole mice were fixed in 10% buffered formalin. Tissues were then routinely processed for histopathology at the Comparative Pathology & Digital Imaging Shared Resource at OSU. Samples were processed on a Leica Peloris 3 Tissue Processor (Leica Biosystems, Buffalo Grove, IL), embedded in paraffin, sectioned at an approximate thickness of 4-5 micrometers, and batch stained with H&E on a Leica ST5020 autostainer (Leica Biosystems, Buffalo Grove, IL) using a routine and quality-controlled protocol.

Targeted Agent and Chemotherapeutic Studies

100k splenocytes from passage three were engrafted via tail vein into 7-8 week old female C57Bl/6J mice. Due to the speed of the model, mice were treated starting on day three post engraftment. Ibrutinib was dosed aqeuously ad lib with 1.6g/L of vehicle. Venetoclax was dosed four days on, three days off, via oral gavage at 12.5 mg/kg or

50mg/kg. PRT382 was dosed was dosed four days on, three days off, via oral gavage at 5mg/kg or 10mg/kg. ERC from disease burden were defined as grossly palpable spleens impeding mobility, severely hunched posture, labored breathing, and/or 20% weight loss.

For the conditioning study, 100k splenocytes from passage three were engrafted subcutaneously into 7-8 week old female C57Bl/6J mice. Once a tumor was palpable, approximately day 15, cyclophosphamide was dosed at 100mg/kg or 200mg/kg IP or mice were irradiated with 1, 2, or 3 gray. Mice were taken on day 21 to determine disease progression.

CAR T Study

To generate anti-CD19 CAR T cells, the iD3-28Z construct [272] was modified with a T2A linker to attach Thy1.1 for selection. Phoenix Eco (ATCC CRL-3214) cells were transfected with this plasmid and cultured for 48 hours. Supernatant was used to transduce T cells selected from healthy C57Bl/6 spleens with a T cell selection kit (StemCell Technologies Catalog # 19851). Cells were stimulated with Con A for 48 hours and allowed to expand for five days. Non-transduced but stimulated and expanded T cells were used as a control.

100k splenocytes from passage three were engrafted via tail vein into 7-8 week old female C57Bl/6J mice. Once a tumor was detectable, mice were irradiated with 3 gray. 1e6 anti-CD19 murine CAR T cells were engrafted via tail vein 24 hours later. ERC was the same as identified for the targeted agents study with the added enlarged lymph nodes and/or a cumulative superficial lymphoid tumor diameter greater than 1.6 cm would satisfy ERC.

3.3 Results

Eμ-SOX11CCND1 mice have shortened life expectancy and develop aberrant expansion of CD5+/CD19+ cells

In order to create the C57BL/6J-Tg(Eμ-sox11-GFP, Eμ-ccnd1), hereafter called the Eμ-SOX11CCND1, model of MCL, we created two colonies of Eμ-CCND1 [16], Eμ-SOX11 [17], and their cross. **Figure 4-1A** shows the genetics of each single transgenic, with both transgenes on the Eμ B cell specific promoter, and the Eμ-SOX11 also containing GFP. The first colony maintained by Dr. Samir Parehk's lab at the Icahn School of Medicine at Mount Sinai, New York, NY, was used to determine survival of the single and double transgenics compared to wild type mice (**Figure 4-1B**). The Eμ-SOX11 and Eμ-SOX11CCND1 colonies had significantly shorter survival compared to wild type mice or Eμ-CCND1 mice. The Eμ-SOX11 and Eμ-SOX11CCND1 did not have significantly different survival from each other.

A second colony was developed and maintained at The Ohio State University by the lymphoma research group. Regular monitoring via cheek bleeds and flow cytometry revealed a significant expansion of aberrant CD5+/CD19+ cells in the Eμ-SOX11 and Eμ-SOX11CCND1 colonies (**Figure 4-2, 4-3**). The Eμ-CCND1 mice closely resembled WT C57Bl/6 mice with a small population of double positive cells and normal proportion of B cells in the CD45+ compartment (**Figure 4-2A, 4-2B**). The Eμ-SOX11 mice, as previously reported [31], saw an expansion of CD5+/CD19+ cells though some maintained a normal population (**Figure 4-2C, Figure 4-3B**). The Eμ-SOX11CCND1 saw a statistically larger population of CD5+/CD19+ cells from weaning with many progressing

to early stage and late stage lymphoma (**Figure 4-2D, 4-2E, 4-3A**). Longitudinal flow cytometry over three months showed that most E μ -SOX11CCND1 mice remain at a low percentage of circulating CD5+/CD19+ cells but once they enter an early stage lymphoma, expansion is rapid (**Figure 4-3A**). Frequent monitoring was essential to detect disease burden as most mice did not show signs of discomfort or illness. Splenomegaly proved to be the most definitive physical marker of disease progress.

The percentage of double positive cells at a single time point was analyzed and showed no significant difference between WT mice, E μ -CCND1 mice, and E μ -SOX11 mice (**Figure 4-3B**). The E μ -SOX11CCND1 showed a significantly larger percent of double positive cells compared to all three groups. Both the E μ -SOX11 and E μ -SOX11CCND1 colonies showed outliers, mice likely developing malignant expansions with mice below 40% considered early stage, and those above late stage.

Age and sex on lymphomagenesis

To compare this model to human MCL incidence, we looked at sex and age. As MCL has a 3:1 male to female presentation, we looked at circulating disease by sex but found difference between sexes in either the E μ -SOX11 or the E μ -SOX11CCND1 colonies (**Figure 4-4A, 4-4B**). Mice in each colony were binned by age and analysis was performed to determine if there was a trend with age and percent CD5+/CD19+ cells circulating. No trend was statistically significant, though mice with early and late stage lymphoma were older than 100 days suggesting an aging component to disease development.

Adoptive transfer model

Due to the unpredictability and long latency of the E μ -SOX11CCND1 transgenic model, we sought to make an adoptive transfer model. This was achieved by taking malignant cells from a donor mouse that had spontaneously developed lymphoma at 625 days of age and engrafting them systemically into irradiated WT C57Bl/6 mice (**Figure 4-5A**). All five of these mice developed lymphoma, reaching ERC between 103 and 230 days post engraftment (**Figure 4-5A, 4-5B**). This process was repeated twice more with similarly conditioned mice and reduced cell numbers each time. By passage four, 100k cells could be engrafted into non-irradiated WT C57Bl/6 mice and ERC would be reached by approximately day 19 (**Figure 4-5A, 4-5B**). Immune profiling of these cells showed them to have a phenotype like human MCL with kappa but not lambda staining, and negativity for IgD (**Figure 4-5C**).

H&E was performed on an adoptive transfer mouse taken at ERC and compared to a WT C57Bl/6 mouse (**Figure 4-6**). Similar to aggressive human MCL, disease could be found throughout the organ systems. The kidneys showed destruction of architecture in addition to lymphocyte infiltration, suggesting dysfunction (**Figure 4-6A**). The liver and spleen both showed high levels of disease infiltration resulting in splenomegaly and likely dysfunction of the hepatic systems (**Figure 4-6B, 4-6C**). Lymphocyte infiltration of these organs, especially the spleen, are common in aggressive extra nodal MCL [1]. The gastrointestinal tract and bone marrow, also common areas of expansion in extra nodal MCL, also show significant disease infiltration (**Figure 4-6D, 4-6E**). This pathology supports the use of this model for aggressive MCL and will allow for study of the disease and host in multiple organ systems.

To further our studies of the tumor microenvironment, we test the adoptive transfer model as a subcutaneous tumor model. 100k cells were engrafted with Matrigel into the flank of WT C57Bl/6 mice. These mice developed subcutaneous tumors as well as systemic disease (data not shown). The subcutaneous model has a slightly delayed ERC compared to the systemic model (**Figure 4-7A**), likely related to the time required for the malignant cells to migrate and circulate.

Spectral flow cytometry was used to immune profile a spleen from a WT, systemically engrafted and subcutaneously engrafted E μ -SOX11CCND1 adoptive transfer mouse (**Figure 4-7B-D**). Clustering on major populations showed the loss of the normal B cell compartment in the subcutaneous and more significant the systemically engrafted mice (dark blue). The CD5⁺/CD19⁺ population indicative of disease cells shows low representation in the WT mouse, as seen in our colony flow but is greatly expanded in the diseased cells. The two double positive populations differ in their expression of GFP, presenting the potential that the adoptive transferred cells are losing GFP expression. Monocyte and T cell populations remain relative preserved in comparison, though all normal cells become less enriched.

We were also able to explore the immune profile in the subcutaneous model, looking at blood, spleen, and tumor of an engrafted mouse (**Figure 4-8A**). The tumor showed heavy dominance of the malignant cells and a small population of normal B cells remaining. The lack of T or NK cells clustered is likely due to relative proportions compared to disease cells as discussed later. The spleen and especially blood maintained a population of normal immune cells allowing for the potential of a host immune response.

These trends are also found focusing on the T cell compartment (**Figure 4-8B, 4-8C**). The proportion of CD4⁺ T cells among all CD3⁺ cells was significantly reduced in the tumor with the more aggressive tumor (#5) showing a greater reduction (**Figure 4-8B**). CD8⁺ T cells were potentially enriched in the tumor compared to spleen and blood but stained dimly compared to lymphatic or circulating T cells. These CD8^{Dim} have been described previously and posited to have greater natural killer effect than CD8^{Bright} cells [273] showing host response to the malignant cells.

Immune function through checkpoints was interrogated in all cell populations in a spleen of a subcutaneously engrafted mouse (**Figure 4-9**). Three populations of interest were identified, CD4⁺ T cells, dendritic cells, and the MCL like lymphoma cells (Circled on **Figure 4-9**). PDL-1 and PD-1 were detected on myeloid and T cells respectively showing immune suppression. Interestingly, the disease cells expressed both, though not concurrently (**Figure 4-9B, C**). This is supportive of a human like immune environment as PD-1 and PDL-1 expression has been reported on MCL cells previously [274].

Targeted therapies in the Eμ-SOX11CCND1

Optimally the Eμ-SOX11CCND1 model of MCL should be useful for both targeted therapies and immune therapy preclinical work so we explored the activity of the BTK inhibitor ibrutinib, the BCL-2 inhibitor venetoclax, and the PRMT5 inhibitor PRT382 [130]. **Figure 4-10A** shows the survival of Eμ-SOX11CCND1 adoptive transfer mice dosed with either a therapeutic (1X) dose or half dose (0.5X) with ibrutinib dissolved and provided as drinking water ad lib. There was not a dose dependent response to this compound though either dose of ibrutinib provided a survival advantage. The tail on both

ibrutinib cohorts suggests either the malignant cells engrafted are still heterogenous resulting in a few responding mice or that engraftment was heterogenous resulting in a delayed ERC. Overall, we would classify this model as ibrutinib resistant.

This model was similarly resistant to venetoclax at the subtherapeutic dose of 12.5mg/kg or therapeutic dose of 50mg/kg (**Figure 4-10B**). This drug was provided via oral gavage starting three days post engraftment four days on, three days off. Interestingly the 12.5mg/kg dose provided a survival advantage while the high dose did not (control 18 days vs 50mg/kg 17.5 days vs 12.5mg/kg 22 days $P < 0.05$). A similar theory holds as above for the mice with significant survival advantage though the 50mg/kg group may have suffered from toxicity. Venetoclax use in the clinic has caused tumor lysis syndrome, resulting in two fatalities in early clinical trials [275]. Tumor lysis syndrome is avoided in clinic through a ramp up in dose that would need to be adjusted for the short duration of disease in this model.

The third compound we tested is the tool compound PRT382, a selective and potent inhibitor of PRMT5. PRMT5 is known to be a key oncogenic protein in lymphomas and has shown promising results in pre-clinical research [111, 127, 130, 260]. PRT382 at 5mg/kg and 10mg/kg was dosed via oral gavage three days post engraftment and dosed four days on, three days off. This treatment provided a dose dependent survival advantage with 10mg/kg increasing the time to ERC more than three-fold (18 days vs 67 days $P < 0.001$). Using spectral flow immune profiling, we began exploring the mechanism of this survival advantage. One of the most distinct differences between treated and untreated mice was in the myeloid compartment (**Figure 4-11B**). There was a shift toward

CD11b+/Ly6Chi/Ly6G- monocytes and a decrease in CD11b+/Ly6Clo/Ly6G+ neutrophils. We also saw a decrease in PD-L1 across all myeloid cells suggesting reduced immune suppression. The increase in monocytes will require additional studies on their development and function as high absolute monocyte counts was found to be a negative prognostic factor in MCL [276].

CAR T Therapy

Chimeric antigen receptor T cells are genetically modified T cells engineered to target a specific oncogenic marker. These are commonly made from the host's own immune cells and then reinfused after the host receives conditioning to increase acceptance of the modified cells. In order to test this therapy in the subcutaneous E μ -SOX11CCND1 adoptive transfer model, we first test two types of conditioning regimens (**Figure 4-12A, 4-12B**). Irradiation is commonly used for murine studies for lymphodepletion while cyclophosphamide is a clinical agent used to condition human patients. Treatment began at day 15 when tumors were palpable. The doses of radiation given increased tumor burden while reducing splenomegaly whereas cyclophosphamide eliminated the cancer as well. Interestingly, a swelling persisted in the cyclophosphamide groups which was measured as a tumor but had no malignant tissue present upon necropsy (data not shown). Irradiation at two gray was used for further experiments to preserve the cancer.

The subcutaneous E μ -SOX11CCND1 adoptive transfer model was used as before to test anti-CD19 CAR T cells generated from syngeneic T cells with the modified the iD3-28Z construct [272] (see methods). Mice were irradiated and treated with either non-transduced T cells or CD19 CAR T cells. There was a significant though relatively small

survival advantage for the CAR T cohort (29 vs 36 days, $P=0.0033$) (**Figure 4-11C**). This result shows that CD19 CAR T cells are effective treatment in this model, similar to human MCL, but also can be improved upon with combinations that could be translated clinically.

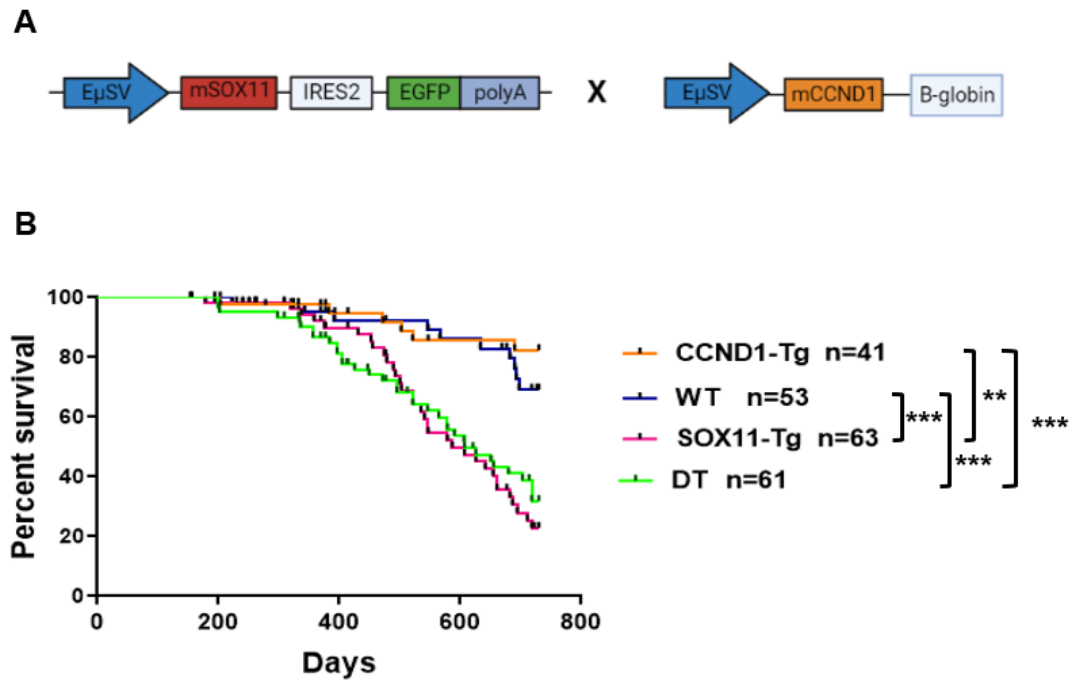


Figure 4-1: Construct of E μ -SOX11CCND1 and survival of single and double transgenic colonies

A) Genetic construct of the E μ -SOX11 and E μ -CCND1 mice that were then crossed to create the E μ -SOX11CCND1 double transgenic (DT) model. B) Kaplan Meier curve of the survival of WT C57Bl/6 mice, E μ -CCND1 (CCND1-Tg), E μ -SOX11 (SOX11-Tg), and E μ -SOX11CCND1 (DT) mice. ** P<0.01 *** P<.001. DT vs. SOX11-Tg and CCND1-Tg vs. WT are N.S. Significance determined with a log-rank test for trend.

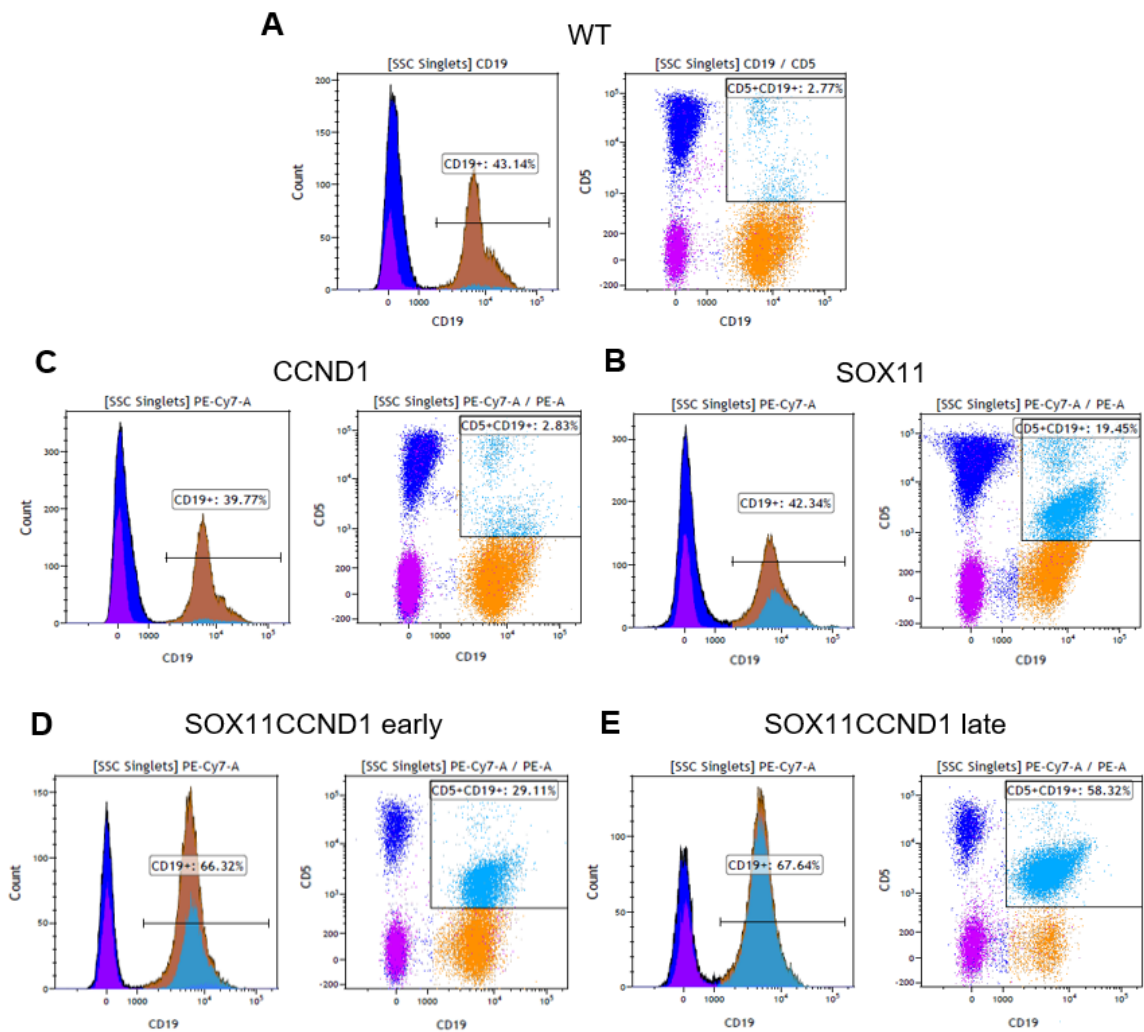


Figure 4-2: Flow cytometry plots of WT, E μ -SOX11, E μ -CCND1 and E μ -SOX11CCND1 showing percentage of CD5+/CD19+ cells

Flow cytometry plots of A) WT, B) E μ -CCND1, C) E μ -SOX11 and two E μ -SOX11CCND1 mice, one with early-stage lymphoma (D), and one with late (E). CD19 histograms show the relative percentage of CD19+ cells circulating and what proportion of those are CD5+/CD19+.

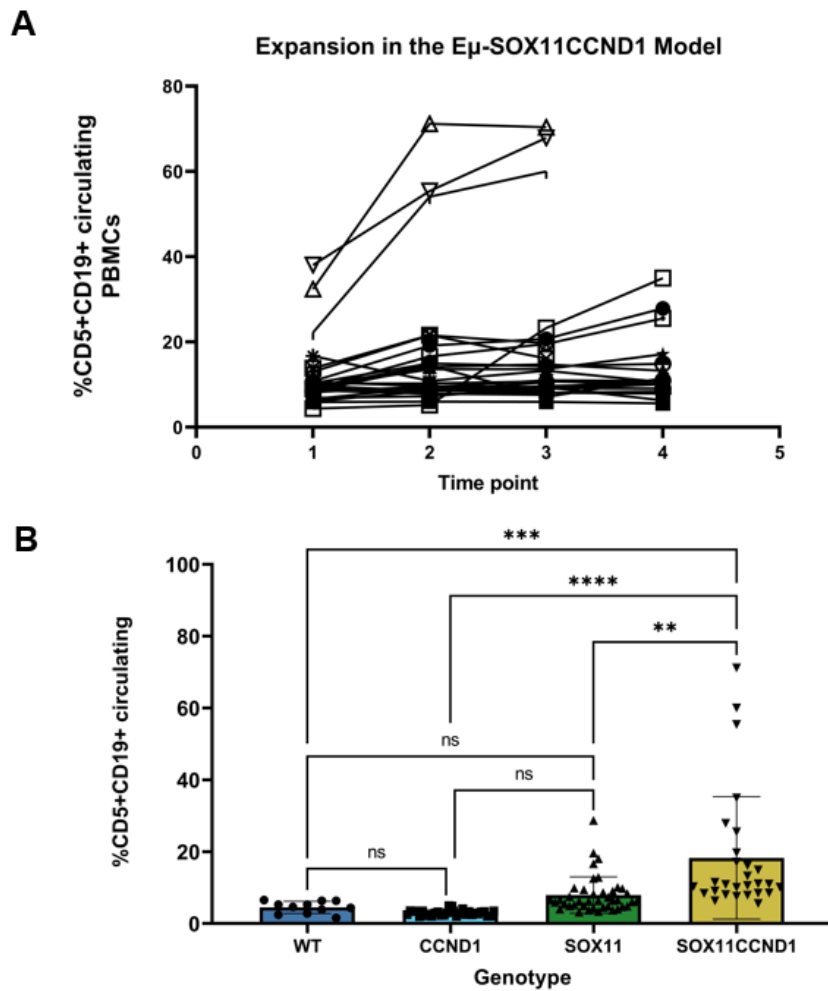


Figure 4-3: Expansion of CD5+/CD19+ cells in the E μ -SOX11CCND1 model

A) The percentage of CD5+/CD19+ cells circulating at four time points as measured via flow cytometry with regular cheek bleeds. Each line represents a separate mouse. B) Aggregated data of WT, E μ -CCND1, E μ -SOX11, and E μ -SOX11CCND1 mice at a single time point. Significance was determined with 2-way ANOVA with Šidák's multiple comparisons test. * P<0.05 ** P<0.01 *** P<0.001 **** P<0.0001 Error bars show standard deviation.

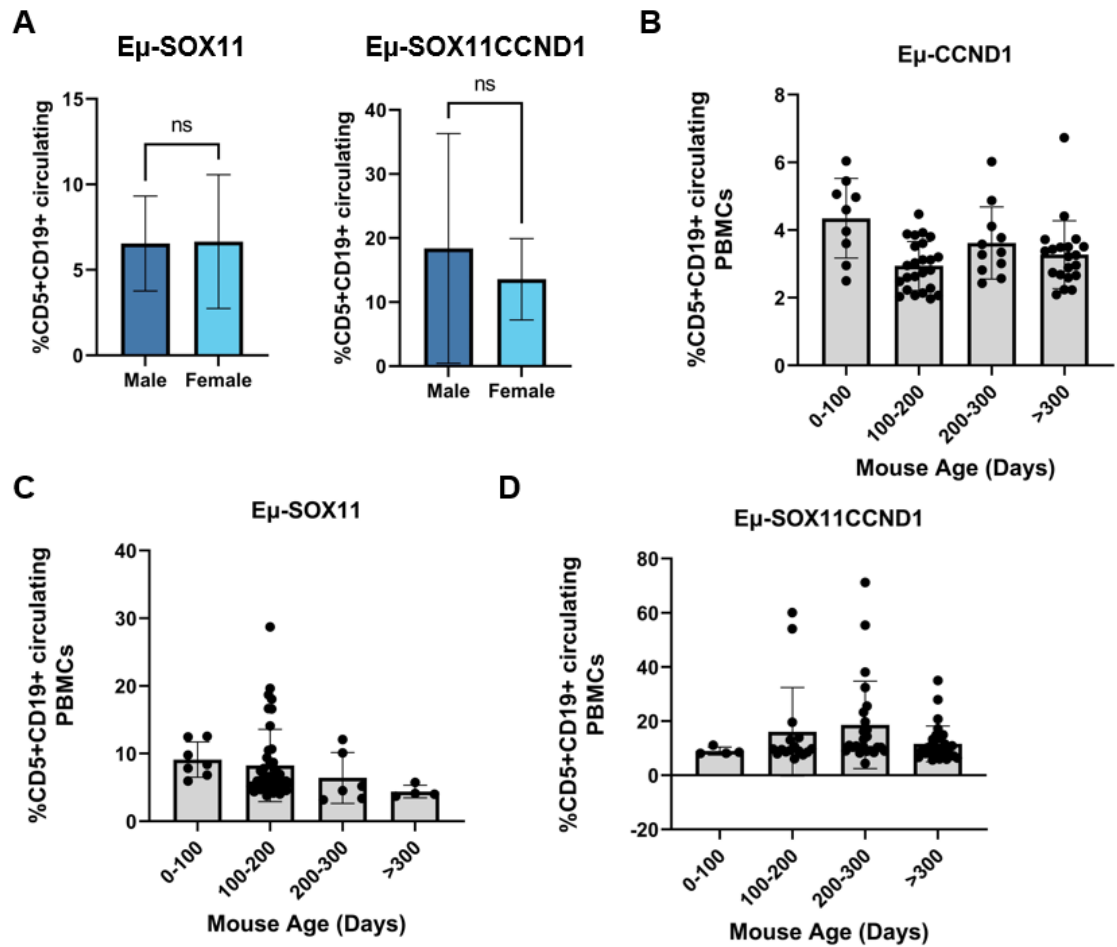


Figure 4-4: Effects of sex and age on lymphomagenesis

A) Circulating CD5+/CD19+ percentage plotted by sex for the Eμ-SOX11 (left), and Eμ-SOX11CCND1 (right) colonies. Circulating CD5+/CD19+ percentage plotted by age for the B) Eμ-CCND1, C) Eμ-SOX11, and D) Eμ-SOX11CCND1 colonies. No statistical significance was found for a linear trend of circulating percentage and age. Statistical significance was determined by students t test in A, and an ordinary one way a nova with linear trend analysis for B, C, and D. Error bars show standard deviation.

A

Mouse	Donor
Passage	0
ERC day	625
Conditioned	N/A
Engraftment number	N/A

Mouse	ATC0003.2	ATC0003.3	ATC0003.4	ATC0003.5	ATC0003.6
Passage	1	1	1	1	1
ERC day	230	201	103	230	172
Conditioned	2 Gy				
Engraftment number	1.00E+07	1.00E+07	7.00E+06	7.00E+06	7.00E+06

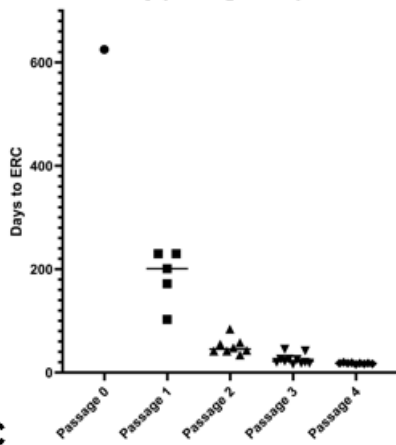
Mouse	C0003.4-1	C0003.4-2	C0003.4-3	C0003.4-4	C0003.4-5	C0003.4-6	C0003.4-7	C0003.4-8	C0003.4-9
Passage	2	2	2	2	2	2	2	2	2
ERC day	84	42	42	34	DNE	58	55	43	48
Conditioned	2 Gy								
Engraftment number	1.00E+07								

Mouse	C0003.4-10	C0003.4.4.31	C0003.4.4.32	C0003.4.4.33	C0003.4.4.34	C0003.4.4.35	C0003.4.4.36	C0003.4.4.37	C0003.4.4.38	C0003.4.4.39	C0003.4.4.40
Passage	3	3	3	3	3	3	3	3	3	3	3
ERC day	45	18	20	16	18	20	42	22	25	26	26
Conditioned	2 Gy	2 Gy	2 Gy	2 Gy	2 Gy	2 Gy	2 Gy	2 Gy	2 Gy	2 Gy	2 Gy
Engraftment number	1.00E+07	1.00E+05									

Mouse	C0003.4.4.32/35-1	C0003.4.4.32/35-2	C0003.4.4.32/35-3	C0003.4.4.32/35-4	C0003.4.4.32/35-5	C0003.4.4.32/35-6	C0003.4.4.32/35-7	C0003.4.4.32/35-8	C0003.4.4.32/35-9	C0003.4.4.32/35-10
Passage	4	4	4	4	4	4	4	4	4	4
ERC day	18	19	DNE	18	16	18	20	17	18	17
Conditioned	None									
Engraftment number	1.00E+05									

B

ERC by passage of Eμ-SOX11CCND1



C

Kappa	B220	CD45	CD11b	CD5	CD11c	CD19	IgD	CD38	IgM
++	Dim	++	-	Dim	-	+	-	+	+

Figure 4-5: Creation and immune profiling of the adoptive transfer Eμ-SOX11CCND1 model.

A) Table of passages 0-4 of the adoptive transfer model of Eμ-SOX11CCND1 detailing time to ERC, conditioning, and engraftment cell number. B) Time to ERC plotted

by passage of E μ -SOX11CCND1 cells. C) Immune profile of the E μ -SOX11CCND1 cell determined by flow cytometry.

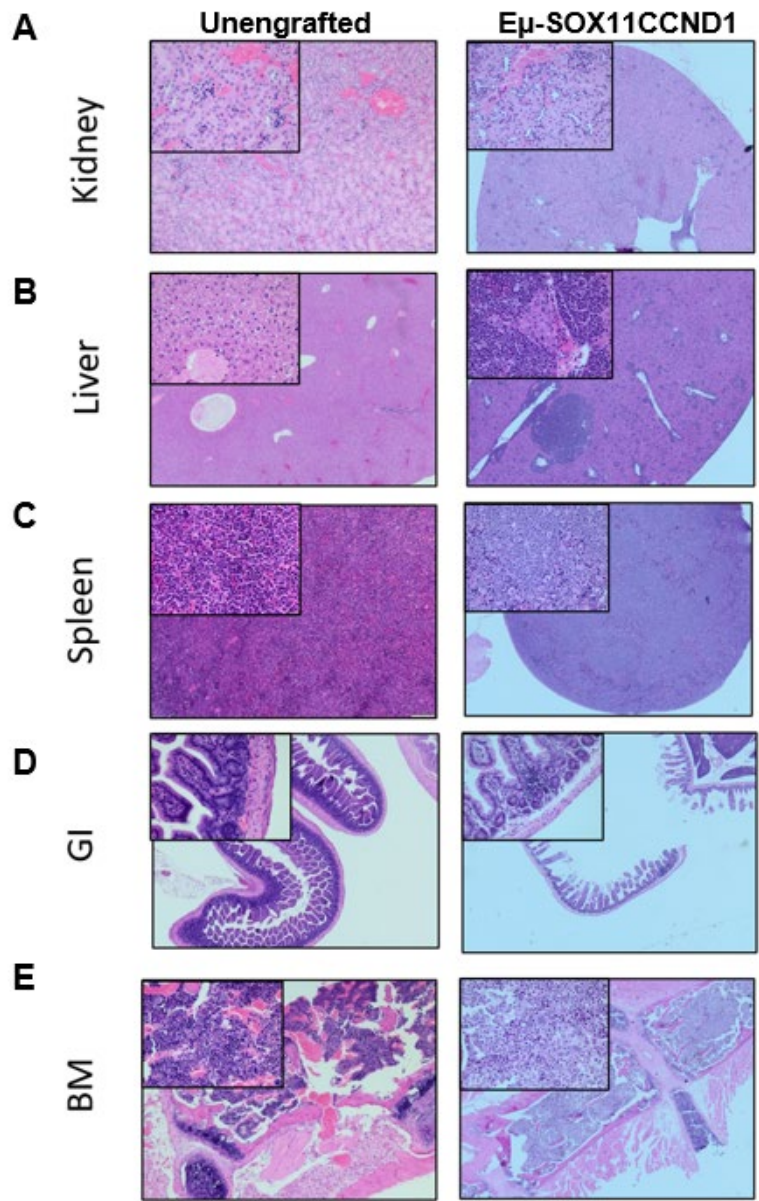


Figure 4-6: H&E of a WT C57Bl/6 mouse and an adoptive transfer E μ -SOX11CCND1 at ERC

Disease spread was detected in the A) kidneys, B) liver, C) spleen, D) gastrointestinal tract (GI), and E) bone marrow (BM).

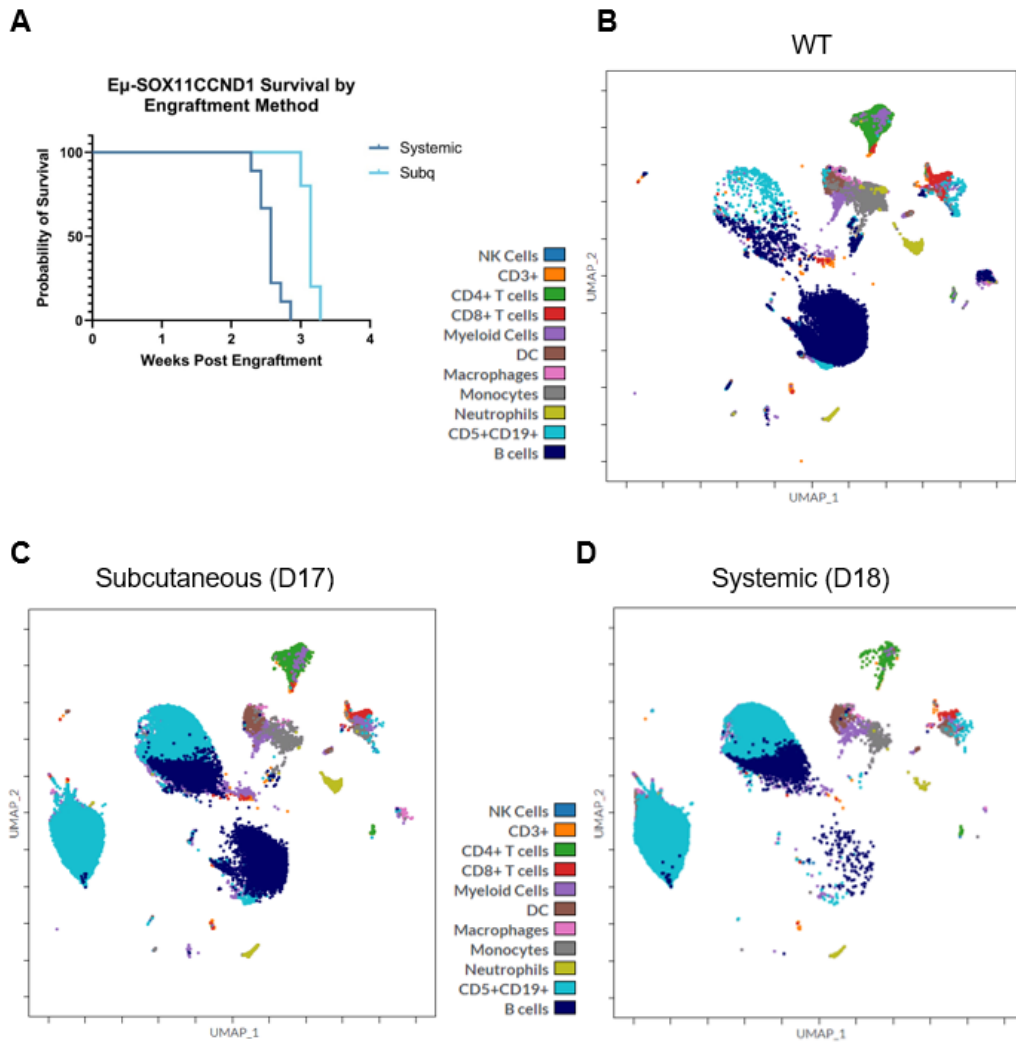


Figure 4-7: Systemic and subcutaneous Eμ-SOX11CCND1 adoptive transfer model survival and immune environment

A) Survival of the systemic and subcutaneous (subq) models of Eμ-SOX11CCND1. Spectral flow data on spleens, dimensionally reduced to UMAP plots, of B) a WT C57Bl6, C) a subcutaneously engrafted mouse sacrificed at day 17, and D) a systemically engrafted mouse sacrificed at day 18. Colors represent major cell types. Analysis and plots created in Cytobank.

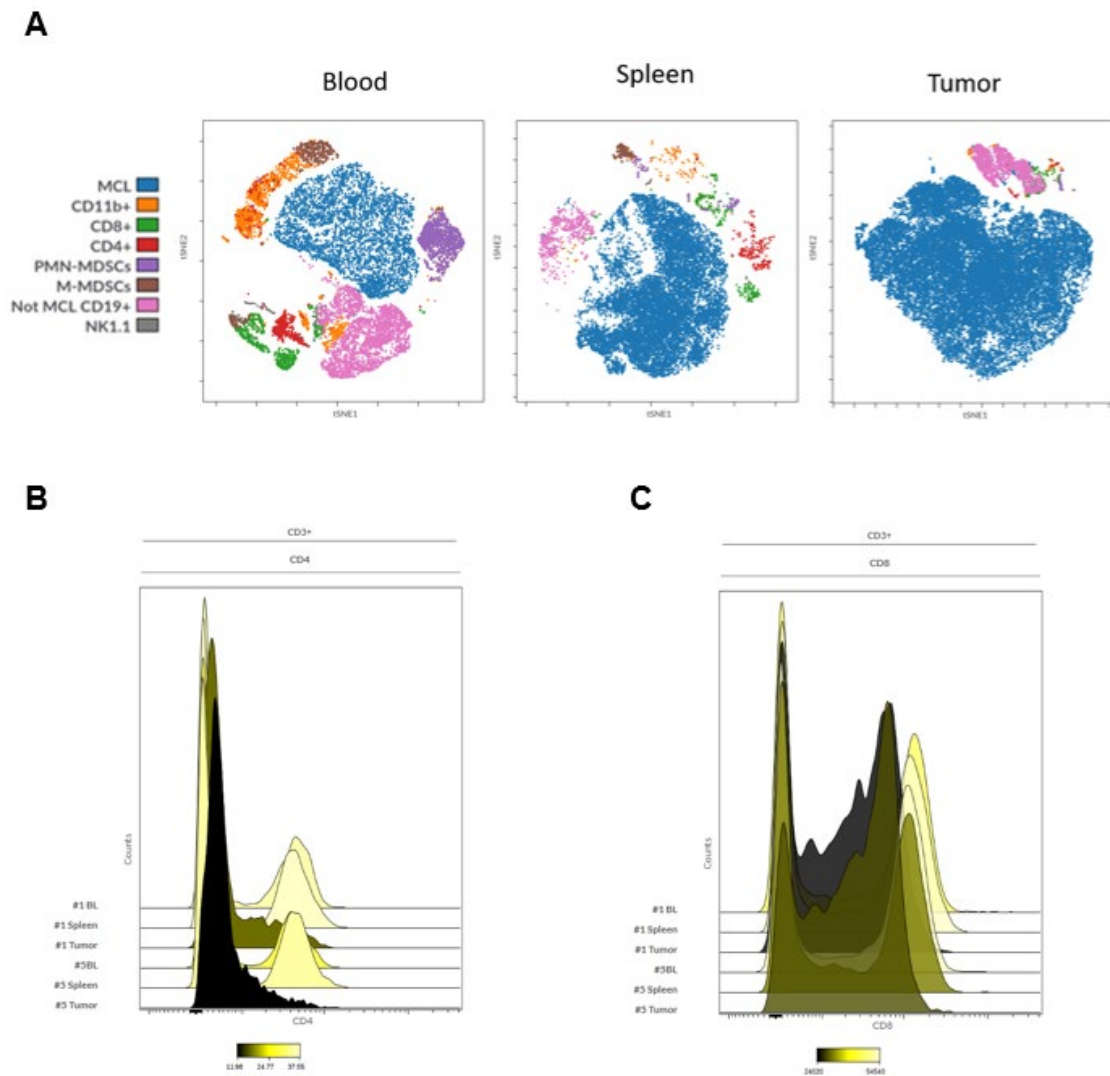


Figure 4-8: Immune analysis of blood, spleen, and tumor for a subcutaneously engrafted E μ -SOX11CCND1 mouse

A) TSNE plots of spectral flow data showing major immune populations in the blood (left), spleen (middle), and tumor (right) of a subcutaneously engrafted E μ -SOX11CCND1 mouse. Histograms of mean fluorescent intensity (MFI) of B) CD4 or C) CD8 on a gated CD3⁺ population in the blood, spleen, and tumor of a less progressed

(#1) and more progressed (#5) mouse. Color indicates percentage in CD4+ gate for C and MFI for D. Data analyzed and plots generated in Cytobank.

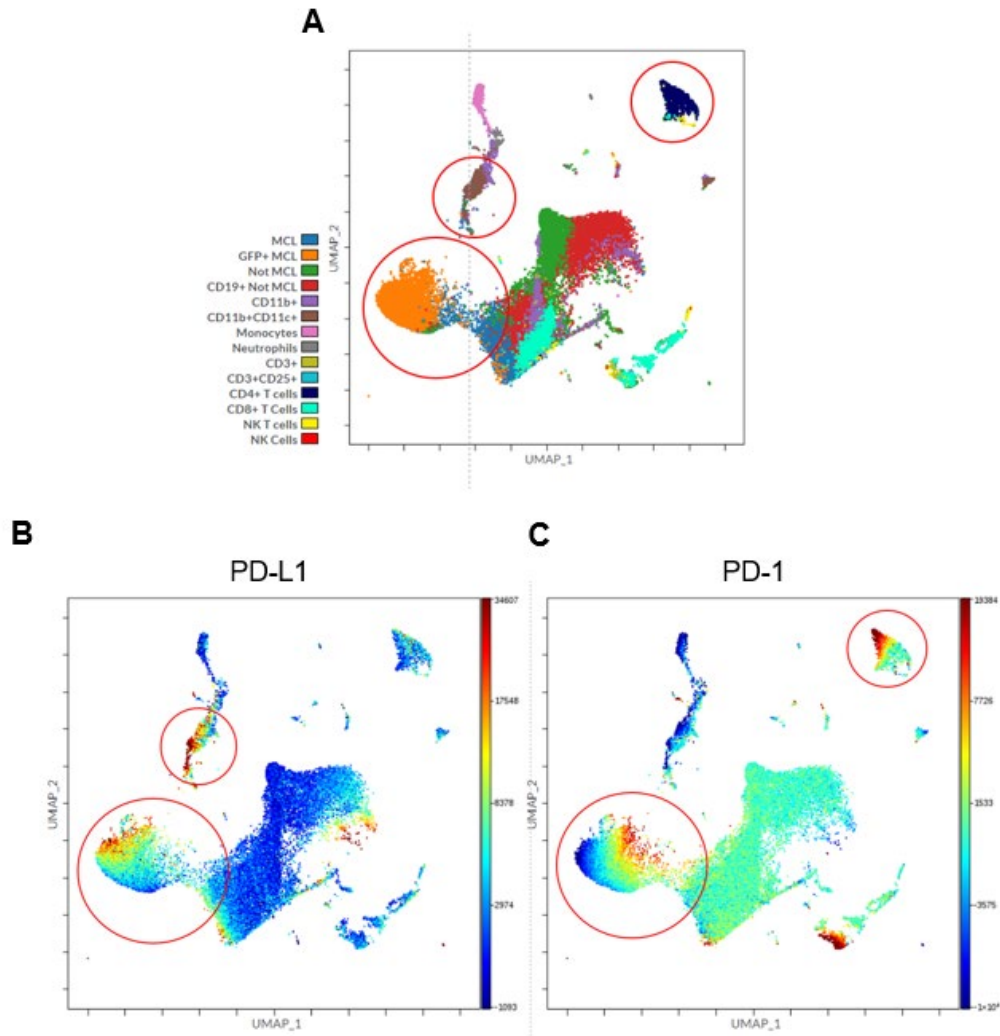


Figure 4-9: PD1 and PD-L1 expression in splenocytes of a subcutaneously engrafted Eμ-SOX11CCND1 mouse

A) Overlay on a UMAP of major immune subsets with CD4+ T cells in dark blue, dendritic (DCs) in brown, and MCL cells in orange and blue circled. Heatmaps of B) PD-L1 and C) PD-1 with the same populations of interested circled as in A. Plots generated in Cytobank.

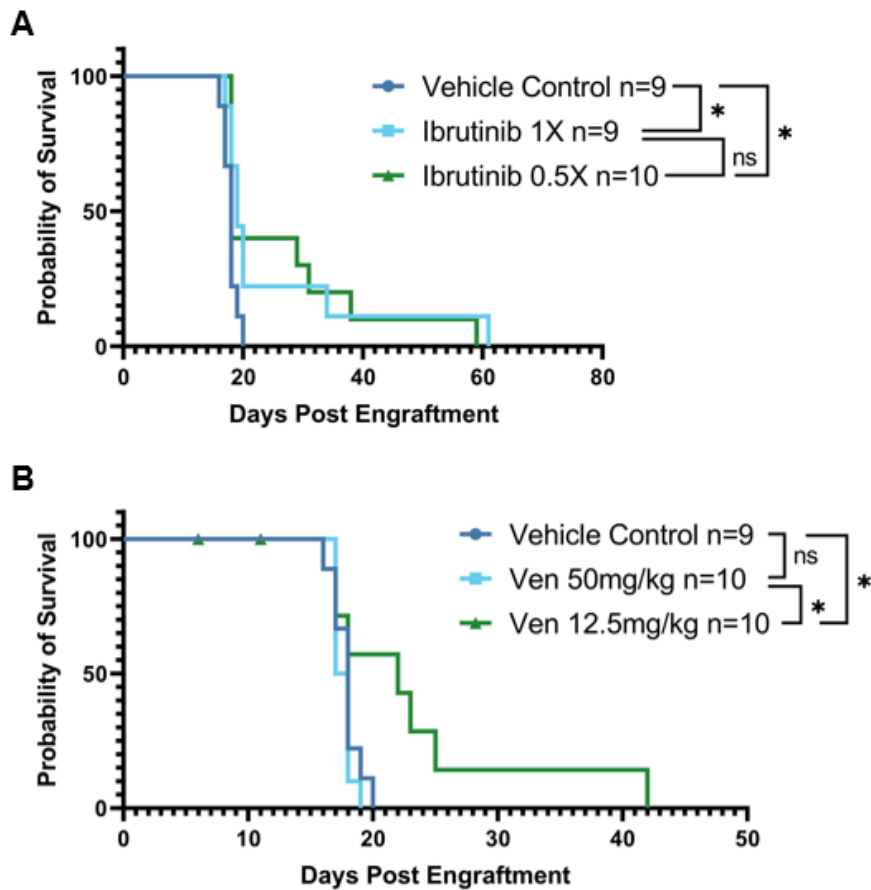


Figure 4-10: Survival curves of ibrutinib and venetoclax in systemically engrafted E μ -SOX11CCND1 mice

A) Kaplan Meier survival curve of systemically engrafted mice treated with 1x or 0.5x ibrutinib in drinking water. B) Kaplan Meier survival curve of systemically engrafted mice treated with 12.5 mg/kg or 50 mg/kg via oral gavage four days on, three days off. A log-rank test for trend was used to determine statistical significance. * P<0.05 **P<0.01 ***P<0.001 ****P<0.0001

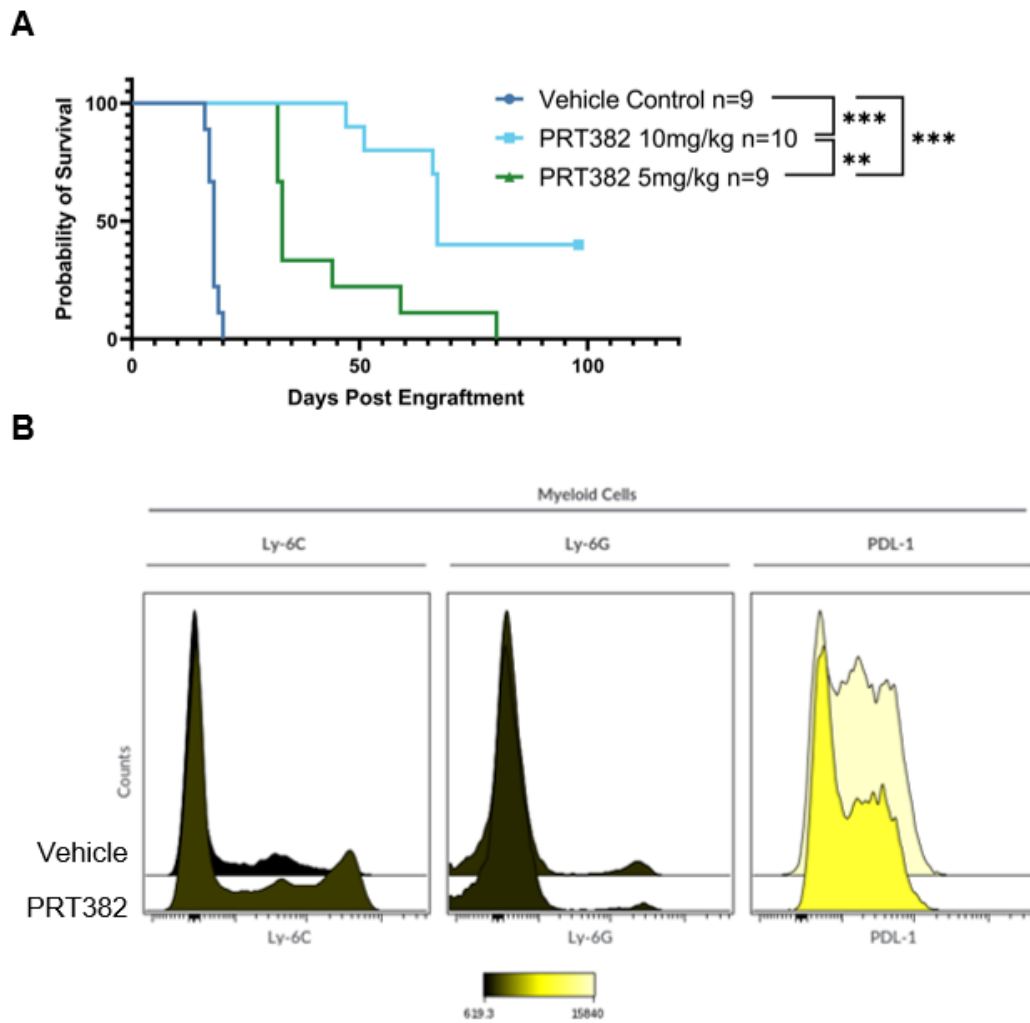


Figure 4-11: PRMT5 inhibition in the E μ -SOX11CCND1 adoptive transfer model

A) Kaplan Meier survival curve of systemically engrafted mice treated with 5mg/kg or 10mg/kg PRT382 via oral gavage dosed 4 days on, 3 days off. B) Histogram of MFI of myeloid markers Ly-6C, Ly-6G, and PD-L1 on a CD11b⁺ gated population in either vehicle or PRT382 treated E μ -SOX11CCND1 adoptive transfer mice. Color represents MFI. Figure generated in Cytobank. A log-rank test for trend was used to determine statistical significance. * P<0.05 **P<0.01 ***P<0.001 ****P<0.0001

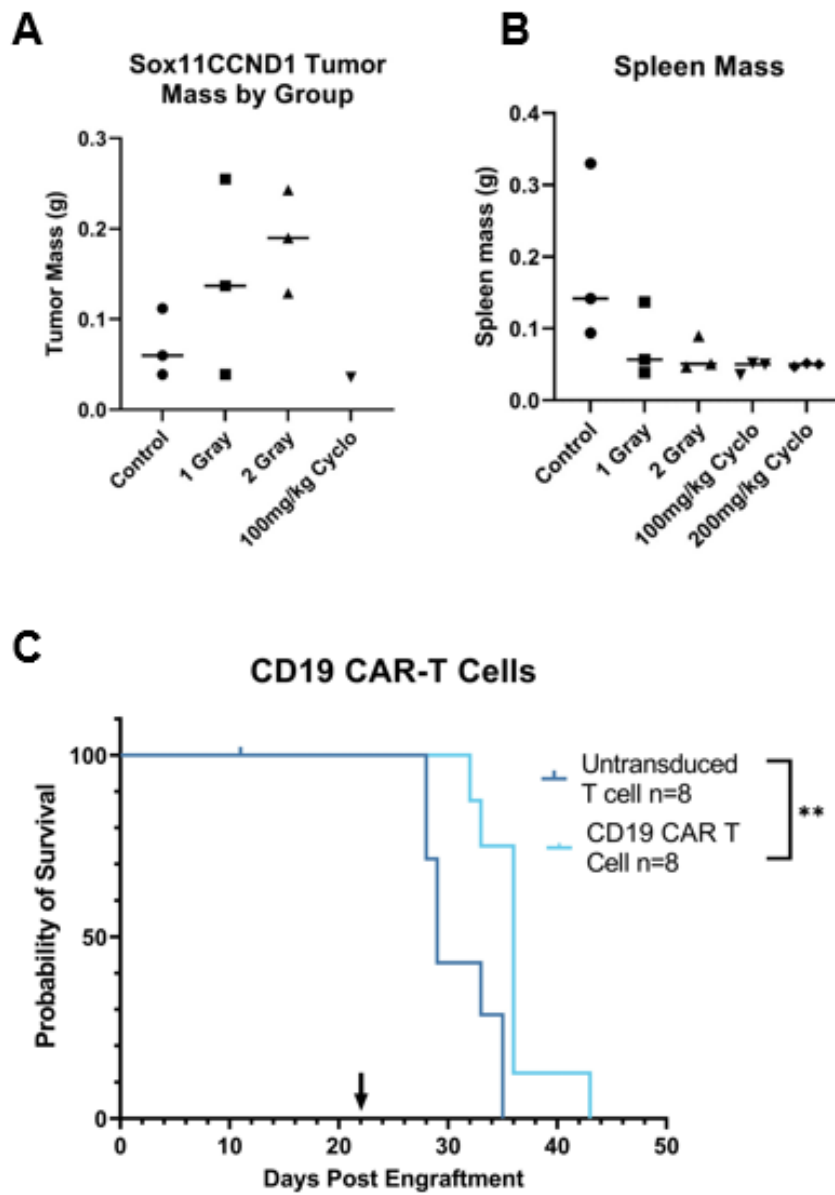


Figure 4-12: CAR T therapy in the E μ -SOX11CCND1 adoptive transfer model

A) Tumor mass on day 21 of mice conditioned with either irradiation measured at 1 or 2 gray or 100mg/kg of cyclophosphamide (cyclo). Two of three mice dosed with 100mg/kg of cyclo and all three mice dosed with 200mg/kg of cyclo did not have a

subcutaneous tumor at experimental end. B) Spleen mass of mice conditioned with either irradiation or cyclophosphamide. C) Kaplan Meier survival curve of subcutaneously engrafted mice irradiated with 2 Gray and subsequently engrafted with 1×10^6 of either untransduced T cells or CD19 CAR T cells. A log-rank test for trend was used to determine statistical significance. * $P < 0.05$ ** $P < 0.01$ *** $P < 0.001$ **** $P < 0.0001$

3.4 Conclusion

With the introduction of brexucabtagene autoleucel as an FDA approved treatment for MCL, we anticipate a renewed focus on immunotherapy for the treatment of MCL. This will require efficient and effective pre-clinical model to study the immune interactions of the host, cancer, and therapeutic agent. The options currently available are poor representations of human MCL, utilizing infrequently dysregulated genes or relying on mutations uncommon in MCL. With the heterogeneous nature of MCL, two genes stand out as overexpressed in over 90% of MCL cases: *SOX11* and *CCND1* [23, 35]. For these reasons, we have created the E μ -SOX11CCND1 transgenic model of MCL.

This study has characterized a novel transgenic model of conventional MCL showing expansion of aberrant CD5 expressing B cells which spontaneously go on to develop lymphomas. This model can also be used for adoptive transfer requiring relatively few passages to decrease the time to ERC. Both the systemically and subcutaneously engrafted models of adoptive transfer show modulated immune responses and differential expression across niches. The immune environment resembles human MCL in the presence of immune suppressive marks such as PD-1 and PD-L1. This model was found to be ibrutinib resistant and sensitive to venetoclax and to a greater degree PRMT5 inhibition. We also used CD19 CAR T cells to show the potential of this model for immunotherapy work.

This model does share characteristics with the previously published E μ -SOX11 model of MCL [31] including a similar reduction in survival, expansion of CD5+ B cells, development of lymphoma, and the ability to adoptively transferred. The

E μ -SOX11CCND1 model improves upon this model by using two key drivers in MCL. CCND1 is over expressed in more than 95% of MCL cases suggesting it plays a necessary, if not sufficient [20], role in lymphomagenesis [35, 277]. We saw a significantly higher parentage of CD5+/CD19+ circulating in our E μ -SOX11CCND1 colony compared to the E μ -SOX11 suggesting a more robust lymphomagenesis in the double transgenic. More work is warranted to investigate the pathways upregulated in both models to compare to human MCL drivers.

A deeper profiling of this model is under way to understand the clonality of disease, genetic drivers, and mutational status. We are also analyzing how these features may change over the course of passaging the adoptive transfer model. While our donor effectively created our adoptive transfer model, it would be advantageous to repeat this process with additional donors to have a portfolio immunocompetent but short duration MCL murine models.

We are currently undergoing additional testing for immunotherapies in this model including novel target CAR T cells and immune check point blockade. While these single agents may provide survival advantages, we are more interested in combining immunomodulatory agents like PRMT5 inhibitors for a combination strategy. PRMT5 inhibition has been shown to reduce graft vs host disease, while preserving the graft vs leukemic effects [108], suggesting immune modulatory activity that would be beneficial for CAR T therapies. The effects on the myeloid compartment are also of interest as PRMT5 regulation of myeloid cells is a poorly understood phenomenon.

In all, this model will be an excellent tool for any MCL researcher looking to explore lymphomagenesis, the tumor microenvironment, or novel immunotherapy strategies. Created on a C57Bl/6 background with high penetrance, this model is accessible and will be easy to establish in other research centers. We are encouraged by the early results of immunotherapy in MCL and hope this model will support further breakthroughs for the treatment of MCL in the clinic.

Chapter 5: Discussion and Future Directions

Mantle cell lymphoma continues to be an incurable cancer. With a highly varied genetic and molecular profile, targeted therapies may be essential for the treatment. Treatment with BTK inhibitors such as ibrutinib, has resulted in significant improvements in outcomes but also results in more aggressive disease upon relapse. Finding options that will work for these patients is vital. Single agent regimens are very rarely given to patients reminding us that combination therapies are not only an option, but historically speaking are more successful at managing cancers. Another avenue of combination therapy beyond two or more targeted agents is immunotherapy and immune modulatory agents. Given the success of immunotherapy in MCL with the anti-CD20 antibody, rituximab, there is hope that new agents in this field including immune checkpoint blocks, bi-specific antibodies, and CAR T or NK cells will result in a breakthrough for the treatment of MCL. The ability to test these agents pre-clinically will be key to translating basic scientific findings into clinical results.

PRMT5 inhibition and BH3 mimetics

Among the agents being tested are PRMT5 inhibitors. PRMT5 is a key oncogene in many cancers including MCL. Previous work from the OSU Lymphoma research group showed that inhibition of this enzyme prevented EBV driven lymphomagenesis [127], suppressed pro-survival WNT beta catenin signaling [30] and restored cell cycle regulation through pRB in MCL [30, 219]. With this understanding CMP 5 was generated at The Ohio State University as a first in class dual target PRMT5 inhibitor [127]. From this compound

second and third generations of compounds were created, including PRT382 (tool for PRT543) and PRT808 (tool for PRT811) from Prelude Therapeutics. PRT543 and PRT811 are being tested in clinical trials and pre-clinical work with these agents support the use of these agents beyond single agent trials.

The work described here shows that PRMT5 inhibition synergizes with BH3 mimetics in *in vitro* and *in vivo* providing support for use of this combination in clinical trials. PRMT5 inhibition was found to reactivate the transcription factor FOXO1 and resulted in the upregulation of a number of pro-apoptotic BCL-2 family proteins including effectors, activators, and sensitizers. These changes in expression resulted in increased sensitivity to mitochondrial insult though response varied by cell line. This is representative of the molecular and genetic heterogeneity seen in MCL cell lines and between patients. Overall, the BH3 mimetics venetoclax (BCL-2i), navitoclax (BCL-2i, BCL-xL, BCL-w), PRT1419(MCL-1i), and A852 (BCL-xL) all showed synergy with PRMT5 inhibition in MCL.

The *in vivo* results from these studies showed impressive survival advantage and reduced circulation of disease but did not prove curative. The mice in the venetoclax study were taken off drug and eventually relapsed (data not shown) while the navitoclax study reached ERC despite low disease burden. Work should be done to determine if venetoclax and PRMT5i could keep mice in remission or if alteration to dosing could result in curative treatments. With a repeat PRT382 and venetoclax study, once mice are in remission, a sentinel cohort could be taken to explore where disease is still located. The bone marrow is a known protective niche for NHLs [278] and may be a difficult location for drugs to

reach. The navitoclax combination also showed impressive survival advantage but all mice reached ERC and never obtained the same remission seen with the venetoclax combination. Samples from these mice should be analyzed to determine what the mechanism of resistance is and if there is a way to work around or through that resistance.

We were able to determine that PRT382 and navitoclax were synergistic in the PDX.AA.MCL model but the MCL-1 inhibitor PRT1419 had no effect in this model as either single agent or in combination. BH3 profiling of vehicle and PRT382 treated cells showed no sensitivity to the MCL-1 targeting NOXA peptide which suggests that MCL-1 inhibition is not a good option for this model. Based on our profiling and access to models, we found that a MCL-1 CDX would be the best choice to test for PRMT5 and MCL-1 synergy. This study is on going and will be included in the publication of this work.

While FOXO1 was found to target multiple pro-survival protein promoters through ChIP seq, ChIP qPCR did not confirm this result for all the cell lines tested. It is likely that multiple transcription factors aid in the regulation of the pro-apoptotic BCL-2 family. p53 is well reported to regulate *BAX* transcription as well as other pro-apoptotic proteins such as Puma [279]. Further mechanistic work to determine which factors associate with the genes in MCL before and after PRMT5 inhibition would provide a deeper understanding of the function of PRMT5 in the support of MCL pathogenesis.

While CDX and PDX models of MCL are useful tools, additional support for PRMT5i and BH3 combination therapy could be obtained through the use of organoid systems to support primary samples. PRMT5 inhibition takes several days to cause changes in signaling and up to six days to see cell death, requiring the ability to culture primary

cells for longer than they will typically last in standard cell culture conditions. Organoid systems have been developed including protocol using Matrigel or other similar hydrogels with promising results. Another mechanism of support is to use CD40L expressing fibroblasts as support cells. Testing these methods may allow us to incorporate more primary sample data in the future.

E μ -SOX11CCND1 Model of MCL

Mouse models are essential for cancer research, acting as a bridge between cell culture and clinical trials. For MCL researchers, CDXs and PDXs have been the only accessible models of MCL that could be used to test novel therapeutic strategies *in vivo*. With the increasing interest in immunotherapy for MCL, there is a great need for a fully immune competent model of MCL. Previous attempts to create a transgenic MCL murine model relied on the overexpression of c-Myc, which while detected in MCL, is heterogenous in its expression and signaling [280]; *CCND1* and second hit that is uncommon in MCL such as *MDM2* [281]; or an alternative cyclin such as *CCND2*. Each of these models has genetic drivers that distance the model from the genetic profile seen in human MCL.

By using *CCND1* and *SOX11* on the E μ promoter, we were able to create a B cell specific over expression of two oncogenes expressed in over 90% of MCL cases and frequently used to diagnose the cancer. This model shows shortened life expectancy, increased circulation of CD5⁺ expressing B cells, and develops lymphoma with pathogenic expansion of CD5⁺/CD19⁺ cells, splenomegaly, and lymphocyte infiltration of liver and kidneys. To make the model more accessible for drug studies or other work that requires

controlled cohorts, we created an adoptive transfer model where disease cells from a spleen or lymph node can be engrafted into a conditioned WT C57Bl/6 mouse, which then goes on to develop lymphoma. Analysis of the systemic and subcutaneous modes of engraftment revealed a major loss in normal B cells as well as differential immune populations in the blood, spleen, and tumor. We also saw evidence of disease cell supported immune suppression with PD-1 and PD-L1 expression being seen on CD5⁺/CD19⁺ cells. Testing targeted therapeutics revealed resistance to the common MCL drug ibrutinib, and a sensitivity to venetoclax and the PRMT5 inhibitor PRT382. We were also able to test murine CD19 CAR T cells as a proof of concept to support the use of this model for testing of novel CAR products or other immune therapies.

Genetic and molecular analysis of the E μ -SOX11CCND1 will be essential for determining the driving pathways and comparing those to human MCL. RNA sequencing, either bulk or single cell could be to answer these questions. Using our colony, we will have samples from different stages of lymphomagenesis allowing us to interrogate what causes a mouse to develop an aggressive lymphoma. B cell receptor sequencing from the sequencing data will answer if the CD5⁺ B cells are mono- or polyclonal and changes during the course of lymphomagenesis. It is possible that these mice have developed tertiary genetic lesions in the form of a mutation that drives proliferation which will also be detected if the mutation is in a gene body. A combination of spectral flow cytometry and single cell RNA sequencing will be essential for understanding how the host and lymphoma interact in specific niches such as the bone marrow, blood, spleen, and lymph nodes. Unlike bulk RNA seq, this question requires the ability to differentiate specific cell

types before performing pathway analysis. We look forward to the results of this work in the near future.

The resistance seen to ibrutinib is a common feature in aggressive MCL. Ibrutinib is currently the second line therapy of choice for MCL and is frequently used for later lines of therapy as well. Unfortunately, progression on ibrutinib is a negative prognostic factor and patients are unlikely to respond to salvage therapy [97]. The response of the E μ -SOX11CCND1 to ibrutinib supports its use as model of aggressive MCL, where novel treatments are the most needed. The response seen to PRT382 also demonstrated the similarity between this model and our PDX and CDX models where dose dependent survival advantages with PRMT5 inhibition were also seen.

The relatively small survival advantage seen with CD19 CAR T cell may actually prove beneficial, as this provides a baseline upon which to improve. Samples from this study will be histologically analyzed to determine the presence and location of the CAR T cells at ERC. As these cells were engrafted systemically, there is the possibility that they were not able to reach the tumor resulting in continued growth. Spectral flow cytometry will also be used to confirm the presence or absence of the CAR T cells, as well as look for other immune subsets and their activating or suppressing marks. Based on human studies of CAR T cells, PD-1/PD-L1 blockade may aid CAR T function, especially given the expression of both marks on the disease cells.

In order to make this model more useful and accessible, additional adoptive transfer models should be developed. While conditioning for the first passage is likely required, testing the speed at which it can be removed and the cell count reduced would be important

for further model development. While the speed of the current adoptive transfer model is a benefit for many drug studies, a slower growing cancer may be preferable to understanding host immune response and how the cancer is able to escape. In humans, cancers often take years to fully mature, a feature difficult to model in mice but a worthy element to try and recreate.

Overview

This dissertation has advanced two key elements of MCL pre-clinical research. First, a novel treatment strategy was developed and tested using compounds currently in clinical trials. The agents chosen were based off a biologic understanding of the drivers of MCL and previous research in the down-stream effects of PRMT5 inhibition. The results were supported through mechanistic studies looking at the response of MCL to mitochondrial insult, ChIP sequencing of a key transcription factor, genetic analysis through RNA sequencing, and knock down studies to determine dependence. The work provides strong rationale for combining PRMT5 inhibitors and BH3 mimetics in future clinical trials. The second advancement is the characterization of a novel transgenic murine model of MCL. The E μ -SOX11CCND1 model opens the door for not just our lab but all MCL researchers who share an interest in the immune response to cancer and how it can be modified. Through spectral flow cytometry, we were able to profile this model as having the same surface markers as human MCL, including expression of both PD-1 and PD-L1 suggesting a potential avenue for immune checkpoint blockade in future treatments. We look forward to seeing what insights and novel immunotherapies are created using this model.

Bibliography

1. Lynch, D.T., et al. *Mantle Cell Lymphoma*. 2022 [cited 2022 November 2nd].
2. Vorobyev, et al., *T(11;14)(q13;q32) in Mantle Cell Lymphoma Patients Is Present Only on Mature Malignant Cells. Fluorescence-Activated Cell Sorting and Fluorescence in Situ Hybridization Analysis*, in *American Society of Hematology (ASH) Annual Meeting*. 2011, Blood.
3. Teras, L.R., et al., *2016 US lymphoid malignancy statistics by World Health Organization subtypes*. *CA Cancer J Clin*, 2016. **66**(6): p. 443-459.
4. Zhou, Y., et al., *Incidence trends of mantle cell lymphoma in the United States between 1992 and 2004*. *Cancer*, 2008. **113**(4): p. 791-8.
5. Cheah, C.Y., J.F. Seymour, and M.L. Wang, *Mantle Cell Lymphoma*. *J Clin Oncol*, 2016. **34**(11): p. 1256-69.
6. Aschebrook-Kilfoy, B., et al., *An upward trend in the age-specific incidence patterns for mantle cell lymphoma in the USA*. *Leuk Lymphoma*, 2013. **54**(8): p. 1677-83.
7. Armitage, J.O. and D.L. Longo, *Mantle-Cell Lymphoma*. *N Engl J Med*, 2022. **386**(26): p. 2495-2506.
8. Swerdlow, S.H., et al., *The 2016 revision of the World Health Organization classification of lymphoid neoplasms*. *Blood*, 2016. **127**(20): p. 2375-90.
9. Maddocks, K., *Update on mantle cell lymphoma*. *Blood*, 2018. **132**(16): p. 1647-1656.
10. Saleh, K., et al., *Tumor Microenvironment and Immunotherapy-Based Approaches in Mantle Cell Lymphoma*. *Cancers (Basel)*, 2022. **14**(13).
11. Martin, P., et al., *Outcome of deferred initial therapy in mantle-cell lymphoma*. *J Clin Oncol*, 2009. **27**(8): p. 1209-13.
12. Khanlari, M. and C.Y. Ok, *Lymphoma & related disorders - Mature B cell neoplasms: Mantle cell lymphoma*. 2023, PathologyOutlines.
13. Liu, H., J. Wang, and E.M. Epner, *Cyclin D1 activation in B-cell malignancy: association with changes in histone acetylation, DNA methylation, and RNA polymerase II binding to both promoter and distal sequences*. *Blood*, 2004. **104**(8): p. 2505-13.
14. Wang, K., et al., *Cell Cycle Dysregulation in Mantle Cell Lymphoma: Genomics and Therapy*. *Hematol Oncol Clin North Am*, 2020. **34**(5): p. 809-823.
15. Salaverria, I., et al., *CCND2 rearrangements are the most frequent genetic events in cyclin D1(-) mantle cell lymphoma*. *Blood*, 2013. **121**(8): p. 1394-402.
16. Lam, E.W., et al., *Cyclin D3 compensates for loss of cyclin D2 in mouse B-lymphocytes activated via the antigen receptor and CD40*. *J Biol Chem*, 2000. **275**(5): p. 3479-84.
17. Chen, B. and J.W. Pollard, *Cyclin D2 compensates for the loss of cyclin D1 in estrogen-induced mouse uterine epithelial cell proliferation*. *Mol Endocrinol*, 2003. **17**(7): p. 1368-81.

18. Fu, M., et al., *Minireview: Cyclin D1: normal and abnormal functions*. *Endocrinology*, 2004. **145**(12): p. 5439-47.
19. Body, S., et al., *Cytoplasmic cyclin D1 controls the migration and invasiveness of mantle lymphoma cells*. *Sci Rep*, 2017. **7**(1): p. 13946.
20. Bodrug, S.E., et al., *Cyclin D1 transgene impedes lymphocyte maturation and collaborates in lymphomagenesis with the myc gene*. *EMBO J*, 1994. **13**(9): p. 2124-30.
21. Lovec, H., et al., *Cyclin D1/bcl-1 cooperates with myc genes in the generation of B-cell lymphoma in transgenic mice*. *EMBO J*, 1994. **13**(15): p. 3487-95.
22. Lecluse, Y., et al., *t(11;14)-positive clones can persist over a long period of time in the peripheral blood of healthy individuals*. *Leukemia*, 2009. **23**(6): p. 1190-3.
23. Mozos, A., et al., *SOX11 expression is highly specific for mantle cell lymphoma and identifies the cyclin D1-negative subtype*. *Haematologica*, 2009. **94**(11): p. 1555-62.
24. Ek, S., et al., *Nuclear expression of the non B-cell lineage Sox11 transcription factor identifies mantle cell lymphoma*. *Blood*, 2008. **111**(2): p. 800-5.
25. Sarkar, A. and K. Hochedlinger, *The sox family of transcription factors: versatile regulators of stem and progenitor cell fate*. *Cell Stem Cell*, 2013. **12**(1): p. 15-30.
26. Dodonova, S.O., et al., *Nucleosome-bound SOX2 and SOX11 structures elucidate pioneer factor function*. *Nature*, 2020. **580**(7805): p. 669-672.
27. Vegliante, M.C., et al., *SOX11 regulates PAX5 expression and blocks terminal B-cell differentiation in aggressive mantle cell lymphoma*. *Blood*, 2013. **121**(12): p. 2175-85.
28. Bhattaram, P., et al., *SOXC proteins amplify canonical WNT signaling to secure nonchondrocytic fates in skeletogenesis*. *J Cell Biol*, 2014. **207**(5): p. 657-71.
29. Gelebart, P., et al., *Constitutive activation of the Wnt canonical pathway in mantle cell lymphoma*. *Blood*, 2008. **112**(13): p. 5171-9.
30. Chung, J., et al., *Protein arginine methyltransferase 5 (PRMT5) promotes survival of lymphoma cells via activation of WNT/ β -catenin and AKT/GSK3 β proliferative signaling*. *J Biol Chem*, 2019. **294**(19): p. 7692-7710.
31. Kuo, P.Y., et al., *SOX11 augments BCR signaling to drive MCL-like tumor development*. *Blood*, 2018. **131**(20): p. 2247-2255.
32. Hill, H.A., et al., *Genetic mutations and features of mantle cell lymphoma: a systematic review and meta-analysis*. *Blood Adv*, 2020. **4**(13): p. 2927-2938.
33. Wu, C., et al., *Genetic heterogeneity in primary and relapsed mantle cell lymphomas: Impact of recurrent CARD11 mutations*. *Oncotarget*, 2016. **7**(25): p. 38180-38190.
34. Jeong, S., et al., *Genetic heterogeneity and prognostic impact of recurrent ANK2 and TP53 mutations in mantle cell lymphoma: a multi-centre cohort study*. *Sci Rep*, 2020. **10**(1): p. 13359.
35. Veloza, L., I. Ribera-Cortada, and E. Campo, *Mantle cell lymphoma pathology update in the 2016 WHO classification*. *Annals of Lymphoma*, 2019. **3**.

36. Nadeu, F., et al., *Genomic and epigenomic insights into the origin, pathogenesis, and clinical behavior of mantle cell lymphoma subtypes*. *Blood*, 2020. **136**(12): p. 1419-1432.
37. Zhang, J., et al., *The genomic landscape of mantle cell lymphoma is related to the epigenetically determined chromatin state of normal B cells*. *Blood*, 2014. **123**(19): p. 2988-96.
38. Salaverria, I., et al., *Specific secondary genetic alterations in mantle cell lymphoma provide prognostic information independent of the gene expression-based proliferation signature*. *J Clin Oncol*, 2007. **25**(10): p. 1216-22.
39. Camacho, E., et al., *ATM gene inactivation in mantle cell lymphoma mainly occurs by truncating mutations and missense mutations involving the phosphatidylinositol-3 kinase domain and is associated with increasing numbers of chromosomal imbalances*. *Blood*, 2002. **99**(1): p. 238-44.
40. Ma, M.C.J., et al., *Subtype-specific and co-occurring genetic alterations in B-cell non-Hodgkin lymphoma*. *Haematologica*, 2022. **107**(3): p. 690-701.
41. Lee, J.H. and T.T. Paull, *Cellular functions of the protein kinase ATM and their relevance to human disease*. *Nat Rev Mol Cell Biol*, 2021. **22**(12): p. 796-814.
42. Mantovani, F., L. Collavin, and G. Del Sal, *Mutant p53 as a guardian of the cancer cell*. *Cell Death Differ*, 2019. **26**(2): p. 199-212.
43. Clot, G., et al., *A gene signature that distinguishes conventional and leukemic nonnodal mantle cell lymphoma helps predict outcome*. *Blood*, 2018. **132**(4): p. 413-422.
44. Jiang, P., A. Desai, and H. Ye, *Progress in molecular feature of smoldering mantle cell lymphoma*. *Exp Hematol Oncol*, 2021. **10**(1): p. 41.
45. Wang, L., et al., *MYC rearrangement but not extra MYC copies is an independent prognostic factor in patients with mantle cell lymphoma*. *Haematologica*, 2021. **106**(5): p. 1381-1389.
46. Lee, J., et al., *Activation of MYC, a bona fide client of HSP90, contributes to intrinsic ibrutinib resistance in mantle cell lymphoma*. *Blood Adv*, 2018. **2**(16): p. 2039-2051.
47. Pinyol, M., et al., *Deletions and loss of expression of p16INK4a and p21Waf1 genes are associated with aggressive variants of mantle cell lymphomas*. *Blood*, 1997. **89**(1): p. 272-80.
48. Streich, L., et al., *Aggressive morphologic variants of mantle cell lymphoma characterized with high genomic instability showing frequent chromothripsis, CDKN2A/B loss, and TP53 mutations: A multi-institutional study*. *Genes Chromosomes Cancer*, 2020. **59**(8): p. 484-494.
49. Serrano, M., et al., *Role of the INK4a locus in tumor suppression and cell mortality*. *Cell*, 1996. **85**(1): p. 27-37.
50. Queirós, A.C., et al., *Decoding the DNA Methylome of Mantle Cell Lymphoma in the Light of the Entire B Cell Lineage*. *Cancer Cell*, 2016. **30**(5): p. 806-821.
51. Leshchenko, V.V., et al., *Genomewide DNA methylation analysis reveals novel targets for drug development in mantle cell lymphoma*. *Blood*, 2010. **116**(7): p. 1025-34.

52. Hasanali, Z., K. Sharma, and E. Epner, *Flipping the cyclin D1 switch in mantle cell lymphoma*. *Best Pract Res Clin Haematol*, 2012. **25**(2): p. 143-52.
53. Wang, Y. and S. Ma, *Risk factors for etiology and prognosis of mantle cell lymphoma*. *Expert Rev Hematol*, 2014. **7**(2): p. 233-43.
54. Smedby, K.E., et al., *Medical history, lifestyle, family history, and occupational risk factors for mantle cell lymphoma: the InterLymph Non-Hodgkin Lymphoma Subtypes Project*. *J Natl Cancer Inst Monogr*, 2014. **2014**(48): p. 76-86.
55. Wang, S.S., et al., *Family history of hematopoietic malignancies and risk of non-Hodgkin lymphoma (NHL): a pooled analysis of 10 211 cases and 11 905 controls from the International Lymphoma Epidemiology Consortium (InterLymph)*. *Blood*, 2007. **109**(8): p. 3479-88.
56. Carbone, P.P., et al., *Report of the Committee on Hodgkin's Disease Staging Classification*. *Cancer Res*, 1971. **31**(11): p. 1860-1.
57. Lister, T.A., et al., *Report of a committee convened to discuss the evaluation and staging of patients with Hodgkin's disease: Cotswolds meeting*. *J Clin Oncol*, 1989. **7**(11): p. 1630-6.
58. Board, P.P.T.E., *Childhood Hodgkin Lymphoma Treatment: Health Professional Version*. 2022, National Cancer Institute.
59. Cheson, B.D., et al., *Recommendations for initial evaluation, staging, and response assessment of Hodgkin and non-Hodgkin lymphoma: the Lugano classification*. *J Clin Oncol*, 2014. **32**(27): p. 3059-68.
60. Seam, P., M.E. Juweid, and B.D. Cheson, *The role of FDG-PET scans in patients with lymphoma*. *Blood*, 2007. **110**(10): p. 3507-16.
61. Cohen, J.B., et al., *Deferred therapy is associated with improved overall survival in patients with newly diagnosed mantle cell lymphoma*. *Cancer*, 2016. **122**(15): p. 2356-63.
62. Lee, C. and P. Martin, *Watch and Wait in Mantle Cell Lymphoma*. *Hematol Oncol Clin North Am*, 2020. **34**(5): p. 837-847.
63. Kumar, A., et al., *Clinical presentation determines selection of patients for initial observation in mantle cell lymphoma*. *Haematologica*, 2019. **104**(4): p. e163-e166.
64. Kumar, A., et al., *Patterns of survival in patients with recurrent mantle cell lymphoma in the modern era: progressive shortening in response duration and survival after each relapse*. *Blood Cancer J*, 2019. **9**(6): p. 50.
65. team, T.A.C.S.m.a.e.c., *Stem Cell or Bone Marrow Transplant Side Effects*. 2020.
66. Tward, J., et al., *Incidence, risk factors, and pathogenesis of second malignancies in patients with non-Hodgkin lymphoma*. *Leuk Lymphoma*, 2007. **48**(8): p. 1482-95.
67. Martin, P., et al., *Treatment Outcomes and Roles of Transplantation and Maintenance Rituximab in Patients With Previously Untreated Mantle Cell Lymphoma: Results From Large Real-World Cohorts*. *J Clin Oncol*, 2023. **41**(3): p. 541-554.

68. Monga, N., et al., *Clinical efficacy and safety of first-line treatments in patients with mantle cell lymphoma: A systematic literature review*. Crit Rev Oncol Hematol, 2021. **158**: p. 103212.
69. Liu, H., et al., *First-Line Autologous Stem Cell Transplantation for Mantle Cell Lymphoma: A Systematic Analysis and Treatment Recommendation*. Front Oncol, 2022. **12**: p. 881346.
70. Eyre, T.A., et al., *BRUIN MCL-321: phase III study of pirtobrutinib versus investigator choice of BTK inhibitor in BTK inhibitor naïve mantle cell lymphoma*. Future Oncol, 2022.
71. Sharman, J., et al., *Treatment patterns and outcomes among mantle cell lymphoma patients treated with ibrutinib in the United States: a retrospective electronic medical record database and chart review study*. Br J Haematol, 2021. **192**(4): p. 737-746.
72. RHEINSTEIN, P.H. and B. AKBARI, *Significant FDA Approvals in 1997*. 1998: American Family Physician. p. 2865-2868.
73. Narkhede, M., et al., *Evaluating real-world treatment patterns and outcomes of mantle cell lymphoma*. Blood Adv, 2022. **6**(14): p. 4122-4131.
74. Administration, U.S.F.a.D., *FDA approves brexucabtagene autoleucel for relapsed or refractory mantle cell lymphoma*. 2020.
75. Daher, M., et al., *CAR-NK cells: the next wave of cellular therapy for cancer*. Clin Transl Immunology, 2021. **10**(4): p. e1274.
76. Marsh, I.R., et al., *Preclinical Pharmacokinetics and Dosimetry Studies of ¹²⁴I/¹³¹I-CLR1404 for Treatment of Pediatric Solid Tumors in Murine Xenograft Models*. J Nucl Med, 2019. **60**(10): p. 1414-1420.
77. *Betalutin*. [cited 2023; Available from: <https://www.nordicanovector.com/what-we-do/our-pipeline/betalutin>].
78. Khanal, R., et al., *Trial in Progress: AB-101, an Allogeneic, Non-Engineered, Cord Blood-Derived Natural Killer (NK) Cell Therapy, As Monotherapy or in Combination with Rituximab in Patients with Relapsed or Refractory Non-Hodgkin Lymphoma*, in *The American Society of Hematology 64th Annual Meeting*. 2022, Blood: New Orleans, LA, USA.
79. Veronika Bachanova , et al., *Gda-201, a Novel Metabolically Enhanced Allogeneic Natural Killer (NK) Cell Product Yields High Remission Rates in Patients with Relapsed/Refractory Non-Hodgkin Lymphoma (NHL): 2-Year Survival and Correlation with Cytokine IL7*, in *American Society of Hematology 63rd Annual Meeting*. 2021, Blood: Atlanta, Georgia, USA.
80. Vose, J.M., *Mantle cell lymphoma: 2017 update on diagnosis, risk-stratification, and clinical management*. Am J Hematol, 2017. **92**(8): p. 806-813.
81. Abrahamsson, A., et al., *Real world data on primary treatment for mantle cell lymphoma: a Nordic Lymphoma Group observational study*. Blood, 2014. **124**(8): p. 1288-95.
82. Hess, G., et al., *Real-world experience among patients with relapsed/refractory mantle cell lymphoma after Bruton tyrosine kinase inhibitor failure in Europe: The SCHOLAR-2 retrospective chart review study*. Br J Haematol, 2022.

83. Cheah, C.Y., et al., *Patients with mantle cell lymphoma failing ibrutinib are unlikely to respond to salvage chemotherapy and have poor outcomes*. *Ann Oncol*, 2015. **26**(6): p. 1175-9.
84. Wang, M., et al., *Three-year follow-up of outcomes with KTE-X19 in patients with relapsed/refractory mantle cell lymphoma in ZUMA-2*. 2022, *Journal of Clinical Oncology*.
85. Cortelazzo, S., et al., *Mantle cell lymphoma*. *Crit Rev Oncol Hematol*, 2012. **82**(1): p. 78-101.
86. Lin, W.J., et al., *The mammalian immediate-early TIS21 protein and the leukemia-associated BTG1 protein interact with a protein-arginine N-methyltransferase*. *J Biol Chem*, 1996. **271**(25): p. 15034-44.
87. Ahmad, A., Y. Dong, and X. Cao, *Characterization of the PRMT gene family in rice reveals conservation of arginine methylation*. *PLoS One*, 2011. **6**(8): p. e22664.
88. Koh, C.M., M. Bezzi, and E. Guccione, *The Where and the How of PRMT5*. *Current Molecular Biology Reports*, 2015(1): p. 19-28.
89. Smith, E., et al., *Recent advances in targeting protein arginine methyltransferase enzymes in cancer therapy*. *Expert Opin Ther Targets*, 2018. **22**(6): p. 527-545.
90. Tang, J., et al., *PRMT1 is the predominant type I protein arginine methyltransferase in mammalian cells*. *J Biol Chem*, 2000. **275**(11): p. 7723-30.
91. Yang, Y., et al., *PRMT9 is a type II methyltransferase that methylates the splicing factor SAPI45*. *Nat Commun*, 2015. **6**: p. 6428.
92. Hadjikyriacou, A., et al., *Unique Features of Human Protein Arginine Methyltransferase 9 (PRMT9) and Its Substrate RNA Splicing Factor SF3B2*. *J Biol Chem*, 2015. **290**(27): p. 16723-43.
93. Pollack, B.P., et al., *The human homologue of the yeast proteins Skb1 and Hsl7p interacts with Jak kinases and contains protein methyltransferase activity*. *J Biol Chem*, 1999. **274**(44): p. 31531-42.
94. Rho, J., et al., *Prmt5, which forms distinct homo-oligomers, is a member of the protein-arginine methyltransferase family*. *J Biol Chem*, 2001. **276**(14): p. 11393-401.
95. Antonysamy, S., et al., *Crystal structure of the human PRMT5:MEP50 complex*. *Proc Natl Acad Sci U S A*, 2012. **109**(44): p. 17960-5.
96. Kim, H. and Z.A. Ronai, *PRMT5 function and targeting in cancer*. *Cell Stress*, 2020. **4**(8): p. 199-215.
97. Blanc, R.S. and S. Richard, *Arginine Methylation: The Coming of Age*. *Mol Cell*, 2017. **65**(1): p. 8-24.
98. Musiani, D., et al., *Proteomics profiling of arginine methylation defines PRMT5 substrate specificity*. *Sci Signal*, 2019. **12**(575).
99. Zhu, F. and L. Rui, *PRMT5 in gene regulation and hematologic malignancies*. *Genes Dis*, 2019. **6**(3): p. 247-257.
100. Tee, W.W., et al., *Prmt5 is essential for early mouse development and acts in the cytoplasm to maintain ES cell pluripotency*. *Genes Dev*, 2010. **24**(24): p. 2772-7.

101. Gkoutela, S., et al., *PRMT5 is required for human embryonic stem cell proliferation but not pluripotency*. Stem Cell Rev Rep, 2014. **10**(2): p. 230-9.
102. Uhlén, M., et al., *A human protein atlas for normal and cancer tissues based on antibody proteomics*. Mol Cell Proteomics, 2005. **4**(12): p. 1920-32.
103. *The Human Protein Atlas*.
104. Liu, F., et al., *Arginine methyltransferase PRMT5 is essential for sustaining normal adult hematopoiesis*. J Clin Invest, 2015. **125**(9): p. 3532-44.
105. Litzler, L.C., et al., *PRMT5 is essential for B cell development and germinal center dynamics*. Nat Commun, 2019. **10**(1): p. 22.
106. Tanaka, Y., et al., *PRMT5 Is Required for T Cell Survival and Proliferation by Maintaining Cytokine Signaling*. Front Immunol, 2020. **11**: p. 621.
107. Strobl, C.D., et al., *Selective PRMT5 Inhibitors Suppress Human CD8*. Mol Cancer Ther, 2020. **19**(2): p. 409-419.
108. Snyder, K.J., et al., *PRMT5 regulates T cell interferon response and is a target for acute graft-versus-host disease*. JCI Insight, 2020. **5**(8).
109. Migliori, V., et al., *Symmetric dimethylation of H3R2 is a newly identified histone mark that supports euchromatin maintenance*. Nat Struct Mol Biol, 2012. **19**(2): p. 136-44.
110. Meister, G. and U. Fischer, *Assisted RNP assembly: SMN and PRMT5 complexes cooperate in the formation of spliceosomal UsnRNPs*. EMBO J, 2002. **21**(21): p. 5853-63.
111. Radzisheskaya, A., et al., *PRMT5 methylome profiling uncovers a direct link to splicing regulation in acute myeloid leukemia*. Nat Struct Mol Biol, 2019. **26**(11): p. 999-1012.
112. Rengasamy, M., et al., *The PRMT5/WDR77 complex regulates alternative splicing through ZNF326 in breast cancer*. Nucleic Acids Res, 2017. **45**(19): p. 11106-11120.
113. Gao, G., S. Dhar, and M.T. Bedford, *PRMT5 regulates IRES-dependent translation via methylation of hnRNP A1*. Nucleic Acids Res, 2017. **45**(8): p. 4359-4369.
114. Lim, J.H., et al., *PRMT5 is essential for the eIF4E-mediated 5'-cap dependent translation*. Biochem Biophys Res Commun, 2014. **452**(4): p. 1016-21.
115. Hsu, J.M., et al., *Crosstalk between Arg 1175 methylation and Tyr 1173 phosphorylation negatively modulates EGFR-mediated ERK activation*. Nat Cell Biol, 2011. **13**(2): p. 174-81.
116. Bandyopadhyay, S., et al., *HOXA9 methylation by PRMT5 is essential for endothelial cell expression of leukocyte adhesion molecules*. Mol Cell Biol, 2012. **32**(7): p. 1202-13.
117. Kim, H., et al., *PRMT5 control of cGAS/STING and NLRC5 pathways defines melanoma response to antitumor immunity*. Sci Transl Med, 2020. **12**(551).
118. Fan, Z., et al., *The arginine methyltransferase PRMT5 regulates CIITA-dependent MHC II transcription*. Biochim Biophys Acta, 2016. **1859**(5): p. 687-96.

119. Harris, D.P., et al., *PRMT5-Mediated Methylation of NF- κ B p65 at Arg174 Is Required for Endothelial CXCL11 Gene Induction in Response to TNF- α and IFN- γ Costimulation*. PLoS One, 2016. **11**(2): p. e0148905.
120. Beketova, E., et al., *Protein Arginine Methyltransferase 5 Promotes pICln-Dependent Androgen Receptor Transcription in Castration-Resistant Prostate Cancer*. Cancer Res, 2020. **80**(22): p. 4904-4917.
121. Webb, L.M., et al., *PRMT5-Selective Inhibitors Suppress Inflammatory T Cell Responses and Experimental Autoimmune Encephalomyelitis*. J Immunol, 2017. **198**(4): p. 1439-1451.
122. Wei, T.Y., et al., *Protein arginine methyltransferase 5 is a potential oncoprotein that upregulates G1 cyclins/cyclin-dependent kinases and the phosphoinositide 3-kinase/AKT signaling cascade*. Cancer Sci, 2012. **103**(9): p. 1640-50.
123. Tsai, W.W., et al., *PRMT5 modulates the metabolic response to fasting signals*. Proc Natl Acad Sci U S A, 2013. **110**(22): p. 8870-5.
124. Shailesh, H., et al., *Protein arginine methyltransferase 5 (PRMT5) dysregulation in cancer*. Oncotarget, 2018. **9**(94): p. 36705-36718.
125. Motolani, A., et al., *The Structure and Functions of PRMT5 in Human Diseases*. Life (Basel), 2021. **11**(10).
126. Xiao, W., et al., *Role of protein arginine methyltransferase 5 in human cancers*. Biomed Pharmacother, 2019. **114**: p. 108790.
127. Alinari, L., et al., *Selective inhibition of protein arginine methyltransferase 5 blocks initiation and maintenance of B-cell transformation*. Blood, 2015. **125**(16): p. 2530-43.
128. Yin, S., et al., *PRMT5-mediated arginine methylation activates AKT kinase to govern tumorigenesis*. Nat Commun, 2021. **12**(1): p. 3444.
129. Jing, P., et al., *The methylation induced by protein arginine methyltransferase 5 promotes tumorigenesis and progression of lung cancer*. J Thorac Dis, 2018. **10**(12): p. 7014-7019.
130. Hing, Z.A., et al., *Dysregulation of PRMT5 in chronic lymphocytic leukemia promotes progression with high risk of Richter's transformation*. Nat Commun, 2023. **14**(1): p. 97.
131. Bao, X., et al., *Overexpression of PRMT5 promotes tumor cell growth and is associated with poor disease prognosis in epithelial ovarian cancer*. J Histochem Cytochem, 2013. **61**(3): p. 206-17.
132. Hu, D., et al., *Interplay between arginine methylation and ubiquitylation regulates KLF4-mediated genome stability and carcinogenesis*. Nat Commun, 2015. **6**: p. 8419.
133. Liang, Z., et al., *Clinicopathological and Prognostic Significance of PRMT5 in Cancers: A System Review and Meta-Analysis*. Cancer Control, 2021. **28**: p. 10732748211050583.
134. Ge, L., et al., *PRMT5 promotes epithelial-mesenchymal transition via EGFR- β -catenin axis in pancreatic cancer cells*. J Cell Mol Med, 2020. **24**(2): p. 1969-1979.

135. Banasavadi-Siddegowda, Y.K., et al., *PRMT5-PTEN molecular pathway regulates senescence and self-renewal of primary glioblastoma neurosphere cells*. *Oncogene*, 2017. **36**(2): p. 263-274.
136. Chiang, K., et al., *PRMT5 Is a Critical Regulator of Breast Cancer Stem Cell Function via Histone Methylation and FOXP1 Expression*. *Cell Rep*, 2017. **21**(12): p. 3498-3513.
137. Jin, Y., et al., *Targeting methyltransferase PRMT5 eliminates leukemia stem cells in chronic myelogenous leukemia*. *J Clin Invest*, 2016. **126**(10): p. 3961-3980.
138. Pal, S., et al., *Low levels of miR-92b/96 induce PRMT5 translation and H3R8/H4R3 methylation in mantle cell lymphoma*. *EMBO J*, 2007. **26**(15): p. 3558-69.
139. Wang, L., S. Pal, and S. Sif, *Protein arginine methyltransferase 5 suppresses the transcription of the RB family of tumor suppressors in leukemia and lymphoma cells*. *Mol Cell Biol*, 2008. **28**(20): p. 6262-77.
140. Lu, Y.F., et al., *LncRNA SNHG16 Functions as an Oncogene by Sponging MiR-4518 and Up-Regulating PRMT5 Expression in Glioma*. *Cell Physiol Biochem*, 2018. **45**(5): p. 1975-1985.
141. Li, Y., et al., *PRMT5 is required for lymphomagenesis triggered by multiple oncogenic drivers*. *Cancer Discov*, 2015. **5**(3): p. 288-303.
142. Bezzi, M., et al., *Regulation of constitutive and alternative splicing by PRMT5 reveals a role for Mdm4 pre-mRNA in sensing defects in the spliceosomal machinery*. *Genes Dev*, 2013. **27**(17): p. 1903-16.
143. AbuHammad, S., et al., *Regulation of PRMT5-MDM4 axis is critical in the response to CDK4/6 inhibitors in melanoma*. *Proc Natl Acad Sci U S A*, 2019.
144. Gerhart, S.V., et al., *Activation of the p53-MDM4 regulatory axis defines the anti-tumour response to PRMT5 inhibition through its role in regulating cellular splicing*. *Sci Rep*, 2018. **8**(1): p. 9711.
145. Qin, Y., et al., *PRMT5 enhances tumorigenicity and glycolysis in pancreatic cancer via the FBW7/cMyc axis*. *Cell Commun Signal*, 2019. **17**(1): p. 30.
146. Shen, Y., et al., *Tadalafil increases the antitumor activity of 5-FU through inhibiting PRMT5-mediated glycolysis and cell proliferation in colorectal cancer*. *Cancer Metab*, 2022. **10**(1): p. 22.
147. Yuan, H.F., et al., *PRMT5 confers lipid metabolism reprogramming, tumour growth and metastasis depending on the SIRT7-mediated desuccinylation of PRMT5 K387 in tumours*. *Acta Pharmacol Sin*, 2022. **43**(9): p. 2373-2385.
148. Chan-Penebre, E., et al., *A selective inhibitor of PRMT5 with in vivo and in vitro potency in MCL models*. *Nat Chem Biol*, 2015. **11**(6): p. 432-7.
149. Fu, S., et al., *Medicinal chemistry strategies targeting PRMT5 for cancer therapy*. *Eur J Med Chem*, 2022. **244**: p. 114842.
150. Kryukov, G.V., et al., *MTAP deletion confers enhanced dependency on the PRMT5 arginine methyltransferase in cancer cells*. *Science*, 2016. **351**(6278): p. 1214-8.

151. Mavrakis, K.J., et al., *Disordered methionine metabolism in MTAP/CDKN2A-deleted cancers leads to dependence on PRMT5*. Science, 2016. **351**(6278): p. 1208-13.
152. Mao, R., et al., *Potent, Selective, and Cell Active Protein Arginine Methyltransferase 5 (PRMT5) Inhibitor Developed by Structure-Based Virtual Screening and Hit Optimization*. J Med Chem, 2017. **60**(14): p. 6289-6304.
153. Lin, H., et al., *Discovery of Potent and Selective Covalent Protein Arginine Methyltransferase 5 (PRMT5) Inhibitors*. ACS Med Chem Lett, 2019. **10**(7): p. 1033-1038.
154. Smith, C.R., et al., *Fragment-Based Discovery of MRTX1719, a Synthetic Lethal Inhibitor of the PRMT5•MTA Complex for the Treatment of*. J Med Chem, 2022. **65**(3): p. 1749-1766.
155. McKinney, D.C., et al., *Discovery of a First-in-Class Inhibitor of the PRMT5-Substrate Adaptor Interaction*. J Med Chem, 2021. **64**(15): p. 11148-11168.
156. Al-Hamashi, A.A., et al., *Discovery of a potent and dual-selective bisubstrate inhibitor for protein arginine methyltransferase 4/5*. Acta Pharm Sin B, 2021. **11**(9): p. 2709-2718.
157. Prabhu, L., et al., *Inhibition of PRMT5 by market drugs as a novel cancer therapeutic avenue*. 2022, Genes & Diseases.
158. Shen, Y., et al., *Discovery of First-in-Class Protein Arginine Methyltransferase 5 (PRMT5) Degraders*. J Med Chem, 2020. **63**(17): p. 9977-9989.
159. Youle, R.J. and A. Strasser, *The BCL-2 protein family: opposing activities that mediate cell death*. Nat Rev Mol Cell Biol, 2008. **9**(1): p. 47-59.
160. Hatok, J. and P. Racay, *Bcl-2 family proteins: master regulators of cell survival*. Biomol Concepts, 2016. **7**(4): p. 259-70.
161. Germain, M., J.P. Mathai, and G.C. Shore, *BH-3-only BIK functions at the endoplasmic reticulum to stimulate cytochrome c release from mitochondria*. J Biol Chem, 2002. **277**(20): p. 18053-60.
162. Edlich, F., et al., *Bcl-x(L) retrotranslocates Bax from the mitochondria into the cytosol*. Cell, 2011. **145**(1): p. 104-16.
163. Lithgow, T., et al., *The protein product of the oncogene bcl-2 is a component of the nuclear envelope, the endoplasmic reticulum, and the outer mitochondrial membrane*. Cell Growth Differ, 1994. **5**(4): p. 411-7.
164. Sevilla, L., et al., *Transcriptional regulation of the bcl-x gene encoding the anti-apoptotic Bcl-xL protein by Ets, Rel/NFkappaB, STAT and API transcription factor families*. Histol Histopathol, 2001. **16**(2): p. 595-601.
165. Senichkin, V.V., et al., *Saga of Mcl-1: regulation from transcription to degradation*. Cell Death Differ, 2020. **27**(2): p. 405-419.
166. Mitchell, K.O., et al., *Bax is a transcriptional target and mediator of c-myc-induced apoptosis*. Cancer Res, 2000. **60**(22): p. 6318-25.
167. Miyashita, T. and J.C. Reed, *Tumor suppressor p53 is a direct transcriptional activator of the human bax gene*. Cell, 1995. **80**(2): p. 293-9.

168. Certo, M., et al., *Mitochondria primed by death signals determine cellular addiction to antiapoptotic BCL-2 family members*. *Cancer Cell*, 2006. **9**(5): p. 351-65.
169. Tsujimoto, Y., et al., *Involvement of the bcl-2 gene in human follicular lymphoma*. *Science*, 1985. **228**(4706): p. 1440-3.
170. Plati, J., O. Bucur, and R. Khosravi-Far, *Dysregulation of apoptotic signaling in cancer: molecular mechanisms and therapeutic opportunities*. *J Cell Biochem*, 2008. **104**(4): p. 1124-49.
171. Tessoulin, B., et al., *BCL2-Family Dysregulation in B-Cell Malignancies: From Gene Expression Regulation to a Targeted Therapy Biomarker*. *Front Oncol*, 2018. **8**: p. 645.
172. Fanidi, A., E.A. Harrington, and G.I. Evan, *Cooperative interaction between c-myc and bcl-2 proto-oncogenes*. *Nature*, 1992. **359**(6395): p. 554-6.
173. Strasser, A., et al., *Novel primitive lymphoid tumours induced in transgenic mice by cooperation between myc and bcl-2*. *Nature*, 1990. **348**(6299): p. 331-3.
174. Eischen, C.M., et al., *Bax loss impairs Myc-induced apoptosis and circumvents the selection of p53 mutations during Myc-mediated lymphomagenesis*. *Mol Cell Biol*, 2001. **21**(22): p. 7653-62.
175. Correia, C., et al., *BCL2 mutations are associated with increased risk of transformation and shortened survival in follicular lymphoma*. *Blood*, 2015. **125**(4): p. 658-67.
176. Tsuyama, N., et al., *BCL2 expression in DLBCL: reappraisal of immunohistochemistry with new criteria for therapeutic biomarker evaluation*. *Blood*, 2017. **130**(4): p. 489-500.
177. Dunleavy, K., *Double-hit lymphomas: current paradigms and novel treatment approaches*. *Hematology Am Soc Hematol Educ Program*, 2014. **2014**(1): p. 107-12.
178. Adams, C.M., et al., *Non-Hodgkin and Hodgkin Lymphomas Select for Overexpression of BCLW*. *Clin Cancer Res*, 2017. **23**(22): p. 7119-7129.
179. Zhou, P., et al., *MCL1 transgenic mice exhibit a high incidence of B-cell lymphoma manifested as a spectrum of histologic subtypes*. *Blood*, 2001. **97**(12): p. 3902-9.
180. Beverly, L.J. and H.E. Varmus, *MYC-induced myeloid leukemogenesis is accelerated by all six members of the antiapoptotic BCL family*. *Oncogene*, 2009. **28**(9): p. 1274-9.
181. Adams, C.M., et al., *Targeting the Bcl-2 Family in B Cell Lymphoma*. *Front Oncol*, 2018. **8**: p. 636.
182. Gu, et al., *BCL-Xl Expression Is Druggable Biomarker Associated with a Poor Clinical Outcome in Relapsed/Refractory Diffuse Large B-Cell Lymphoma (DLBCL)*, in *American Society of Hematology 62nd Annual Meeting*. 2019, Blood.
183. Agarwal, B. and K.N. Naresh, *Bcl-2 family of proteins in indolent B-cell non-Hodgkin's lymphoma: study of 116 cases*. *Am J Hematol*, 2002. **70**(4): p. 278-82.

184. Luanpitpong, S., et al., *Bcl-2 Family Members Bcl-xL and Bax Cooperatively Contribute to Bortezomib Resistance in Mantle Cell Lymphoma*. *Int J Mol Sci*, 2022. **23**(22).
185. Phillips, D.C., et al., *Loss in MCL-1 function sensitizes non-Hodgkin's lymphoma cell lines to the BCL-2-selective inhibitor venetoclax (ABT-199)*. *Blood Cancer J*, 2015. **5**(11): p. e368.
186. Nijhawan, D., et al., *Elimination of Mcl-1 is required for the initiation of apoptosis following ultraviolet irradiation*. *Genes Dev*, 2003. **17**(12): p. 1475-86.
187. Tagawa, H., et al., *Genome-wide array-based CGH for mantle cell lymphoma: identification of homozygous deletions of the proapoptotic gene BIM*. *Oncogene*, 2005. **24**(8): p. 1348-58.
188. Mestre-Escorihuela, C., et al., *Homozygous deletions localize novel tumor suppressor genes in B-cell lymphomas*. *Blood*, 2007. **109**(1): p. 271-80.
189. Wang, J.D., et al., *Proapoptotic protein BIM as a novel prognostic marker in mantle cell lymphoma*. *Hum Pathol*, 2019. **93**: p. 54-64.
190. Diepstraten, S.T., et al., *The manipulation of apoptosis for cancer therapy using BH3-mimetic drugs*. *Nat Rev Cancer*, 2022. **22**(1): p. 45-64.
191. Davids, M.S., et al., *Preliminary Results of a Phase I/Ib Study of Ibrutinib in Combination with TGR-1202 in Patients with Relapsed/Refractory CLL or MCL*. 2016: Congress of the European Hematology Association.
192. Tam, C.S., et al., *Ibrutinib plus Venetoclax for the Treatment of Mantle-Cell Lymphoma*. *N Engl J Med*, 2018. **378**(13): p. 1211-1223.
193. Wang, M., et al., *Concurrent ibrutinib plus venetoclax in relapsed/refractory mantle cell lymphoma: the safety run-in of the phase 3 SYMPATICO study*. *J Hematol Oncol*, 2021. **14**(1): p. 179.
194. Thus, Y.J., et al., *Tipping the balance: toward rational combination therapies to overcome venetoclax resistance in mantle cell lymphoma*. *Leukemia*, 2022. **36**(9): p. 2165-2176.
195. Wang, H., et al., *Targeting MCL-1 in cancer: current status and perspectives*. *J Hematol Oncol*, 2021. **14**(1): p. 67.
196. Tse, C., et al., *ABT-263: a potent and orally bioavailable Bcl-2 family inhibitor*. *Cancer Res*, 2008. **68**(9): p. 3421-8.
197. Plieth, J., *Asco 2022 – Abbvie goes back to basics with navitoclax*. 2022, Evaluate Vantage: Evaluate Vantage.
198. Ravikrishna n, J., et al., *Characterization of LP-118, a Novel Small Molecule Inhibitor of Bcl-2 and Bcl-Xl in Chronic Lymphocytic Leukemia Resistant to Venetoclax*, in *American Society of Hematology 63rd Annual Meeting*. 2021, Blood: Atlanta Georgia.
199. Patterson, C.M., et al., *Design and optimisation of dendrimer-conjugated Bcl-2/x*. *Commun Biol*, 2021. **4**(1): p. 112.
200. Zhang, X., et al., *Discovery of PROTAC BCL-X*. *Eur J Med Chem*, 2020. **192**: p. 112186.
201. Pal, P., et al., *Discovery of a Novel BCL-X*. *J Med Chem*, 2021. **64**(19): p. 14230-14246.

202. Papatzimas, J.W., et al., *From Inhibition to Degradation: Targeting the Antiapoptotic Protein Myeloid Cell Leukemia 1 (MCL1)*. J Med Chem, 2019. **62**(11): p. 5522-5540.
203. Zhang, L., et al., *B-Cell Lymphoma Patient-Derived Xenograft Models Enable Drug Discovery and Are a Platform for Personalized Therapy*. Clin Cancer Res, 2017. **23**(15): p. 4212-4223.
204. Townsend, E.C., et al., *The Public Repository of Xenografts Enables Discovery and Randomized Phase II-like Trials in Mice*. Cancer Cell, 2016. **29**(4): p. 574-586.
205. Smith, M.R., et al., *Murine model for mantle cell lymphoma*. Leukemia, 2006. **20**(5): p. 891-3.
206. Anderson, P.N. and M. Potter, *Induction of plasma cell tumours in BALB-c mice with 2,6,10,14-tetramethylpentadecane (pristane)*. Nature, 1969. **222**(5197): p. 994-5.
207. Smith, M.R., et al., *Murine mantle cell lymphoma model cell line*. Leukemia, 2013. **27**(7): p. 1592-4.
208. Gladden, A.B., et al., *Expression of constitutively nuclear cyclin D1 in murine lymphocytes induces B-cell lymphoma*. Oncogene, 2006. **25**(7): p. 998-1007.
209. Katz, S.G., et al., *Mantle cell lymphoma in cyclin D1 transgenic mice with Bim-deficient B cells*. Blood, 2014. **123**(6): p. 884-93.
210. Ford, R.J., et al., *Development of a murine model for blastoid variant mantle-cell lymphoma*. Blood, 2007. **109**(11): p. 4899-906.
211. Vincent-Fabert, C., et al., *A defect of the INK4-Cdk4 checkpoint and Myc collaborate in blastoid mantle cell lymphoma-like lymphoma formation in mice*. Am J Pathol, 2012. **180**(4): p. 1688-701.
212. Fiancette, R., et al., *A p53 defect sensitizes various stages of B cell development to lymphomagenesis in mice carrying an IgH 3' regulatory region-driven c-myc transgene*. J Immunol, 2011. **187**(11): p. 5772-82.
213. Pieters, T., et al., *Cyclin D2 overexpression drives B1a-derived MCL-like lymphoma in mice*. J Exp Med, 2021. **218**(10).
214. Smolewski, P., D. Rydygier, and T. Robak, *Clinical management of mantle cell lymphoma in the elderly*. Expert Opin Pharmacother, 2019: p. 1-13.
215. Freedman, A.S. and J.W. Friedberg *Initial treatment of mantle cell lymphoma*. 2019.
216. Administration, U.F.a.D., *FDA approves brexucabtagene autoleucel for relapsed or refractory mantle cell lymphoma*. 2020: <https://www.fda.gov/drugs/resources-information-approved-drugs/fda-approves-brexucabtagene-autoleucel-relapsed-or-refractory-mantle-cell-lymphoma>.
217. Branscombe, T.L., et al., *PRMT5 (Janus kinase-binding protein 1) catalyzes the formation of symmetric dimethylarginine residues in proteins*. J Biol Chem, 2001. **276**(35): p. 32971-6.
218. Tarighat, S.S., et al., *The dual epigenetic role of PRMT5 in acute myeloid leukemia: gene activation and repression via histone arginine methylation*. Leukemia, 2016. **30**(4): p. 789-99.

219. Chung, J., et al., *Protein arginine methyltransferase 5 (PRMT5) inhibition induces lymphoma cell death through reactivation of the retinoblastoma tumor suppressor pathway and polycomb repressor complex 2 (PRC2) silencing*. J Biol Chem, 2013. **288**(49): p. 35534-47.
220. Scoumanne, A., J. Zhang, and X. Chen, *PRMT5 is required for cell-cycle progression and p53 tumor suppressor function*. Nucleic Acids Res, 2009. **37**(15): p. 4965-76.
221. Wei, H., et al., *PRMT5 dimethylates R30 of the p65 subunit to activate NF- κ B*. Proc Natl Acad Sci U S A, 2013. **110**(33): p. 13516-21.
222. Lu, X., et al., *PRMT5 interacts with the BCL6 oncoprotein and is required for germinal center formation and lymphoma cell survival*. Blood, 2018. **132**(19): p. 2026-2039.
223. Cho, E.C., et al., *Arginine methylation controls growth regulation by E2F-1*. EMBO J, 2012. **31**(7): p. 1785-97.
224. Pastore, F., et al., *PRMT5 Inhibition Modulates E2F1 Methylation and Gene-Regulatory Networks Leading to Therapeutic Efficacy in JAK2*. Cancer Discov, 2020. **10**(11): p. 1742-1757.
225. Zhang, S., et al., *Targeting PRMT5/Akt signalling axis prevents human lung cancer cell growth*. J Cell Mol Med, 2018.
226. Yan, F., et al., *Genetic validation of the protein arginine methyltransferase PRMT5 as a candidate therapeutic target in glioblastoma*. Cancer Res, 2014. **74**(6): p. 1752-65.
227. Sabnis, R.W., *Novel PRMT5 Inhibitors for Treating Cancer*. ACS Med Chem Lett, 2021. **12**(10): p. 1537-1538.
228. Lin, H. and J.I. Luengo, *Nucleoside protein arginine methyltransferase 5 (PRMT5) inhibitors*. Bioorg Med Chem Lett, 2019. **29**(11): p. 1264-1269.
229. Manning, B.D. and A. Toker, *AKT/PKB Signaling: Navigating the Network*. Cell, 2017. **169**(3): p. 381-405.
230. Golding, S.E., et al., *Pro-survival AKT and ERK signaling from EGFR and mutant EGFRvIII enhances DNA double-strand break repair in human glioma cells*. Cancer Biol Ther, 2009. **8**(8): p. 730-8.
231. Alt, J.R., et al., *Phosphorylation-dependent regulation of cyclin D1 nuclear export and cyclin D1-dependent cellular transformation*. Genes Dev, 2000. **14**(24): p. 3102-14.
232. Ogawara, Y., et al., *Akt enhances Mdm2-mediated ubiquitination and degradation of p53*. J Biol Chem, 2002. **277**(24): p. 21843-50.
233. Sugiyama, M.G., G.D. Fairn, and C.N. Antonescu, *Akt-ing Up Just About Everywhere: Compartment-Specific Akt Activation and Function in Receptor Tyrosine Kinase Signaling*. Front Cell Dev Biol, 2019. **7**: p. 70.
234. Zhang, Y., et al., *FoxO family members in cancer*. Cancer Biol Ther, 2011. **12**(4): p. 253-9.
235. Kim, C.G., et al., *Role of Forkhead Box Class O proteins in cancer progression and metastasis*. Semin Cancer Biol, 2018. **50**: p. 142-151.

236. Rena, G., et al., *Phosphorylation of the transcription factor forkhead family member FKHR by protein kinase B*. J Biol Chem, 1999. **274**(24): p. 17179-83.
237. Dengler, H.S., et al., *Distinct functions for the transcription factor Foxo1 at various stages of B cell differentiation*. Nat Immunol, 2008. **9**(12): p. 1388-98.
238. Yusuf, I., et al., *Optimal B-cell proliferation requires phosphoinositide 3-kinase-dependent inactivation of FOXO transcription factors*. Blood, 2004. **104**(3): p. 784-7.
239. Medema, R.H., et al., *AFX-like Forkhead transcription factors mediate cell-cycle regulation by Ras and PKB through p27kip1*. Nature, 2000. **404**(6779): p. 782-7.
240. Ramaswamy, S., et al., *A novel mechanism of gene regulation and tumor suppression by the transcription factor FKHR*. Cancer Cell, 2002. **2**(1): p. 81-91.
241. Zhao, Y., et al., *Cytosolic FoxO1 is essential for the induction of autophagy and tumour suppressor activity*. Nat Cell Biol, 2010. **12**(7): p. 665-75.
242. Zhang, J., et al., *Histone deacetylase inhibitors induce autophagy through FOXO1-dependent pathways*. Autophagy, 2015. **11**(4): p. 629-42.
243. Cheong, J.W., et al., *Constitutive phosphorylation of FKHR transcription factor as a prognostic variable in acute myeloid leukemia*. Leuk Res, 2003. **27**(12): p. 1159-62.
244. Grupp, K., et al., *FOXO1 overexpression and loss of pSerine256-FOXO1 expression predicts clinical outcome in esophageal adenocarcinomas*. Sci Rep, 2018. **8**(1): p. 17370.
245. Zhu, F., et al., *PRMT5 is upregulated by B-cell receptor signaling and forms a positive-feedback loop with PI3K/AKT in lymphoma cells*. Leukemia, 2019.
246. Di Veroli, G.Y., et al., *Combenefit: an interactive platform for the analysis and visualization of drug combinations*. Bioinformatics, 2016. **32**(18): p. 2866-8.
247. Hwang, I., et al., *CIC is a critical regulator of neuronal differentiation*. JCI Insight, 2020. **5**(9).
248. Sloan, S., et al., *Targeting PRMT5 to Circumvent Acquired Ibrutinib Resistance in Mantle Cell Lymphoma*, in American Society of Hematology 61st Annual Meeting. 2019, Blood: Orlando, Florida.
249. Obsil, T. and V. Obsilova, *Structural basis for DNA recognition by FOXO proteins*. Biochim Biophys Acta, 2011. **1813**(11): p. 1946-53.
250. FDA, U., *Venetoclax (Venclexta) Tablets*. 2016.
251. LOEWE, S., *The problem of synergism and antagonism of combined drugs*. Arzneimittelforschung, 1953. **3**(6): p. 285-90.
252. Jain, P. and M. Wang, *Mantle cell lymphoma: 2019 update on the diagnosis, pathogenesis, prognostication, and management*. Am J Hematol, 2019. **94**(6): p. 710-725.
253. Jeon, Y.W., et al., *Clinical outcomes for ibrutinib in relapsed or refractory mantle cell lymphoma in real-world experience*. Cancer Med, 2019. **8**(16): p. 6860-6870.
254. Jain, P., et al., *Long-term outcomes and mutation profiling of patients with mantle cell lymphoma (MCL) who discontinued ibrutinib*. Br J Haematol, 2018. **183**(4): p. 578-587.

255. Jang, J.Y., et al., *A FOXO1-dependent transcription network is a targetable vulnerability of mantle cell lymphomas*. J Clin Invest, 2022.
256. NCBI, *Gene: 10419 PRMT5*. 2021, NCBI: NCBI online database.
257. Jain, P. and M.L. Wang, *Mantle cell lymphoma in 2022-A comprehensive update on molecular pathogenesis, risk stratification, clinical approach, and current and novel treatments*. Am J Hematol, 2022. **97**(5): p. 638-656.
258. Inamdar, A.A., et al., *Mantle cell lymphoma in the era of precision medicine- diagnosis, biomarkers and therapeutic agents*. Oncotarget, 2016. **7**(30): p. 48692-48731.
259. Martin, P., et al., *Postibrutinib outcomes in patients with mantle cell lymphoma*. Blood, 2016. **127**(12): p. 1559-63.
260. Brown, F., et al., *PRMT5 Inhibition Drives Therapeutic Vulnerability to BCL-2 Inhibition with Venetoclax and Provides Rationale for Combination Therapy in Mantle Cell Lymphoma*. Blood, 2019. **134**(Supplement_1): p. 302-302.
261. Fong, J.Y., et al., *Therapeutic Targeting of RNA Splicing Catalysis through Inhibition of Protein Arginine Methylation*. Cancer Cell, 2019. **36**(2): p. 194-209.e9.
262. Subramanian, A., et al., *Gene set enrichment analysis: A knowledge-based approach for interpreting genome-wide expression profiles*. Proceedings of the National Academy of Sciences, 2005. **102**(43): p. 15545-15550.
263. Hanel, W., et al., *A sumoylation program is essential for maintaining the mitotic fidelity in proliferating mantle cell lymphoma cells*. Exp Hematol Oncol, 2022. **11**(1): p. 40.
264. de Groot, R.P., et al., *STAT5-Dependent CyclinD1 and Bcl-xL expression in Bcr-Abl-transformed cells*. Mol Cell Biol Res Commun, 2000. **3**(5): p. 299-305.
265. Mohamad Anuar, N.N., et al., *Clinical Review: Navitoclax as a Pro-Apoptotic and Anti-Fibrotic Agent*. Front Pharmacol, 2020. **11**: p. 564108.
266. Bhagwat, N., et al., *Preclinical characterization of PRT1419, a potent, selective and orally available inhibitor of MCL1, in American Association for Cancer Research Annual Meeting 2021*. 2021, AACR: Philadelphia, PA.
267. Yadav, B., et al., *Searching for Drug Synergy in Complex Dose-Response Landscapes Using an Interaction Potency Model*. Comput Struct Biotechnol J, 2015. **13**: p. 504-13.
268. Price, A.M., et al., *Epstein-Barr virus ensures B cell survival by uniquely modulating apoptosis at early and late times after infection*. Elife, 2017. **6**.
269. Fitzsimmons, L. and G.L. Kelly, *EBV and Apoptosis: The Viral Master Regulator of Cell Fate?* Viruses, 2017. **9**(11).
270. Abrisqueta, P., et al., *Observation as the initial management strategy in patients with mantle cell lymphoma*. Ann Oncol, 2017. **28**(10): p. 2489-2495.
271. Ondrejka, S.L., et al., *Indolent mantle cell leukemia: a clinicopathological variant characterized by isolated lymphocytosis, interstitial bone marrow involvement, kappa light chain restriction, and good prognosis*. Haematologica, 2011. **96**(8): p. 1121-7.

272. Kochenderfer, J.N., et al., *Adoptive transfer of syngeneic T cells transduced with a chimeric antigen receptor that recognizes murine CD19 can eradicate lymphoma and normal B cells*. *Blood*, 2010. **116**(19): p. 3875-86.
273. Prince, H.E., S. Bermudez, and S. Plaeger-Marshall, *Preparation of CD8bright and CD8dim lymphocyte populations using two positive selection methods in tandem*. *J Immunol Methods*, 1993. **165**(2): p. 139-48.
274. Harrington, B.K., et al., *Modulation of immune checkpoint molecule expression in mantle cell lymphoma*. *Leuk Lymphoma*, 2019. **60**(10): p. 2498-2507.
275. Fischer, K., O. Al-Sawaf, and M. Hallek, *Preventing and monitoring for tumor lysis syndrome and other toxicities of venetoclax during treatment of chronic lymphocytic leukemia*. *Hematology Am Soc Hematol Educ Program*, 2020. **2020**(1): p. 357-362.
276. Haydaroglu Sahin, H., *Can the prognosis of mantle cell lymphoma be predicted by simple CBC counts?* *Medicine (Baltimore)*, 2019. **98**(30): p. e16180.
277. Zlamalikova, L., et al., *Expression of D-type cyclins in mantle cell and diffuse large B-cell lymphomas*. *Oncol Rep*, 2016. **35**(5): p. 2673-80.
278. Jalali, S. and S.M. Ansell, *Role of the Bone Marrow Niche in Supporting the Pathogenesis of Lymphoid Malignancies*. *Front Cell Dev Biol*, 2021. **9**: p. 692320.
279. Hemann, M.T. and S.W. Lowe, *The p53-Bcl-2 connection*. *Cell Death Differ*, 2006. **13**(8): p. 1256-9.
280. Chisholm, K.M., et al., *Expression profiles of MYC protein and MYC gene rearrangement in lymphomas*. *Am J Surg Pathol*, 2015. **39**(3): p. 294-303.
281. Hartmann, E., et al., *Increased MDM2 expression is associated with inferior survival in mantle-cell lymphoma, but not related to the MDM2 SNP309*. *Haematologica*, 2007. **92**(4): p. 574-5.
282. Hwang, I., et al., *Cellular stress signaling activates type-I IFN response through FOXO3-regulated lamin posttranslational modification*. *Nat Commun*, 2021. **12**(1): p. 640.

Appendix A. Active Clinical Trials with Targeted Therapies

Target	Compound	Clinical Trial
CDK9	VIP152	NCT02635672 NCT05371054
BCL-2	LOXO-388	NCT05024045
IRAK4	CA-4948	NCT03328078
BCL-2	Venetoclax	NCT03112174 NCT03557619 NCT03955783 NCT03223610 NCT04739813 NCT05529069 NCT05371054 NCT02992522 NCT03583424 NCT03713580 NCT05053659
BTK	Nemtabrutinib (ARQ-53)	NCT03162536
BCL-2	BGB-11417	NCT04277637
P300/CBP	CCS1477	NCT04068597
PI3K delta	Parsaclisib (INCB050465)	NCT03235544 NCT04809467
GSK-3beta	9-ING-41	NCT03678883
NOTCH	CB-103	NCT03422679
BTK	BGB-16673	NCT05006716
RAD51	CYT-0851	NCT03997968
TrkA	VMD-928	NCT03556228
TBL1	Tegavivint (BC2059)	NCT04851119
PARP	Veliparib (ABT-888)	NCT00576654 NCT00740805
STAT3	KT-333	NCT05225584
BCL-2/BCL-xL	Navitoclax (ABT-263)	NCT00788684
ATR	BAY1895344	NCT03188965
MALT1	JNJ-67856633	NCT04657224 NCT03900598
PI3K delta	ACP-319	NCT02328014
EED	APG-5918	NCT05415098
BTK	TT-01488	NCT05275504

Continued

Table A-1: List of clinical trials open with targeted therapies for NHLs including MCL.

Table A-1 continued

Target	Compound	Clinical Trial
MALT1	SGR-1505	NCT05544019
BET	ZEN003694	NCT05053971
Class I PI3K isoforms, DNA-PK, and mTORC1/2	Samotolisib (LY3023414)	NCT03213678
HDAC	Romidepsin	NCT01755975
EZH1/2	DS-3201b	NCT02732275
CRBN	CC-122	NCT01421524
A2AR	NIR178	NCT03207867
IKZF1/3	CFT7455	NCT04756726
SAE2	TAK-981	NCT04074330
EZH2	Tazemetostat	NCT05627245
HDAC	Belinostat	NCT05627245
BTK	DTRM-12	NCT04305444
mTOR	Everolimus	NCT04305444
PRMT5	GSK3326595	NCT02783300
PI3K delta	Zandelisib (ME-401)	NCT04745832
Syk	HMPL-523	NCT03779113
CRBN	CC-220	NCT05169515
CRBN	CC-99282	NCT05169515 NCT03930953
Pan PI3K	Copanlisib (BAY 80-6946)	NCT01660451 NCT02626455 NCT02367040
BCL-2/BCL-xL	LP-118	NCT04771572
EZH1/2	HH2853	NCT04390737
BCL-2	VOB560	NCT04702425
MCL-1	MIK665	NCT04702425
PRMT5	JNJ-64619178	NCT03573310
XPO1	Selinexor	NCT03955783 NCT02303392 NCT03147885 NCT04640779
GSPT1 and IKZF1/3	BTX-1188	NCT05144334
BTK	Zanubrutinib	NCT04002297
BTK and FLT3	CG-806	NCT03893682
CDK9	KB-0742	NCT04718675
PI3K	Duvelisib	NCT05065866 NCT01882803 NCT05044039

Continued

Table A-1 continued

Target	Compound	Clinical Trial
BCL-2/BCL-xL	AZD0466	NCT05205161
IRAK4 and IMiD	KT-413	NCT05233033
Aurora A kinase	Alisertib	NCT01695941
BTK	Pirtobrutinib (LOXO-305)	NCT03740529
CARD11/BCL10/MALT1	XL114	NCT05144347
NEDD8	Pevonedistat	NCT03479268
CK1a and CDK7/9	BTX-A51	NCT04872166
PI3K delta and CD1-epsilon	Umbralisib (TGR-1202)	NCT03283137
BTK	JNJ-64264681	NCT04657224 NCT04210219
PI3K delta	ME-401	NCT02914938
PIKfyve kinase	LAM-002A	NCT02594384

Appendix B. Active Clinical Trials with Immunotherapeutic Agents

Mechanism	Biologic	Clinical Trial
Allogenic anti-CD19 CAR NK Cells	NKX019	NCT05020678
Anti-CD19 CAR T Cells	Lisocabtagene Maraleucel (JCAR017)	NCT03310619 NCT03743246 NCT02631044
Anti-ROR1 antibody linked to monomethyl auristatin E	Zilovertamab Vedotin (MK-2140) (VLS-101)	NCT03833180
Anti-DR5 antibody	IGM-8444	NCT04553692
Anti-CD74 antibody	STRO-001	NCT03424603
Anti-PD1 antibody	Nivolumab	NCT03038672 NCT04205409 NCT03015896 NCT05272384 NCT03749018
Anti-CD27 antibody	Varlilumab (CDX-1127)	NCT03038672
Anti-CD79b antibody linked to monomethyl auristatin E	Polatuzumab Vedotin	NCT04659044
Anti-CD73 antibody	CPI-006	NCT03454451
Allogeneic anti-CD19 CAR NK T-Cells	KUR-502	NCT05487651
Anti-CD74 antibody	Evorpaccept (ALX148)	NCT03013218 NCT05025800
Allogeneic anti-CD19 CAR T-Cells	CTX110	NCT04035434
Autologous CD19 CAR-T Cell Therapy + Orthogonal IL-2	SYNCAR-001 + STK-009	NCT05665062
Anti-CD3/CD20 bispecific antibody	GEN3013	NCT03625037
Allogeneic anti-CD20 conjugated Vdelta2 gamma/delta T cells	ACE1831	NCT05653271
Anti-CD19 antibody conjugated to SG3199 (alkylating agent)	loncastuximab tesirine	NCT05453396 NCT04970901 NCT05053659
Anti-PD-1 antibody	PDR001	NCT03207867

Continued

Table B-1: Active Clinical Trials using immunotherapeutic agents

Table B-1 continued

Mechanism	Biologic	Clinical Trial
Autologous anti-CD19 CAR T-Cells	IC19/1563	NCT04892277
Anti-CD19/CD28 bispecific antibody	RO7443904	NCT05219513
Anti-CD20xCD3 bispecific antibody	Odronextamab	NCT02290951 NCT03888105
Anti-PD-1 Antibody	Pembrolizumab (MK-3475)	NCT03278782 NCT02981914 NCT03210662 NCT03035331 NCT03283137 NCT04827862
Anti-CD20xCD3 bispecific antibody	XmAb13676	NCT02924402
Anti-CD19x4-1BB bispecific antibody	RO7227166	NCT04077723
Anti-CD37 antibody	GEN3009	NCT04358458
Autologous CAR-20/19-T Cells	Unnamed	NCT04186520
Anti-CTLA4 antibody	Ipilimumab	NCT01919619
Autologous anti-CD19 CAR T-Cells	JCAR017	NCT03575351
Autologous anti-CD19 NEX-T CAR T-Cells	CC-97540	NCT04231747
Anti-CD20xCD3 bispecific antibody	Mosunetuzumab	NCT05207670 NCT05169515 NCT02500407 NCT03677141 NCT03671018 NCT05315713 NCT05260957
CRISPR-Edited Allogeneic Anti-CD19 CAR-T Cell	CB-010	NCT04637763
Anti-CD38/CD28xCD3 trispecific antibody	SAR442257	NCT04401020
Anti-PD-L1 antibody	Atezolizumab	NCT02500407 NCT03533283 NCT05315713

Continued

Table B-1 continued

Mechanism	Biologic	Clinical Trial
Anti-CD20xCD3 bispecific antibody	IGM-2323	NCT04082936
Allogeneic anti-CD19 CAR NK T Cells	ANCHOR	NCT03774654
Anti-PD-L1/4-1BB bispecific antibody	ATG-101	NCT04986865
Autologous anti-CD19 CAR T-Cells	Axicabtagene Ciloleucel	NCT03105336 NCT04257578
Anti-TIGIT antibody	Tiragolumab	NCT04045028 NCT05315713
Anti-CD19xCD3 bispecific antibody	TNB-486	NCT04594642
Autologous anti- CD22 CAR T Cells	Unnamed	NCT04088890
Anti-CD19xCD3 bispecific antibody	Blinatumomab	NCT02568553 NCT02811679 NCT03114865
Anti-CD20xCD3 bispecific antibody	Glofitamab	NCT03533283 NCT03075696 NCT03467373
Anti-CD79b antibody	Polatuzumab	NCT03533283 NCT04739813 NCT03671018 NCT03467373 NCT05260957
Anti-CD22xCD3 bispecific antibody	JNJ-75348780	NCT04540796
Anti-CD38 antibody fused with Shiga-like toxin-A subunit (SLTA)	MT-0169	NCT04017130
Anti-CD20xCD3 bispecific antibody	Epcoritamab	NCT04663347 NCT05283720
Anti-CD22 antibody conjugated to calicheamicin (cytotoxin)	Inotuzumab ozogamicin	NCT03104491
Anti-CD20/CD79bxCD3 trispecific antibody	JNJ-80948543	NCT05424822
Anti-BAFF antibody	VAY736	NCT04903197

Continued

Table B-1 continued

Mechanism	Biologic	Clinical Trial
Anti-CD20 antibody	Obinutuzumab	NCT03075696 NCT03311126 NCT02992522 NCT02393157
Anti-CD47 antibody	Magrolimab (Hu5F9-G4)	NCT02953509
Autologous anti-CD19 CAR T-Cells	Tisagenlecleucel	NCT03570892
Anti-CD19 antibody	Tafasitamab	NCT04809467
Autologous anti-CD19 CAR T cells	Unnamed	NCT02153580
Anti-CD19 CAR NK cells	Unnamed	NCT03056339
Anti-CCR7 antibody conjugated to maytansinoid DM4	JBH492	NCT04240704
Allogenic anti-CD19 CAR T cells	PBCAR0191	NCT03666000
Anti-CD19 CAR T cells	Unnamed	NCT02050347 NCT00586391
Anti-CD5 CAR T cells	Unnamed	NCT03081910
Anti-CD19 CAR NK cells	TAK-007	NCT05020015
Allogenic anti-CD19 CAR NK cells	CNTY-101	NCT05336409
Anti-CD19/CD20/CD22 CAR T-cells	Unnamed	NCT05418088
Anti-CD19/CD20xCD3 trispecific antibody	1A46	NCT05348889
Anti-CD20/CD47 antibody	CPO107	NCT04853329
Anti-CD19/CD20/CD22 CAR T cells	Unnamed	NCT05094206
Anti-CD20 CAR T cells	MB-106	NCT05360238 NCT03277729
Autologous anti-CD20/CD19 CAR T cells	bbT369	NCT05169489
Anti-CD19 CAR T cells	Unnamed	NCT04732845
Autologous anti-CD19/kappa CAR T cells	Unnamed	NCT04223765
Anti-CD19 CAR T cells	TC-110	NCT04323657
Anti-CD19 CAR T cells	Unnamed	NCT01318317
Anti-CD19 CAR T cells	huJCAR014	NCT03103971
Anti-CD19 CAR T cells	Unnamed	NCT04545762

Continued

Table B-1 continued

Mechanism	Biologic	Clinical Trial
Anti-CD19 CAR T cells	Unnamed	NCT01853631
Anti-CD19 CAR T cells	Unnamed	NCT01840566
Autologous anti-CD20/CD19 CAR T cells	C-CAR039	NCT05421663
Anti-BAFF CAR T cells	LMY-920	NCT05312801
Anti-CD19 CAR T cells	UF-KURE19	NCT05400109
Anti-BAFFR CAR T cells	Unnamed	NCT05370430
Anti-CD19/CD22 CAR T cells	Unnamed	NCT05098613
Anti-CD19 CAR T cells	huCART19-IL18	NCT04684563
Anti-CD19 CAR T cells	UCD19	NCT04240808
Anti-CD20/CD22 CAR T cells	UCART20x22	NCT05607420

Appendix C: Supplemental Table 1 for Chapter 2

Cell Line	PRT382 Dose	Venetoclax Dose
Jeko	300nM	1uM
CCMCL1	100nM	1uM
Z-138	150nM	10nM
Mino	450nM	10nM
Maver-1	1uM	10nM
Granta-519	50nM	1uM
Rec-1	50nM	25nM
UPN-1	450nM	1uM
SP53	50nM	1uM

Table C-1: PRT382 and venetoclax doses used in Chapter 2

Doses used throughout the study for each cell line for both single agent and combination treatment unless otherwise stated. Doses were chosen based on IC50 studies to preserve the viability above 70% at time of collection.

Appendix D: Supplemental Table 2 for Chapter 2

ChIP qPCR primers		
BAX	Forward	CGGGACCAAACCTCCCGA
	Reverse	CTGAACGTGCGTCCTTCAC
BAK	Forward	CAGAGACCTCCCAAGGTACCAG
	Reverse	AGCCTCAGGTTGGAAATGGAC
BIM	Forward	TCGGACTGAGAAACGCAAGG
	Reverse	CTCCAGCGCTAGTCTTCCTTC
BIK	Forward	TTCCTGAGTTATGGAACCACACAG
	Reverse	GCTGGTTACGTTGTCATCGG
BBC3	Forward	CCAGCTGGCTTGTTTTACCAC
	Reverse	CTGCACCCATGTGCTTTAGG
NOXA1	Forward	CGTTGTTGACAAAGGTTCCA
	Reverse	GTTACCCAAATTTCCAGCA
BMF	Forward	TGACCACGGATCCATCTTG
	Reverse	TCCCTGATAGAGGCTCCAAAGA
qPCR primers		
BAX	Forward	TTACCGCCATCAGCAGGAACAG
	Reverse	GGAACTCTGAGTCATAGCGTCG
BAK	Forward	CAAGAGTTGCGGCGTATTGGAG
	Reverse	ACACCAGGCGGACAATGTAACG
BIM	Forward	GGAGGTTCTTGGCATGACTGAC
	Reverse	TGAGGCTCACGTCCATCTCGTC
BIK	Forward	ACGACCTCAACGCACAGTACGA
	Reverse	CCTAATTGGGCTCCATCTCGGG
BBC3	Forward	TTACCGCCATCAGCAGGAACAG
	Reverse	GGAACTCTGAGTCATAGCGTCG
NOXA1	Forward	CTCGATGCAGAGACAGAGGTCG
	Reverse	AGGAGCCTGTTTGCCAACTTGC
BMF	Forward	CAGTGGCAACATCAAGCAGAGG
	Reverse	GCAAGGTTGTGCAGGAAGAGGA

Table D-1: ChIP qPCR and qPCR primers used for Chapter 2

Appendix E: Supplementary Materials and Methods for Chapter 2

Cell lines, culture, and drugging protocol

Nine cell lines were used in this work: Jeko, Rec1, SP53, UPN-1, CCMCL1, Z-138, Mino, Maver-1, and Granta-519. All lines were cultured at 37 degrees Celsius, 5% CO₂, in RPMI 1640 (Gibco, Thermo Fisher Cat#2180-084) supplemented with 10% FBS (Sigma Aldrich #F4135), 1% glutamax (Gibco, Thermo Fisher #35050-061), and 1% penicillin/streptomycin (Gibco #15140-122). Cell lines were validated by STR typing within one year of data collection. Mycoplasma testing (Lonza #LT07-518) was performed monthly.

PRT382 was generously supplied by Prelude Therapeutics. Venetoclax (ABT-199) (Cat HY-15531) was purchased from MedChemExpress. To administer drug *in vitro*, cells were seeded at 0.3e6 cells/ml in fresh full RPMI media. PRT382 was solubilized at 100mM in DMSO (Fisher Chemical #D128-500) and log fold dilutions in DMSO were made. These were stored at -20 degrees Celsius for no longer than one month or ten freeze thaw cycles, whichever came first. Venetoclax was solubilized at 50mM in DMSO and then diluted to 10mM with log fold dilutions following. These were also stored at -20 degrees Celsius for no more than one month or ten freeze thaw cycles, whichever came first. No more than 0.1% DMSO v/v was added to a given culture. Approximate IC₇₀ of PRT382 at day nine and Venetoclax at day three, as determined by single agent IC₅₀ studies, described below, were used for each line for western blots, qPCR, and the other *in vitro* experiments performed. For six and nine day experiments, cells were pelleted and resuspended in fresh drugged media at 0.3e6 cell/ml every three days.

Chromatin Immunoprecipitation and Sequencing

ChIP analysis was performed following previous report [282]. In brief, the cells were cultured with or without PRT 100 nM for 24h. 3×10^7 cells were washed with PBS and then, were cross-linked for 5 min with 1% paraformaldehyde and quenched with 125 mM glycine for 5 min at room temperature. After nuclei isolation, the chromatin was sheared in shearing buffer (50 mM Tris-HCl, 10 mM EDTA, and 0.1% SDS) using the Covaris M220 (Covaris Inc., Woburn, MA) focused-ultrasonicator according to the manufacturer's instructions. Immunoprecipitation was performed with 10 μ g of anti-FOXO1 (custom raised rabbit polyclonal) overnight at 4°C. 30 μ l of pre-cleared Dynabeads® Protein G (#10004D, ThermoFisher Scientific, Agawam, MA) was added and incubated for 3 h at 4°C. The beads were washed by RIPA buffer (including LiCl) and eluted with elution buffer (50 mM Tris-HCl, 10 mM EDTA, and 1% SDS). After RNase and Proteinase K treatment, eluted DNA was reverse-crosslinked by 65°C incubation overnight. DNA was extracted using NucleoSpin Gel and PCR clean-up DNA extraction kit (#740609.250, Macherey-Nagel, Bethlehem, PA) and size-selection was carried out to obtain <400 bp size DNA fragments using SPRIselect Reagent (#B23317, Beckmann Coulter Inc., Brea, CA). qRT-PCR was performed using specific primers as described in **Appendix D**.

Quantitative Real Time PCR (qRT-PCR)

The cells were cultured with or without PRT 100 nM for 24h. Total RNAs were extracted from cells by using NucleoSpin RNA kit (#740955.250, Macherey-Nagel,

Bethlehem, PA). Reverse transcription was carried out on 200 ng of total RNA using utilizing RevertAid RT kit (#K1691, ThermoFisher Scientific, Agawam, MA). RT-qPCR was performed on cDNA samples using the PowerUp™ SYBR® Green Master Mix (#A25742, ThermoFisher Scientific, Agawam, MA) on the 7500 Fast Real-time PCR system (ThermoFisher Scientific, Agawam, MA). All samples were run in duplicate and the mRNA level of each sample was normalized to that of ACTB mRNA. The relative mRNA level was presented as unit values of $2^{-\Delta Ct}$ ($=Ct$ of ACTB- Ct of gene). Primers for both ChIP qPCR and qPCR are shown in supplemental table 2.

Immunofluorescence

Slides were prepared using the cytopsin protocol and then fixed in 4% paraformaldehyde for 15 minutes at room temperature (RT). The cells were permeabilized in 0.2% TX100 in PBS for 5 minutes at RT. Slides were rinsed with three changes of PBS and incubated with the primary antibody (1:100 FOXO1 antibody CST cat# 2880S) in 1.5% BSA/PBS overnight at 4 degrees Celsius. These were rinsed with two changes of PBS. The secondary antibody (1:1,000 alexa488-conjugated donkey anti rabbit IgG: ThermoFisher Scientific cat# R37118) for between 30 minutes and one hour at RT. They were also stained with DAPI. The secondary was rinsed with three changes of PBS and slides were mounted (ProLong Gold ThermoFisher Scientific cat# P36934). Slides were imaged with a EVOS FL Cell Auto Imaging System (ThermoFisher Scientific Cat#AMAFD1000) at 40x magnification. Z-138 con (6), Z-138 PRT (9), CCMCL1 con (11), and CCMCL1 PRT (13) view fields were quantified for the number of cells enriched with FOXO1 in the nucleus.

Antibodies and Western blotting assay

Cells were cultured and drugged as described above. Viability was collected on the day of collection as well as on days the culture was refed using trypan blue (Sigma Aldrich Cat# T8154) and DeNovix automated cell counter. At least 5×10^6 cells were collected for western blotting and 2×10^6 for RNA extraction. The calculated quantity of media for western blots and RNA extraction was centrifuged at 315 g for 8 minutes. The pellet was aspirated as dry as possible and then re-suspended in 1 ml of ice-cold PBS (Fisher Scientific Cat# 10010049). 200ul was transferred to a second microcentrifuge tube for RNA extraction. Both tubes were centrifuged at 6785g at 4 degrees Celsius for 10 minutes. These were aspirated dry and stored at -80 degrees Celsius for later use.

Protein extraction, immunoblotting, and immunoprecipitation were performed as described previously (10, 12, 51). Dry pellets were lysed in RIPA buffer (Thermo Scientific Cat# 89901) with phosphatase and protease inhibition cocktails (Thermo Scientific Cat# 78441), using approximately 80ul per 10×10^6 cells. Samples were vortexed vigorously every 10 minutes for 30 minutes, incubating on ice between mixings. These were then pelleted at max speed (~ 13200 g) in a microcentrifuge at 4 degrees Celsius and the supernatant transferred to a new microcentrifuge tube. The quantity of protein in each sample was determined by BCA using the supplied protocol (Thermo Scientific Cat# 23222). Between 20 to 30 micrograms of protein were separated on a 4-20% SDS-PAGE gel (Bio-Rad Cat# 456-1096) using between 80 and 120 volts in TGS running buffer (Bio-Rad Cat# 1610772). The protein was transferred onto polyvinylidene difluoride (PVDF) membrane (Bio-Rad Cat# 1704274) using the semidry transfer system and Turbo transfer blotting buffer (Bio-

Rad Cat# 1704274). After the transfer, membranes were briefly rinsed in DI water to remove residual salts and allowed to dry fully. Blots were then reactivated in methanol and blocked in LiCor Intercept Blocking Buffer (LI-COR Biosciences Cat# 927-60001) for at least one hour, at room temperature with constant rocking. Primary antibodies were used at a 1:1000 dilution in TBS-t (0.01% tween) with the exception of GAPDH which was used at a 1:3000 dilution. Probing was completed overnight at 4 degrees Celsius with constant rocking. Blots were then washed with TBS-t for 10 minutes three times, before being blocked with LiCor fluorescent secondary antibodies (LI-COR Biosciences Cat# 926-68073 and Cat# 926-33210). These antibodies were used at a 1:20,000 dilution in TBS-t for at least one hour at room temperature with constant rocking. A second 30-minute wash with TBS-t was performed as before. The blots were detected on a CLX LiCor scanner. ImageStudio was used to optimize images as well as quantify bands. Bands of interest were normalized against GAPDH or relevant loading control. Primary antibodies used are as follows: GAPDH (CST 67166), FOXO1 (CST 2880), BAX (CST 5023), BAK1 (CST 12105), BBC3 (AKA Puma) (CST 98672), PRMT5 (CST 79998), BCL-2 (CST 4223), Caspase 3 (CST 9663), Caspase 9 (CST 9502), Caspase 8 (CST 4790), Beta-Tubulin (CST 86298)

IC50 and synergy studies

IC50s were determined with two different protocols. Based on our previous work [30, 127, 219, 248], we measured the impact of PRMT5 inhibition on survival in MCL cell lines on day nine. Cells were seeded at 0.3×10^6 in multi well plates. On days three and six,

one quarter volume of each well was transferred to a new plate and the volume was refilled with fresh drugged media. On day nine, cells were transferred to flow cytometry tubes and pelleted at 1500rpm for 5 mins. The tubes were decanted and 100ul of Annexin binding buffer was added to each (BD cat# 556454). Each tube also received 1ul of PI (BD cat# 556463). and 2ul of Annexin V (BD cat# 556419). The tubes were gently vortexed and then allowed to incubate for 15min at room temp in the dark. Before flow was run, an additional 200ul of PBS was added to each tube. The percentage of cells staining double negative, as set with single color controls, was recorded as the percent of live cells. As Venetoclax has maximal effect within 24 hours (data not shown), three days was considered sufficient to determine the effect of Venetoclax on the cell lines. Cells were plated, drugged, stained, and analyzed the same as for PRMT5 inhibition.

When testing for synergy, cells were plated at 0.3e6 cells/ml in 96 well plates (Falcon Cat# 353072). Biologic quadruplicate was used for each experiment. Cells were cultured for six days with either a level of PRT382 or DMSO. On day three, one quarter of the volume was transferred to a new 96 well plate with fresh drugged media used to replace the volume. On day six, Venetoclax conditions were added in combination with PRT382 treatments to the fresh media in a gridded fashion. On day nine, MTS reagent (Abcam Cat# ab197010) was added per provided protocol and incubated for at least 1.5 hours. The absorbance was measured at 492nm. The four wells for each condition were averaged and normalized to the DMSO/DMSO condition. Combenefit, a synergy analysis software developed at Cambridge University [246], was used to create dose response curves to

confirm the expected results of drugging, Lowe model [251] based synergy grids, and a weighted overall synergy score.

Knock Down Lines

In order to knock down the genes of interest, we used shRNA against transcripts. The shRNA sequences were purchased from Sigma Aldrich in glycerol stock form. A small scraping of this stock was placed in terrific broth (Invitrogen cat# 22711022) which had been previously autoclaved. This was placed in an incubator and allowed to remain overnight at 37 degrees Celsius temp and with shaking at 250 RPM. The resulting bacterial culture was purified using a Maxi Prep Kit (Qiagen cat# 12163). The quantity of plasmid DNA was determined by nanodrop.

To generate the virus, 150mm plates were coated with 20mls of 0.6mg/ml Polybran for 10 minutes and then aspirated. 10e6 LentiX 293T cells were seeded per plate in DMEM (Gibco cat# 11995-065) with 10% FBS and 1% sodium pyruvate. The next day, the old media was replaced with 21mls of new media. The DNA mixture was prepared in 4.5ml of OptiMEM media (Thermo Fisher Cat# 51985091) as follows: 13ug of the target vector as determined previously, 9ug of psPAX2 packaging plasmid (addgene plasmid# 12260) and 4.5ug of pHMM-G envelope plasmid (DNASU plasmid repository). In a second tube, 100ul of Lipofectamine 2000 (Thermo Fisher Cat# 11668027) was added to 4.5ml of OptiMEM. Each tube was mixed in circular motion briefly before incubating at room temperature for five minutes. The second tube was added to the first, mixed briefly as before, and then the combined tube was incubated at room temperature for 20 minutes,

during which the solution turns slightly cloudy. This solution was pipetted up and slowly added to the LentiX 293T cells plated earlier, taking care to spread out the flow of solution to cover the entire plate. The plate was rotated gently once and then allowed to incubate in a cell incubator overnight. The next morning all 30ml of media was replaced with fresh, full DMEM. 24 hours after the refeed, the media was removed as viral supernatant. This was spun at 2000 g for 10min and then filtered through a 0.45um filter. The resulting supernatant could be used immediately or frozen at -80 degrees Celsius for later use.

To transduce the cells of interest, cells were resuspended in at 1×10^6 /ml in viral supernatant and placed in micro centrifuge tubes. They were spun at 1428g for 90 min at 32 degrees Celsius. The viral supernatant was aspirated off and the cells seeded in normal growth media. This process was repeated the next day. After the cells rest for 24 hours post the second round of transduction, puromycin was added for selection. The concentration of puromycin was experimental determined (data not shown).

Prior to use in experiments, knockdown was determined via western blot. Between the two vectors, the more efficiently knocked down line for each protein was chosen. Cells were then treated with either DMSO, PRT382, venetoclax, or the combination for four days. On the fourth day, cells were stained with Annexin V/PI and flow cytometry was used to determine the viability of each combination.

Bax(1) TRCN0000312626

Sequence:CCGGCCTTACGTGTCTGATCAATCCCTCGAGGGATTGATCAGACAC
GTAAGGTTTTTG

Bax(2) TRCN0000312625

Sequence:CCGGGACGAACTGGACAGTAACATGCTCGAGCATGTTACTGTCCAG
TTCGTCTTTTTG

BAK1(1) TRCN0000033466

Sequence:CCGGTGGTACGAAGATTCTTCAAATCTCGAGATTTGAAGAATCTTCG
TACCATTTTTG

BAK1(2) TRCN0000234974

Sequence:CCGGATGAGTACTTCACCAAGATTGCTCGAGCAATCTTGGTGAAGT
ACTCATTTTTTG

The empty vector control was also purchased as a glycerol stock (Sigma Aldrich MISSION pLKO.1-puro Empty Vector Control Plasmid DNA Cat#SHC001).

In Vivo Studies

Two PDX (PDX.AA.MCL, PDX.IR.96069) and two CDX (CCMCL1, Granta-519) models were used during this study. For all experiments mice were kept at no more than five mice per cage and no fewer than two per cage when possible. Food and water were provided regularly, with both the researchers and institutional employees monitoring the animals daily. Animal condition was determined through behavioral observation, body scores, and weights taken at least twice weekly. Palliative care including creating “mash” (dry pellets softened in sterile water), administering subcutaneous fluids, and providing high calorie nutrition supplements were provided as needed. ERC was defined as greater than 20% weight loss in one week, a body score lower than 2, a tumor volume of over 3000mm³ and/or disease burden reaching greater than 80% by flow cytometry. Toxicity

was monitored through body weight measurements and observation of mice. When mice reached ERC, they were sacrificed and a necropsy was performed. Notes on organ condition were noted as well as any possible signs of toxicity. 10% of the spleen and the rest of the mouse body were preserved in 10% formalin. The remaining spleen, and any possible tumors were dissociated and stored in 90%FBS/10%DMSO at -80 degrees Celsius before being stored long term in liquid nitrogen. This process was performed as sterilely as possible to allow these cells to be used in future work.

The CCMCL1 CDX model was used at The Ohio State University under protocol 2009A0094-R4. Briefly, CCMCL1 MCL cells were expanded in complete RPMI media, harvested and pelleted, washed with PBS, counted and resuspended at 20e6 cells per ml of sterile PBS. Female NSG (NOD.Cg-Prkdc^{scid} Il2rg^{tm1Wjl}/SzJ, RRID:IMSR_JAX:005557) mice between six and eight weeks of age were engrafted with 100ul of cells resuspended in sterile PBS. The percentage of circulating disease was quantified with flow cytometry by staining for Human-CD19+ (BD Biosciences Cat# 555413, RRID:AB_395813) MCL cells in peripheral blood from weekly cheek bleeds gated on the lymphoid compartment by forward scatter: side scatter (FS:SS). Treatment began on day 15 with four cohorts: vehicle control, PRT382 5mg/kg daily, PRT382 10mg/kg 4 days on, 3 days off, and PRT382 10mg/kg daily.

The Granta-519 flank model was performed at Crown Bioscience on behalf of Prelude Therapeutics under the appropriate ethical compliances. Granta-519 cells were

maintained *in vitro* with DMEM medium supplemented with 10% fetal bovine serum at 37°C with 5% CO₂. The cells in exponential growth phase were harvested and quantitated by cell counter before tumor inoculation. Each mouse was inoculated subcutaneously in the right front flank region with Granta-519 cells (1x 10⁷) in 0.1 ml of PBS mixed with Matrigel (1:1) for tumor development. The date of tumor cell inoculation is denoted as day 0. Randomization was performed when the mean tumor size reached approximately 100-150mm³. 20 mice were randomly allocated to four study groups. Randomization was performed based on “Matched distribution” method using the multi-task method (StudyDirector™ software, version 3.1.399.19)/ randomized block design.

After tumor cell inoculation, the animals were checked daily for morbidity and mortality. During routine monitoring, the animals were checked for any effects of tumor growth and treatment on behavior such as mobility, food and water consumption, body weight gain/loss (body weights were measured twice per week after randomization), eye/hair matting and any other abnormalities. Mortality and observed clinical signs were recorded for individual animals in detail.

Tumor volumes were measured twice per week in two dimensions using a caliper, and the volume was expressed in mm³ using the formula: “ $V = (L \times W \times W)/2$ ”, where V is tumor volume, L is tumor length (the longest tumor dimension) and W is tumor width (the longest tumor dimension perpendicular to L). The body weights and tumor volumes were calculated using StudyDirector™ software (version 3.1.399.19).

Dosing began on day nine with vehicle, PRT543 30mg/kg, venetoclax 100mg/kg, or PRT543 and venetoclax. At day 14, venetoclax was reduced to 50mg/kg for both the

single agent and combo groups. Holidays were given in the groups as needed based on a body weight loss of 10% or higher between weigh ins.

The PDX.AA.MCL and PDX.IR.96069 studies were performed at The Ohio State University under protocol 2009A0094-R4 and IACUC approval. The PDX.AA.MCL model was developed by the Baiocchi and Alinari labs [263] by engrafting 100e6 PBMCs from an ibrutinib resistant MCL patient systemically via tail vein. Splenocytes were collected from mice who developed lymphoma and serially passaged. Dr. Lalit Segal at The Ohio State University provided the PDX-96069 (PRoXe Cat# DFBL- 96069-V1) mouse model.

Female NSG (NOD.Cg-Prkdc^{scid} Il2rg^{tm1Wjl}/SzJ, RRID:IMSR_JAX:005557) mice between six and eight weeks of age were engrafted with 10e6 cells of either the PDX.AA.MCL model, passage six, or the PDX.IR.96069 model from passage five. These cells were resuspended in 100uL of sterile PBS and engrafted via a tail vein. Disease progression was also monitored by flow cytometry on the blood of the mice. Once weekly approximately 50ul of blood was acquired from each mouse and stabilized in an EDTA tube. This was transferred to flow tubes and stained with one test worth of CD5 Fitc (BD cat#555352) and CD19 PE (BD cat# 555413) antibodies. Blood from unengrafted NSG was used as a negative control. For the PDX.AA.MCL model, treatment was to begin once the average circulating MCL cells constituted 1% of the blood. Treatment for the PDX.IR.96069 model was started on day 11 based on previous experience with the model.

Treatment consisted of oral gavage 4 days a week and a break for 3 days. Each drug was administered in 100ul. 4mg/kg of PRT382 was solubilized in a solution made of (0.5% methyl cellulose (w/v) (MP BioMedicals cat# 155492) and 0.1% Tween-80 (v/v) (Fisher cat# T164-500) in sterile water. The vehicle was combined and mixed and heated for approximately one hour. The solution was allowed to incubate overnight at 37 degrees Celsius or until the solution appeared uniformly cloudy. Cooling the solution at 4 degrees for one hour clarified the solution. 12.5 mg/kg of venetoclax was dissolved in sterile ethanol (Sigma Aldrich cat# E7023), before adding Peg400 (Fisher cat# P167-1) and Phosal 50 PG (MedChemExpress cat# HY-Y1903). The final ratio was 10% ethanol, 30% Peg800, and 60% Phosal. Both drugs were sonicated as needed and vortexed immediately before dosing. Mice were censored if engraftment failed or death was not due to disease burden, i.e. gavage injury. Age-matched, strain matched, un-engrafted mice were used as controls.

Statistics

An unpaired Student's t test was used for p53 status analysis, ChIP qPCR, q-PCR results, and protein quantities. A Spearman's Correlation Variable was used to compare two variables for correlation. A two-way ANOVA with multiple comparisons was used to compare shRNA rescue results. To compare changes in disease burden over time, we used Generalized Estimating Equations (GEE) with autoregressive correlation structure to test the differences of slopes between groups. For this exploratory pre-clinical study, p-values

were not adjusted for potential multiple comparisons. A log rank test was used to determine significance for Kaplan Meier curves.

All studies using patient lymphoma samples, which had no patient identifiers, abide by the declaration of Helsinki principles and were approved by The Ohio State University Comprehensive Cancer Center Institutional Review Board (IRB protocol no. 1997CO194) and conducted in agreement with the approved guidelines (IBC protocol no. 2006R0017-R1-AM6). Similarly, all animal studies were performed in compliance with guidelines approved by the Federal and The Ohio State University Institutional Animal Care and Use Committee (IACUC protocol no. 2009A0094-R4) or Crown Bioscience's ethical policies.

